

國立臺灣大學工學院應用力學研究所

博士論文

Graduate Institute of Applied of Mechanics

College of Engineering

National Taiwan University

Doctoral Dissertation

四面體雙聚體分子之量子化學計算與分子動力學模擬

Molecular Dynamics Simulations of Tetrahedral Molecule

Dimers Properties Using *Ab Initio* Intermolecular

Interaction Potentials

李皇德

Arvin Huang-Te Li

指導教授：趙聖德 博士

Advisor: Sheng D. Chao, Ph.D.

中華民國 99 年 6 月

June, 2010

國立臺灣大學博士學位論文
口試委員會審定書

四面體雙聚體分子之量子化學計算與分子動力學模擬

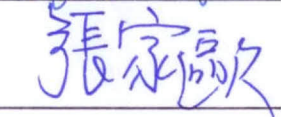
Molecular Dynamics Simulations of Tetrahedral
Molecule Dimers Properties Using *Ab Initio*
Intermolecular Interaction Potentials

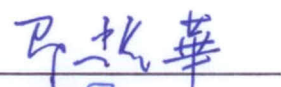
本論文係李皇德君（學號：D93543004）在國立臺灣大學應用力學研究所完成之博士學位論文，於民國 99 年 6 月 3 日承下列考試委員審查通過及口試及格，特此證明

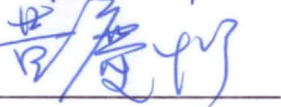
口試委員：

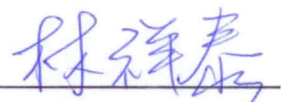
趙聖德 
(指導教授)

張建成 

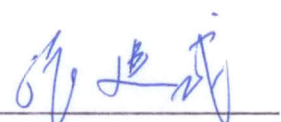
張家歐 

邵耀華 

黃慶怡 

林祥泰 

李寬容 

所 長 張建成 

Acknowledgment

在此要感謝我的爸爸、媽媽以及家人給我的支持與鼓勵，讓我得以無慮的完成博士班的學業，謝謝您們。再者也要感謝這幾年來讓我在知識與見識上增長的恩師趙聖德老師與師母，感謝您的諄諄教誨與提攜讓我如沐春風，亦師亦友、同舟共濟的革命情感相信日後會更加珍惜。也謝謝所長 張建成老師的知遇之恩，讓自己可以在所內發揮所長。謝謝所上的教過自己的老師讓我獲得許多新知，吳光鐘老師、張正憲老師、朱錦洲老師、王立昇老師、沈弘俊老師、邵耀華老師、陳國慶老師、陳瑞琳老師等等，謝謝您們。感謝所有口試委員對自己的肯定，相信自己日後會更加努力。

感謝多年來實驗室的學弟、研究與行政助理們，謝謝您們的幫忙。謝謝本實驗室學弟：景政、宏吉、士緯、守正、光惟、宜興、熙葆、俊傑、陳楠、碩峰、育德、佑儒、思哲，研究助理：奕翔、宛儀、馨瑩、以謝，行政助理：逸璇、書閔、欣瑩、婷婷、薔涵等等的幫忙。謝謝其他實驗室：在欣、玉清、哲宇、祺皓、銘儒、義慶、宏志、明峰、冠榮、佳暉、萬霖、大發等等的幫助。所上翁文斌技士、李孟賢技佐、所辦許文珍小姐、張素端小姐、李瑩蘭小姐的幫忙。清大生科所的林志侯老師、李寬容老師、張晃猷老師的鼓勵，以及清大的大鈞學長、昭芬學姐。謝謝當兵時候嘉義縣新港國中的老師們，謝謝您們。

感謝家昕當時候的支持與陪伴，由衷的感謝。謝謝好友瑞苓、瑞玲、Ivo、育嘉、Amy、Nancy、Yichi、Helen、璽凱、小顏、膺任、彥城、俊甫、珣玨、啟昌、良玉、慧怡、謝迺岳老師等等的幫忙。

謝謝家人、老師、同儕、朋友，您們都是我的明燈與貴人，萬分感謝。

皇德 謹誌于

國立台灣大學 應用力學所
跨尺度動力學實驗室 R 325A

中華民國 99 年 6 月

摘要

本論文主要探討四面體雙聚體分子之量子化學計算與分子動力學模擬探討熱力學性質。我們從最簡單的四面體甲烷分子開始研究並推廣到矽烷與四氯化碳分子。我們首先準確的架構並計算出 12 個不同方位的能量曲線，探討方位、中間氫原子數目對能量關係、吸引力、斥力、剛體與非剛體對能量造成的影響。

在量子計算方面主要使用的方法有 Hartree-Fock (HF)、Density Function Theory (DFT)、Second-order Møller-Plesset Perturbation Theory (MP2) 與 Single-point Coupled Cluster with Single and Double and Perturbative Triple Excitations CCSD(T) 等計算方法。基底方面使用 Pople 的方法從小的基底到 6-311++G (3df, 3pd)，並使用 Dunning 的基底 [cc-pVXZ 與 aug-cc-pVXZ，其中 X = D、T、Q、5] 進行一連串完整的計算並探討能量收斂狀況。計算時中心原子距離從 3.0 \AA 到 9.0 \AA ，並使用四種近似法 (Extrapolation methods) 與完整基底極限展開法 (Complete Basis set limit) 得到鍵結最低能量極限值，與目前光譜實驗量測所可以測得的容許差值約在 0.03 kcal/mol 之內。

而在分子動力學模擬方面主要是利用 Lennard-Jones (L-J) potential function 去做擬合並建構力場，先分別探討 4-site 與 5-site 的影響。4-site 需要決定四個擬合參數 16 條方程式，5-site 需要決定六個擬合參數 25 條方程式。利用得到的擬合參數去模擬在不同溫度、密度與壓力下 Radial Distribution Function (RDF) 的平衡性質並探討溫度效應與實驗值做比較。而動態性質方面主要是研究沿著汽化線做 Velocity Autocorrelation Function (VAF) 的模擬，求得擴散係數 (Diffusion Coefficient) 並與文獻上既有的實驗值做比較。最後做 X-ray 散射 與 Neutron 散射模擬研究皆與真實文

獻上實驗吻合。由上述結果可知，就我們目前所做的量子化學勢能曲線 (Potential Energy Surface) 理論計算結果與所得到的 5-site 理論擬合參數值皆可精準與實驗相驗證。



關鍵字：Hartree-Fock (HF)， Density Function Theory(密度泛函理論)， Second-order Møller-Plesset Perturbation Theory (二階 Møller-Plesset 微擾理論)， Single-point Coupled Cluster with Single and Double and Perturbative Triple Excitations CCSD(T)， Radial Distribution Function (徑向分布函數)， Velocity Autocorrelation Function (速度自相關函數)， Diffusion Coefficient (擴散係數)， X-ray 散射與 Neutron 散射。

Abstract

In this study, intermolecular interaction energy data for the tetrahedral molecule dimers have been calculated at a spectroscopic accuracy and employed to construct an *ab initio* potential energy surface (PES) for molecular dynamics (MD) simulations of tetrahedral molecule properties. The full potential curves of the tetrahedral molecule dimers at 12 symmetric conformations were calculated by the supermolecule counterpoise-corrected Hartree-Fock (HF), Density Function Theory (DFT), second-order Møller-Plesset (MP2) perturbation theory and single-point coupled-cluster with single and double and perturbative triple excitations [CCSD(T)] calculations were also carried out to calibrate the MP2 potentials. We employed Pople's medium size basis sets [up to 6-311++G (3df, 3pd)] and Dunning's correlation consistent basis sets (cc-pVXZ and aug-cc-pVXZ, X = D, T, Q, 5). For each conformer, the intermolecular carbon-carbon separation was sampled in a step 0.1 Å for a range of 3.0 ~ 9.0 Å. The MP2 binding curves display significant anisotropy with respect to the relative orientations of the dimer. The potential curves at the complete basis set (CBS) limit were estimated using well-established analytical extrapolation schemes and while a large basis set (aug-cc-pVTZ) is required to converge the binding energy at a chemical accuracy (~0.03 kcal/mol). A 4-site and 5-site potential models were used to fit the *ab initio* potential data. We performed molecular dynamics

simulations using the *ab initio* force field and compared the simulation results to experiments. Quantitative agreements for the atomwise radial distribution functions, the self-diffusion coefficients, and the X-ray and Neutron diffraction scattering functions over a wide range of experimental conditions can be obtained, thus validating the *ab initio* force field without using experimental data *a priori*.



Keyword : Hartree-Fock (HF), Density Function Theory (DFT), Second-order Møller-Plesset Perturbation Theory(MP2), Single-point Coupled Cluster with Single and Double and Perturbative Triple Excitations CCSD(T),Radial Distribution Function (RDF), Velocity Autocorrelation Function (VAF), Diffusion Coefficient, X-ray and Neutron diffraction scattering function.

Contents

口試委員會審定書.....	i
Acknowledgment.....	ii
Chinese Abstract.....	iii
English Abstract.....	v
Contents	vii
Figure Contents	ix
Table Contents	xiv
Chapter 0 General Introduction	17
Chapter 1 Theoretical Studies on the Methane Dimers.....	22
1.1 Intermolecular Interaction Potentials of Dispersion-Bound Methane Dimer From Coupled Cluster Method at Complete Basis Set Limit.....	22
1.2 Intermolecular Potentials of the Methane Dimer Calculated with Møller- Plesset Perturbation Theory and Density Functional Theory and comment on "Intermolecular Interaction Potential of the Methane Dimer From the Local Density Approximation".....	42
1.3 Molecular Dynamics Simulations of Fluid Methane Properties Using <i>Ab</i> <i>Initio</i> Intermolecular Interaction Potentials.....	93
Chapter 2 Theoretical Studies on the Silane Dimers.....	131
2.1 Intermolecular Potentials of the Silane Dimer Calculated with Hartree-Fock Theory, Møller-Plesset Perturbation Theory and Density Functional Theory.....	131
2.2 Determination of a Silane Intermolecular Force Field Potential Model From an <i>Ab Initio</i> Calculation.....	169
Chapter 3 Theoretical Studies on the Carbon Tetrachloride Dimers.....	187

3.1 Molecular dynamics simulation of liquid carbon tetrachloride using <i>AbInitio</i> force field.....	187
3.2 Intermolecular Potential of the Carbon Tetrachlorid Dimer Calculated with Møller-Plesset Perturbation Theory and Density Function Theory.....	213
Chapter 4 Conclusion	232



Figure Contents

Fig. 0.0-1... tetrahedral molecule dimers.....	18
Fig. 0.0-2...Standard operating procedure(SOP).....	19
Fig. 0.0-3... 4-site model.....	20
Fig. 0.0-4... 5-site model.....	20
Fig. 0.0-5... Radial distribution function.....	21
Fig. 0.0-6...Velocity autocorrelation function.....	21
Fig. 1.1-1... The BSSE corrected HF, MP2, and CCSD(T) interaction potentials of the methane dimer using the aug-cc-pVQZ basis set.....	40
Fig. 1.1-2... The estimated CCSD(T)/CBS potential curves using the direct extrapolation scheme with the four extrapolation methods on the cc-pVXZ potential data..	40
Fig. 1.1-3... The estimated CCSD(T)/CBS potential curves using the direct extrapolation scheme with the four extrapolation methods on the aug-cc-pVXZ potential data.....	41
Fig. 1.2-1... The calculated intermolecular interaction potentials using a series of exchange-correlation functionals.....	84
Fig. 1.2-2... Comparison of the calculated data with the fittings using the L-J function and the exponential function.....	85
Fig. 1.2-3... The BSSE corrected HF interaction potentials of the methane dimer using several basis sets.....	86
Fig. 1.2-4... The BSSE corrected (CP) and uncorrected (NCP) MP2 potentials of the methane dimer using a series of basis sets.....	86
Fig. 1.2-5... Comparison of the BSSE corrected MP2 potential curve calculated at the aug-cc-pVQZ basis set and the sum of the HF potential and the long range	

dispersion potentials.....	87
Fig. 1.2-6... The BSSE corrected DFT intermolecular potential curves using the PW91 as the exchange or correlation functional.....	87
Fig. 1.2-7... The GGA exchange enhancement factor as a function of s for the B88, HCTH, OPTX, MPW, PBE, and PW91 exchange functionals.....	88
Fig. 1.2-8... The GGA correlation enhancement factor as a function of s for the TPSS, PBE, PW91, P86, and HCTH correlation functionals. Here $r_s=10$	88
Fig. 1.2-9... The r_s dependence of the GGA correlation enhancement factor as a function of s for the P86 correlation functional.....	89
Fig. 1.2-10... The BSSE corrected potential curves with varying exchange functionals by fixing (a) PBE, (b) PW91, (c) VWN, (d) VP86 and (e) LYP correlation functionals, respectively.....	89
Fig. 1.2-11... The BSSE corrected potential curves selective using several hybrid functionals.....	92
Fig. 1.2-12... The asymptotic behavior of selective DFT potentials versus the MP2 potential via a analysis of the long-range data.....	92
Fig. 1.3-1... The twelve symmetric conformers of the methane dimer considered in this paper.....	118
Fig. 1.3-2... Comparison of the potentials with (rigid) and without (non-rigid) the rigid monomer assumption for the J conformer.....	119
Fig. 1.3-3... The MP2/aug-cc-pVQZ potentials of the methane dimer for the 12 conformers.....	120
Fig. 1.3-4... Comparison of the HF (repulsive) and MP2-HF (attractive) potentials for the 12 conformers.....	121
Fig. 1.3-5... The MP2/CBS potential curves using the extrapolation method of Halgaker et al.	121

Fig. 1.3-6... A schematic plot of the 4-site model where the sites are located at the hydrogen positions only.....	122
Fig. 1.3-7... Comparison of the fitting curves and the calculated potential data.....	123
Fig. 1.3-8... The six-dimension PES.....	124
Fig. 1.3-9... Comparison of the experimental (EXP) and the molecular dynamics (MD) radial distribution functions (RDFs) as a function of R.....	125
Fig. 1.3-10... Velocity autocorrelation functions as a function of time for several experimental conditions.....	127
Fig. 1.3-11... The diffusion coefficient as a function of temperature for different cell sizes and r_{cut}	128
Fig. 1.3-12... Comparison of the experimental (EXP) and the molecular dynamics (MD) X-ray scattering as a function of K.....	129
Fig. 1.3 -13... Comparison of the experimental (EXP) and the molecular dynamics (MD) thermal effect as a function of K.....	130
Fig. 2.1-1... The BSSE corrected MP2 potentials using the aug-cc-pVTZ basis set for the D_{3d} and C_{3v} conformers of the silane dimer.....	162
Fig. 2.1-2... The BSSE corrected HF interaction potentials of the silane dimer using several basis sets.....	162
Fig. 2.1-3... The BSSE corrected (CP) and uncorrected (NCP) MP2 potentials of the silane dimer using a series of basis sets.....	163
Fig. 2.1-4... Comparison of the BSSE corrected MP2 potential curve calculated at the aug-cc-pVQZ basis set and the sum of the HF potential and the long-range dispersion potentials.....	163
Fig. 2.1-5... The basis set dependence of the DFT potentials calculated with the PW91PW91 functional (left panel).....	164
Fig. 2.1-6... The GGA correlation enhancement factor as a function of s for the TPSS,	

PBE, PW91, P86, and HCTH correlation functionals.....	164
Fig. 2.1-7... The BSSE corrected DFT potential curves with varying exchange functionals by fixing (a) PBE, (b) PW91, (c) VWN, (d) VP86, and (e) LYP correlation functionals, respectively. (f) The DFT potentials using several hybrid functionals (B3LYP, B3P86, BHandH, MPW1PW91, O3LYP, and PBE1PBE)	165
Fig. 2.1-8... The asymptotic behaviors of selective DFT potentials versus the MP2 potential via an analysis of the long-range data.....	168
Fig. 2.2-1... The twelve symmetric conformers of the silane dimer.....	183
Fig. 2.2-2... The HF potentials for the 12 orientations using the aug-cc-pV5Z basis set..	184
Fig. 2.2-3... The MP2 potentials for the 12 orientations using the aug-cc-pV5Z basis set.	184
Fig. 2.2-4... The MP2-HF potentials for the 12 orientations using the aug-cc-pV5Z basis set.....	185
Fig. 2.2-5... The C_6 coefficient value has been obtained by fitting to intermolecular potential energy from ab initio calculation.....	185
Fig. 2.2-6... Comparison of the fitting curves (line) and the potential data (symbol).....	186
Fig. 3.1-1... The twelve symmetric conformers of the carbon tetrachloride dimer.....	208
Fig. 3.1-2... The HF potentials for the 12 orientations using the aug-cc-pVTZ basis set. .	209
Fig. 3.1-3... The MP2 potentials for the 12 orientations using the aug-cc-pVTZ basis set.....	209
Fig. 3.1-4... The MP2-HF potentials for the 12 orientations using the aug-cc-pVTZ basis set.	210
Fig. 3.1-5... Comparison of the fitting curves (line) and the potential data (symbol).....	210
Fig. 3.1-6... The calculated C-C, C-Cl and Cl-Cl radial distribution function g_{CC} , g_{CCl} , g_{ClCl} for a range of thermodynamic conditions.....	211
Fig. 3.1-7... Comparison of theory curve (line) and neutron scattering functions	

(symbol).....	212
Fig. 3.1-8... Comparison of theory curve (line) and X-ray scattering functions	
(symbol).....	212
Fig. 3.2-1... The BSSE corrected MP2 potentials using the aug-cc-pVTZ basis set for the D _{3d} and C _{3v} conformers of the carbon tetrachloride dimer.....	229
Fig. 3.2-2... The BSSE corrected HF interaction potentials of the carbon tetrachloride dimer using several basis sets.....	229
Fig. 3.2-3... The BSSE corrected (CP) and uncorrected (NCP) MP2 interaction potentials of the carbon tetrachloride dimer using a series of basis sets.....	230
Fig. 3.2-4... The BSSE corrected DFT potential curves with varying exchange functional by fixing VWN5 correlation functionals.....	230
Fig. 3.2-5... The BSSE corrected DFT potential curves with varying exchange functional by fixing PL correlation functionals.....	231

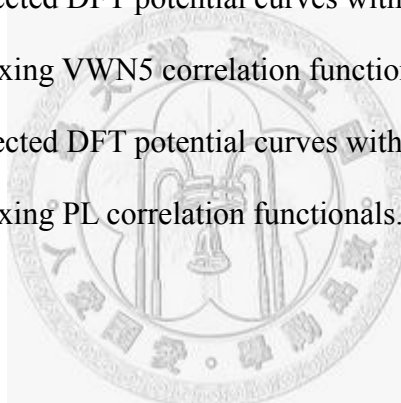


Table Contents

Table 1.1-1 ... The basis set dependence of important potential parameters of the BSSE corrected CCSD(T) intermolecular potentials.....	37
Table 1.1-2 ... Comparison the estimated CCSD(T) and MP2 binding energies at the complete basis set limit using the four extrapolation methods.....	38
Table 1.1-3 ... Basis set dependence of the estimated potential parameters of the CCSD(T)/CBS potential.....	39
Table 1.2-1 ... The basis set dependence of important potential parameters using the BSSE corrected HF and MP2 intermolecular potentials.....	80
Table 1.2-2 ... Comparison of the bond lengths and the binding energies calculated using the several exchange-correlation functionals with the MP2 results using the 6-311++G (3df,3pd) basis set.....	81
Table 1.2-3 ... Comparison of the bond lengths calculated with the 90 exchange-correlation functionals using the 6-311++G (3df, 3pd) basis set.....	82
Table 1.2-4 ... Comparison of the binding energies calculated with the 90 exchange-correlation functionals using the 6-311++G (3df, 3pd) basis set.....	83
Table 1.3-1 ... The basis set dependence of important potential quantities extracted from the MP2 potentials for the 12 conformers.....	112
Table 1.3-2 ... The MP2/CBS binding energies using the four extrapolation methods....	114
Table 1.3-3 ... Comparison of the MP2/aug-cc-pVQZ and MP2/CBS potential data with the CCSD(T)/aug-cc-pVQZ data for the J conformer.....	115
Table 1.3-4 ... Comparison of the experimental (EXP) and molecular dynamics (MD) self-diffusion coefficients for a wide range of thermodynamic conditions.....	116

Table 1.3-5 ... The deviation of the fit data from the ab initio data. <i>ABSper</i> and <i>ABSerr</i> represent the root mean square errors.....	117
Table 2.1-1 ... The basis set dependence of important potential parameters using the BSSE corrected HF and MP2 intermolecular potential.....	158
Table 2.1-2 ... Comparison of the binding energies using the BSSE corrected MP2 and CCSD(T) intermolecular potentials calculated at several basis sets.....	159
Table 2.1-3 ... Comparison of the bond lengths calculated with the 108 exchange-correlation functionals using the 6-311++G (3df,3pd) basis set.....	160
Table 2.1-4 ... Comparison of the binding energies calculated with the 108 exchange-correlation functionals using the 6-311++G (3df, 3pd) basis set.....	161
Table 2.2-1 ... The basis set dependence of MP2 potentials for the G and H conformers.	180
Table 2.2-2 ... Predicted C ₆ coefficient value with literature in twelve conformers.....	181
Table 2.2-3 ... The estimated MP2/CBS binding energies for the G conformer using the three extrapolation methods described in the text.....	182
Table 3.1-1 ... The basis set dependence of some potential parameters of the HF and MP2 potentials for the J conformer.....	204
Table 3.1-2 ... The estimated MP2/CBS binding energies for the J conformer. using the four extrapolation methods described in the text.....	205
Table 3.1-3 ... Comparison of the calculated peak and valley positions of the RDF with the experiment	206
Table 3.1-4... The self-diffusion coefficients using the Green-Kubo formula as compared to the available experimental data.....	207
Table 3.2-1 ... The basis set dependence of some potential parameters for the HF and MP2 potentials.....	226
Table 3.2-2 ... Comparison of the bond lengths of the interaction potential calculated with the 80 exchange-correlation functionals using the aug-cc-pVTZ	

basis set.....227

Table 3.2-3 ... Comparison of the binding energies of the potential calculated with
the 80 exchange-correlation functionals using the aug-cc-pVTZ basis
set.....228



Chapter 0 General Introduction

We performed refined quantum chemistry calculations of the intermolecular interactions for dimers of methane, silane, and tetrachloromethane in Fig.0.0-1. For arbitrary molecule in quantum chemistry calculations, the energy can be expansion in Hamiltonian formula,

$$\hat{H} = -\frac{\hbar^2}{2m_e} \sum_i \nabla_i^2 - \frac{e^2}{4\pi\epsilon_0} \sum_{i,C} \frac{Z_C}{r_{i,C}} + \frac{e^2}{4\pi\epsilon_0} \sum_{i>j} \frac{1}{r_{i,j}} - \sum_C \frac{\hbar^2}{2m_C} \nabla_C^2 + \frac{e^2}{4\pi\epsilon_0} \sum_{C>C'} \frac{Z_C Z_{C'}}{R_{C,C'}}$$

for total energy (Born-Oppenheimer energy)

$$E_{total} = E_{elec} + U_{c'c}$$

Our *ab initio* calculations focused on the minimum energy curves for a specific relative configuration of the dimers considered. We performed at the HF, DFT, MP2 and CCSD(T) theory

$$HF: E_{slater} = \int \psi^* \hat{H}_{elec} \psi d\tau = 2 \int \phi_i^*(1) \left(-\frac{\hbar^2}{2m_e} \nabla_1^2 - \sum_C \frac{Z_C}{4\pi\epsilon_0 r_{1,C}} \right) \phi_i(1) d\tau_1 + \sum_{i=1}^n \sum_{j=1}^n (2J_{ij} - K_{ij})$$

$$DFT: E = U_{Ne} + K_s + U_{ee} + E_{xc}$$

$$MP2: E = E_{HF} + E_0^{(2)} = E_{HF} + \sum_{m \neq 0} \frac{|\int \psi_m^{(0)*} \hat{H} \psi_0^{(0)} d\tau|^2}{E_0^{(0)} - E_m^{(0)}} = E_{HF} + \sum_{a,b,i,j} \frac{|(ij|ab) - (ia|jb)|^2}{\epsilon_i + \epsilon_j - \epsilon_a + \epsilon_b}$$

$$CCSD(T): \psi = e^{\hat{T}} \phi_{HF}$$

and higher level *ab initio* calculations for other relative configurations to model the anisotropy of intermolecular interactions of the chosen functional groups. We also perform a nonlinear modeling using force matching and other minimization schemes. The liquid methane, silane, and tetrachloromethane properties, structural and dynamical, can be well reproduced via molecular dynamics simulations in Fig.0.0-2 ~

Fig. 0.0-6.

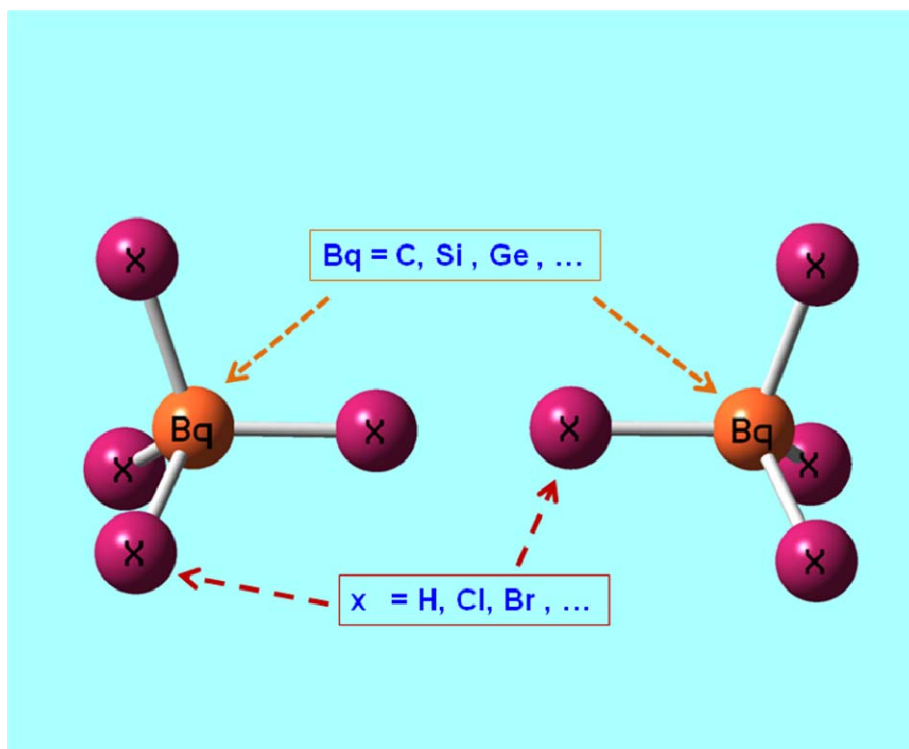


Fig. 0.0-1

Standard operating procedure (SOP)

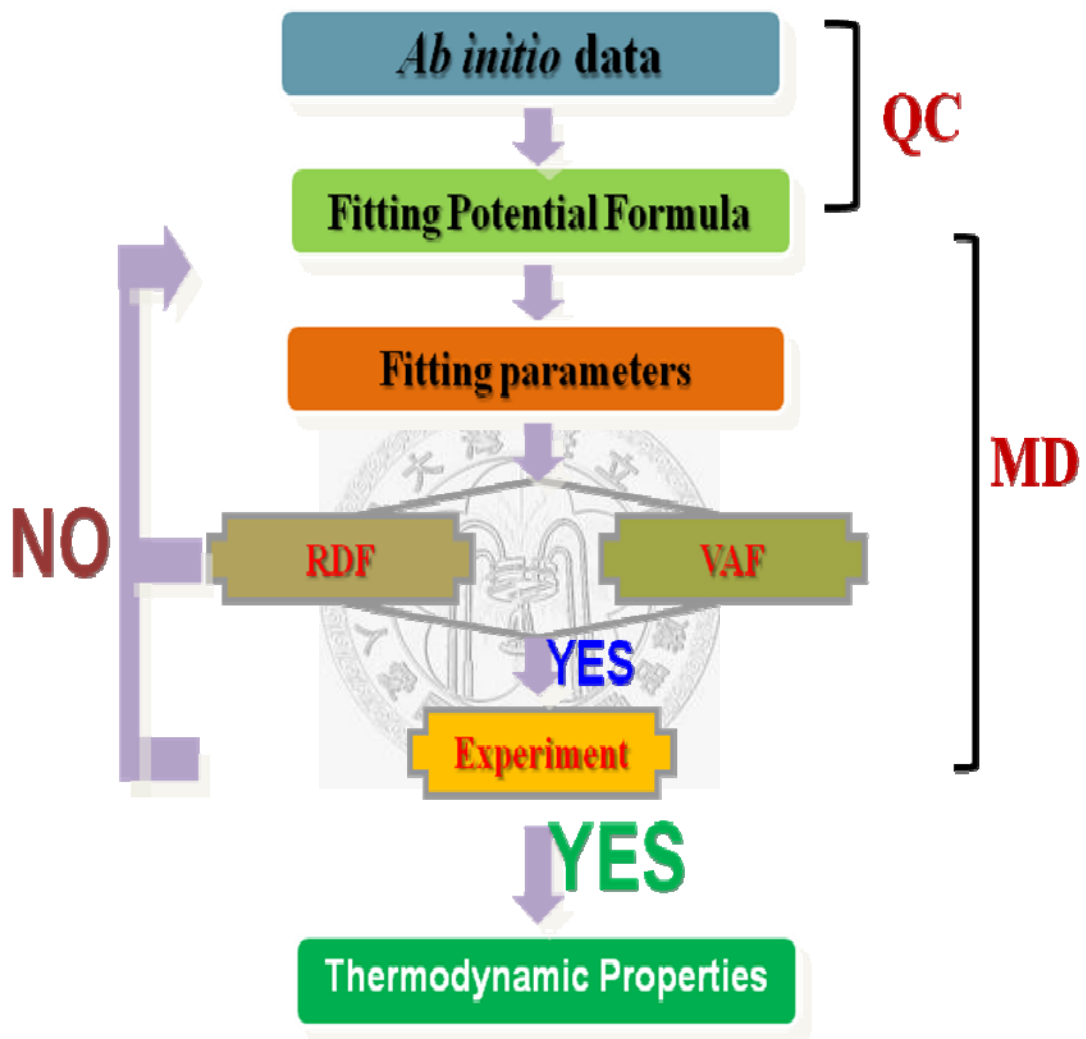
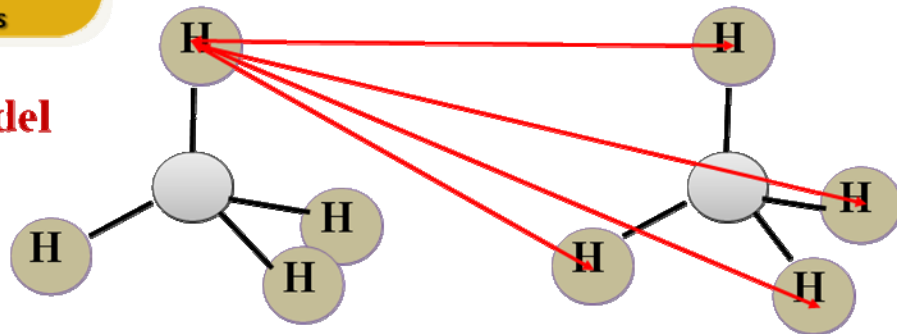


Fig. 0.0-2

4-Site model

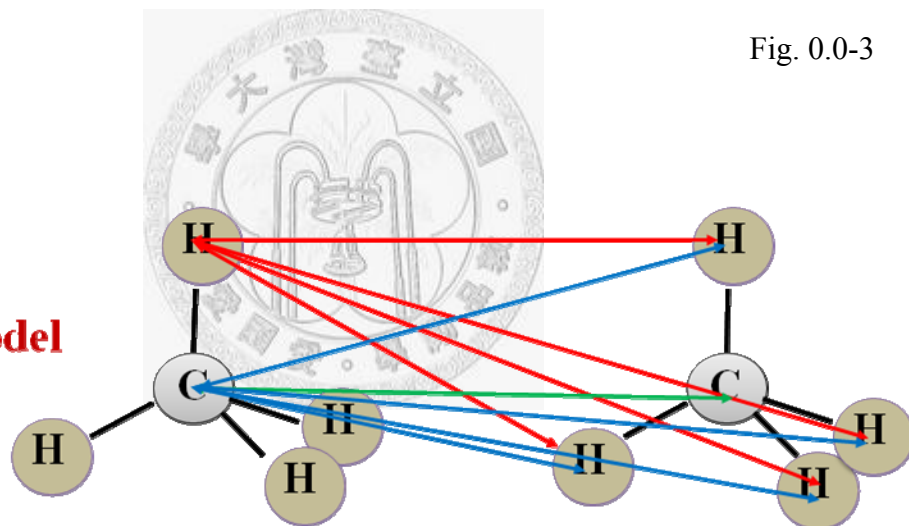


$$U(r) = 4\epsilon \left[\left(\frac{\sigma}{r} \right)^{12} - \left(\frac{\sigma}{r} \right)^6 \right]$$

$$\hookrightarrow U(r) = 4\epsilon_{HH} \left[\left(\frac{\sigma_{HH}}{r} \right)^{12} - \left(\frac{\sigma_{HH}}{r} \right)^6 \right]$$

Fig. 0.0-3

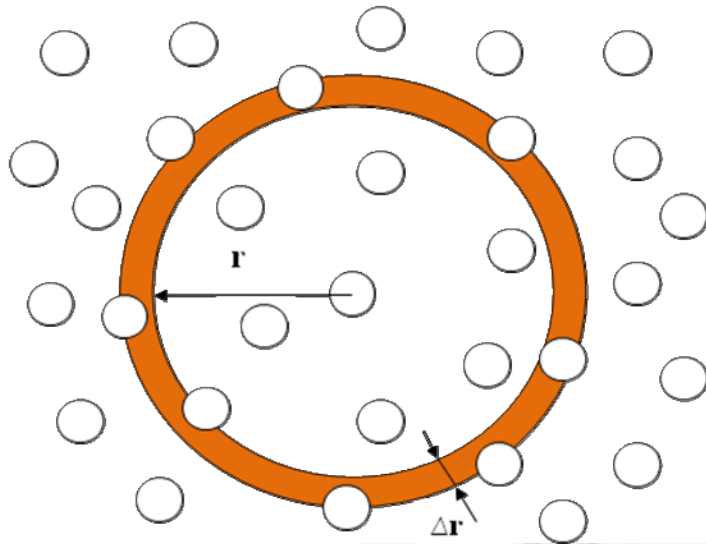
5-Site model



$$U(r) = 4\epsilon_{HH} \left[\left(\frac{\sigma_{HH}}{r} \right)^{12} - \left(\frac{\sigma_{HH}}{r} \right)^6 \right] + 4\epsilon_{CH} \left[\left(\frac{\sigma_{CH}}{r} \right)^{12} - \left(\frac{\sigma_{CH}}{r} \right)^6 \right] + 4\epsilon_{CC} \left[\left(\frac{\sigma_{CC}}{r} \right)^{12} - \left(\frac{\sigma_{CC}}{r} \right)^6 \right]$$

Fig. 0.0-4

RDF (Radial Distribution Function)

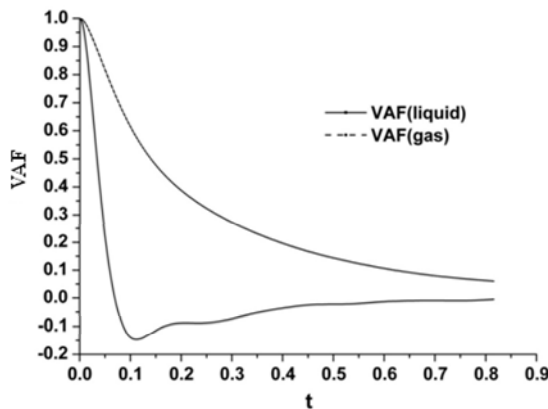


$$g(r) = \frac{n(r)}{\rho 4\pi r^2 \Delta r}$$

Fig. 0.0-5

VAF (Velocity Autocorrelation Function)

➔ Diffusion coefficient



$$D = \frac{1}{3N} \int_0^{\infty} \left\langle \sum_i^N \mathbf{v}_i(t) \cdot \mathbf{v}_i(0) \right\rangle dt$$

Green Kubo expression

Fig. 0.0-6

Chapter 1 Theoretical Studies on the Methane Dimers

1.1 Intermolecular Interaction Potentials of Dispersion-Bound Methane Dimer From Coupled Cluster Method at Complete Basis Set Limit

1. Introduction

The hydrocarbon interactions are very crucial in determining the packing morphology of molecular solids and soft matters such as lipid bi-layer assembly of membranes and active conformation of proteins [1-3]. The potential energy functions are also requested for mesoscale modeling of macromolecules [4] because the hydrocarbon interactions dominate the surface energies, from which many important properties relevant to organic nanostructures can be derived. Determining intermolecular interactions among dispersion-bound complexes from solely experimental measurements is a notoriously challenging task [5-7], mainly due to limited sampling of the potential energy surface. One alternative is to use first-principles electronic structure calculations, at least for small molecular systems [8-10].

Methane molecular interactions can be regarded as a prototype system of any hydrocarbon interactions or of any segment containing hydrocarbons and thus have been intensely studied [11-23]. Jurecka *et al.* [21] have obtained the CCSD(T) binding

energies of the methane dimer at the complete basis set (CBS) limit using an approximation scheme (see Eq. (1) below). Tsuzuki *et al.* [22] have estimated the CCSD(T)/CBS binding energies using the method of Halgaker *et al.* [32] and the method of Feller [34]. Previous CCSD(T) studies on the methane dimer mainly focused on the equilibrium region of the potentials with relatively few discussion on the full potential curve. Nevertheless, to construct a reliable force field model for molecular simulations, the full intermolecular potential surfaces are required. Recently, Takatani *et al.* [24] have obtained a CCSD(T)/CBS potential curve for the methane dimer using a specific extrapolation scheme. However, the basis set effects using the CCSD(T) method and the performance of various extrapolation methods to obtain the CBS data have not been systematically investigated. Therefore, in this paper we perform a comprehensive study on interaction potentials of the prototype methane dimer in terms of the CCSD(T) method at the complete basis set limit. The relative performance of several extrapolation methods to obtain the CBS values is thoroughly discussed. The full potential curves are presented to see the overall scope of the interactions.

2. Methods and Calculations

Supermolecular approach has been taken to calculate the interaction energy in which

the intermolecular potential is defined as the total energy difference between the supermolecule and the isolated subsystems. The calculation of electron correlation energies depends on the level of the correlation method, the size of the basis set, and the correction of the BSSE. State-of-the-art choice of the correlation method is the coupled cluster method with iterative single and double substitutions and with noniterative triple excitations [CCSD(T)] method [26]. It has been widely recognized that the CCSD(T) results with large basis sets are close to the results at the complete basis set limit [27]. To study the basis set effects, we have employed a wide range of basis sets from the Slater-type orbitals fitted with Gaussian functions (STO-nG, n=3~6) [28], Pople's medium size basis sets [up to 6-311++G (3df, 3pd)] [29] to Dunning's correlation consistent basis sets (cc-pVXZ and aug-cc-pVXZ, X=D, T, Q) [30]. The basis set superposition error (BSSE) was corrected by the counterpoise (CP) method of Boys and Bernardi [31]. The CCSD(T) binding energy at the complete basis set limit has been estimated using the methods of Helgaker *et al.* [32], Martin [33], Feller [34], and a numerical extrapolation method based on the 3-term Lagrangian formula [35]. The analytic extrapolation formulas are summarized as follows.

$$\text{Helgaker } et al.: \quad E_X = E_\infty + bX^{-3}$$

$$\text{Martin: } E_{\infty} = \frac{(X+3/2)^4}{(X+3/2)^4 - (X+1/2)^4} E_{X+1} - \frac{(X+1/2)^4}{(X+3/2)^4 - (X+1/2)^4} E_X$$

$$\text{Feller: } E_X = E_{\infty} + b e^{-cX}$$

All the calculations are performed using the Gaussian 03 program package [36] on a single node 1-processor IBM 1350 PC cluster with distributed memory. To obtain the most stable intermolecular geometry, the methane molecule was first optimized at the CCSD(T)/aug-cc-pVTZ and the obtained C-H bond length is 1.085 Å. Next we calculated the binding energies of the 12 symmetric dimer conformers such as those considered by Tsuzuki *et al.* [15] using MP2/aug-cc-pVTZ and found the minimum-energy conformation corresponds to the D_{3d} symmetry conformer. This optimized conformer has been explained in terms of the interplay of the steric stabilization of repulsive hydrogen in opposite monomers [11]. Subsequently the C-C distance was sampled for a quite large range of intermolecular separation (normally 3~9 Å), resulting in a total of 11 configuration points for each basis set. During the scan we first fix the monomer geometry (rigid monomer assumption) and the conformer symmetry. Next, because inclusion of the intramolecular vibrational relaxation could be relevant to molecular dynamics simulations using flexible models [37], validity of the rigid monomer assumption should be checked. We repeat the

above procedure while allowing the C-H bonds to relax during the scan. We found little effect (normally within 0.01 *kcal/mol* in energy difference) when including the vibrational relaxation. Therefore, in this paper we present the potential data under the rigid monomer assumption in order to compare them with previous studies.

3. Results and Discussions

In Fig. 1.1-1 we compare the BSSE corrected HF, MP2, and CCSD(T) potentials of the methane dimer using the aug-cc-pVQZ basis set. The HF and MP2 potentials are obtained from our previous calculations [23]. It is seen that the HF potential is purely repulsive while the MP2 and CCSD(T) potentials display potential wells. The CCSD(T) potential shown in Fig. 1.1-1 displays a clear minimum and a long range attractive potential tail. Because the contributions from the electrostatic and induction energies are small [11], the dispersion energy is mainly responsible for the attractions. The sharp difference between the HF calculations and the CCSD(T) calculations indicates the importance of including the correlation corrections in the wave function calculations. The MP2 potential is close to the CCSD(T) potential in this case. We also find very strong dependence of the interaction potentials on the BSSE corrections, even using the aug-cc-pVTZ basis set. Only the BSSE corrected potential curves bear the proper trend of systematic convergence. This is similar to our previous studies

using the MP2 method [23].

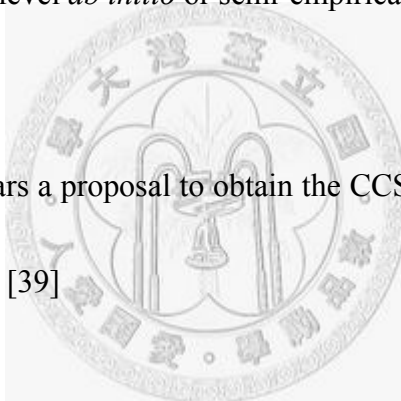
In Table 1.1-1 we provide a detailed editing of the basis set effects on the equilibrium bond length, the binding energy, and the harmonic frequency. R_0 is the distance at which the potential is zero and can be obtained from a two point interpolation of the calculated data. The bond length R_m , the binding energy E_b and the intermolecular vibration frequency ω can be obtained through a harmonic modeling of the three lowest potential data near the equilibrium regions. It is seen that the interaction energy becomes deeper with more polarization and diffuse functions added. Small cc-pVDZ and cc-pVTZ basis sets lead to underestimation of the binding energy but augmentation of the diffuse functions improves much on the binding energy. The basis set effects presented here are qualitatively similar to previous studies on methane and silane dimers using the MP2 method [23, 38-39]. These observations are expected to apply to other dispersion-bound systems also.

The strong basis set dependence and the slow convergence on the dispersion energy call for an estimation of the important potential features at the complete basis set limit in a calculated potential. Complete basis set limit of the binding energy can be estimated using Dunning's basis sets with an extrapolation method. We consider three

analytical methods [32-34] and a numerical method [35] and the results are shown in Table 1.1-2. The binding energies obtained at the complete basis set limit (using the potential data calculated at Dunning's basis sets, aug-cc-pVXZ, X=D, T, Q) are -0.509, -0.512, -0.507, and -0.510 *kcal/mol* using the methods of Helgaker *et al.* [32], Martin [33], Feller [34] and the numerical method [35], respectively. These values are very close to the results obtained by Tsuzuki *et al.* [22] (-0.500 *kcal/mol*) and Zhao *et al.* [25] (-0.510 *kcal/mol*), while a little smaller (in absolute magnitudes) than those obtained by Jurecka *et al.* [21] (-0.530 *kcal/mol*) and Takatani *et al.* [24] (-0.541 *kcal/mol*). Notice that the estimated binding energies using the data calculated at the cc-pVXZ basis sets exhibit large deviation among the extrapolation methods. In particular, using the method of Feller with the cc-pVDZ data overestimates much of the energy. This latter observation is at variance with the results of Tsuzuki *et al.* [22] while is more in line with other criticisms on using Feller's method with the cc-pVDZ potential data to obtain the complete basis set limit binding energy [40]. For the other potential parameters, we used the numerical extrapolation based on the vanishing inverse of the number of basis function [35]. We note that the large vibration frequency, or equivalently the zero point energy correction to the binding energy, indicates that the anharmonicity of the dispersion potential well should be considered for comparison with spectroscopic measurements.

Using the above extrapolation methods, the CCSD(T)/CBS binding energies can be estimated. However, our ultimate objective is to obtain the full potential curve. Because we have obtained the potential curve at each basis set, we can use a direct extrapolation scheme where for each sampled C-C distance the potential data calculated at a series of basis sets are used to extrapolate to the CBS potential energy. We can then evaluate the effects of the potential data quality and the extrapolation methods on the CCSD(T)/CBS potential curves. In Fig. 1.1-2 and Fig. 1.1-3 we present the CBS potential curves obtained from the above four extrapolation methods [32-35], using the cc-pVXZ and aug-cc-pVXZ potential data, respectively. In Fig. 1.1-2 we see that using the cc-pVXZ data, the estimated CCSD(T)/CBS potential curves exhibit large deviation among the extrapolation methods. On the other hand, as shown in Fig. 3, using the aug-cc-pVXZ data, the CBS potential curves are all close to each other except for that obtained by Feller's method, which exhibits spurious long-range behavior. It is thus clear that the estimated potential curve depends sensitively on the quality of the calculated potential data which in turn depends on the basis sets used and the precision of the extrapolation methods. By all means one should check the consistency of using the extrapolation methods to obtain the CBS potential curve before any definite conclusion can be made. In the present case, the

CBS potential curves obtained by the methods of Helgaker *et al.* [32], Martin [33] are more self-consistent than those using the method of Feller [34], in particular if the potential data calculated at small basis sets were used to perform extrapolations. Our potential curve using the method of Helgaker *et al.* [32] is very close to that of Takatani *et al.* [24], although they did not compare the results using different extrapolation methods. Therefore, we believe that these data are reliable and serve as an operational standard for further experimental verifications and theoretical calibrations of other lower level *ab initio* or semi-empirical methods.



In the literature there appears a proposal to obtain the CCSD(T)/CBS potential energy by an approximate formula [39]

$$\begin{aligned}
 E_{CCSD(T)}^{CBS} &\approx E_{MP2}^{CBS} + \Delta E \\
 \Delta E &= E_{CCSD(T)}^{small-basis} - E_{MP2}^{small-basis}
 \end{aligned}
 \tag{1}$$

Underlying this formula is the assumption that ΔE is relatively basis set independent. We would like to check this assumption more quantitatively by examining the basis set dependence of ΔE . Using the CCSD(T) data in Table 1.1-1 and our previous MP2 data [23] we can estimate the CCSD(T)/CBS binding energy with Eq. (1) for each basis set we employed. In this way we can determine the

applicability of the above approximation more quantitatively. The results are shown in Table III, where our previous MP2 results are also presented as a reference. We see that using the aug-cc-pVDZ is good enough to obtain a binding energy within a 0.01 *kcal/mol* error with respect to the CBS energy. It is also interesting to study how far this idea can be applied to estimate the CBS values for other potential quantities; namely, we propose the formula

$$\begin{aligned}
 Q_{CCSD(T)}^{CBS} &\approx Q_{MP2}^{CBS} + \Delta Q \\
 \Delta Q &= Q_{CCSD(T)}^{small-basis} - Q_{MP2}^{small-basis}
 \end{aligned}
 \tag{2}$$

where $Q = R_0, R_m, \omega$, etc. To estimate the CBS values for the bond distance and harmonic frequency. The results are shown in Table III. We see that the estimation is surprisingly good. Using even the 6-31G* basis set we have obtained an estimation of the CBS bond distance within a 0.05 \AA precision and of the CBS frequency within a 15 cm^{-1} precision. Using the aug-cc-pVDZ data almost all the potential quantities can be obtained exactly. It remains to be seen whether this kind of good agreement can be extended to other systems.

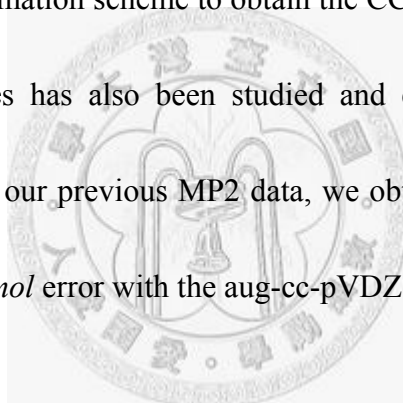
In passing we would like to comment on comparison of the calculated potential energy with the “empirical” or “semi-empirical” one. Actually the potential energy

itself is not a direct observable in experiments while it depends on auxiliary theoretical modeling. Experimental potentials are often isotropic and depend on thermodynamic conditions so the consistency with the potential retrieved from experiments does not guarantee the correctness and accuracy of the calculated potential. It is highly possible to obtain a potential curve using smaller basis sets (and/or without the BSSE correction) which incidentally is close to the “empirical” potential. However, this kind of agreement is largely accidental and should not be taken too seriously. Error cancelation can happen from many sources including correlation energy corrections, basis truncation errors, BSSE, and extrapolation approximations. This precaution should also be taken while using lower-level correlation methods or density functional theory using semi-local functionals to obtain the dispersion energies [42-43]. In case of lacking direct experimental verification, a benchmark study like the present one is ultimately required to unambiguously determine the *ab initio* intermolecular potential.

4. Conclusion

In this paper we have calculated intermolecular potentials of the methane dimer at the most stable D_{3d} conformation using the CCSD(T) method at complete basis set (CBS) limit. With Dunning’s correlation-consistent polarized valence basis sets, we

estimated the CCSD(T)/CBS potential curve using the extrapolation methods of Helgaker *et al.* [32], Martin [33], Feller [34] and a numerical method [35] on the potential data over the entire potential curve. The relative performance of these extrapolation methods has been carefully evaluated. Depending on the basis set quality, the CBS potential curves obtained by the methods of Helgaker *et al.* [32] and Martin [33] are more self-consistent than those using the method of Feller [34], in particular if the potential data calculated at small basis sets were used to perform extrapolations. An approximation scheme to obtain the CCSD(T)/CBS binding energy utilizing the MP2 energies has also been studied and extended to estimate other potential quantities. Using our previous MP2 data, we obtained an estimated binding energy within a 0.01 *kcal/mol* error with the aug-cc-pVDZ basis set.



5. Bibliography

- [1] J. D. Wright, *Molecular Crystals* (Cambridge University Press, Cambridge, 1987).
- [2] P. Hobza and R. Zahradnik, *Intermolecular Complexes : the role of van der Waals systems in physical chemistry and in the biodisciplines* (Elsevier, New York, 1988).
- [3] G. A. Jeffrey and W. Saenger, *Hydrogen Bonding in Biological Structures* (Springer-Verlag, Berlin, 1991).

- [4] S. D. Chao, J. D. Kress, and A. Redondo, *J. Chem. Phys.* **122**, 234912 (2005).
- [5] A. van der Avoird, P. E. S. Wormer, and R. Moszynski, *Chem. Rev.* **94**, 1931 (1994).
- [6] G. Chalasinski and M. M. Szczesniak, *Chem. Rev.* **100**, 4227 (2000).
- [7] A. K. Rappe and E. R. Bernstein, *J. Phys. Chem. A* **104**, 6117 (2000).
- [8] C. E. Dykstra, G. Frenking, K. S. Kim, and G. E. Scuseria (Eds.), *Theory and Applications of Computational Chemistry : The first forty years* (Elsevier, Amsterdam, 2005).
- [9] G. C. Groenenboom, E. M. Mas, R. Bukowski, K. Szalewicz, P. E. S. Wormer, and A. van der Avoird, *Phys. Rev. Lett.* **84**, 4072 (2000).
- [10] R. Bukowski, K. Szalewicz, G. C. Groenenboom, and A. van der Avoird, *Science*, **315**, 1249 (2007).
- [11] M. M. Szczesniak, G. Chalasinski, S. M. Cybulski, and S. Scheiner, *J. Chem. Phys.* **93**, 4243 (1990).
- [12] S. Tsuzuki and K. Tanabe, *J. Phys. Chem.* **95**, 2272 (1991).
- [13] J. J. Novoa, M.-H. Whangho, and J. M. Williams, *J. Chem. Phys.* **94**, 4835 (1991).
- [14] D. H. Gay, H. Dai, and D. R. Beck, *J. Chem. Phys.* **95**, 9106 (1991).
- [15] S. Tsuzuki, T. Uchimaru, K. Tanabe, and S. Kuwajima, *J. Phys. Chem.* **98**, 1830

(1994).

[16] J. Nagy, D. F. Weaver, and V. H. Smith, *Mol. Phys.* **85**, 1179 (1995).

[17] E. Frascini and A. J. Stone, *J. Comput. Chem.* **19**, 847 (1998).

[18] S. Tsuzuki, T. Uchimaru, and K. Tanabe, *Chem. Phys. Lett.* **287**, 202 (1998).

[19] R. L. Rowley and T. Pakkanen, *J. Chem. Phys.* **110**, 3368 (1999).

[20] S. Tsuzuki and H. P. Luthi, *J. Chem. Phys.* **114**, 3949 (2001).

[21] P. Jurecka, J. Sponer, J. Cerny, and P. Hobza, *Phys. Chem. Chem. Phys.* **8**, 1985

(2006).

[22] S. Tsuzuki, K. Honda and T. Uchimaru, M. Mikami, *J. Chem. Phys.* **124**, 114304

(2006).

[23] A. H.-T. Li and S. D. Chao, *J. Chem. Phys.* **125**, 094312 (2006).

[24] T. Takatani and C. D. Sherrill, *Phys. Chem. Chem. Phys.* **9**, 6106 (2007).

[25] Y. Zhao and D. G. Truhlar, *J. Chem. Theory Comput.* **1**, 415 (2005).

[26] J. A. Pople, M. Head-Gordon, and K. Raghavachari, *J. Chem. Phys.* **87**, 5968

(1987).

[27] R. J. Bartlett and M. Musial, *Rev. Mod. Phys.* **79**, 291 (2007).

[28] A. Szabo, N. S. Ostlund, *Modern Quantum Chemistry. Introduction to Advanced*

Electronic Structure Theory (Dover, New York, 1996).

[29] R. Krishnan, J. S. Binkley, R. Seeger and J. A. Pople, *J. Chem. Phys.* **72**, 650

(1980)

- [30] T. H. Dunning, Jr., *J. Chem. Phys.* **90**, 1007 (1989).
- [31] S. F. Boys and F. Bernardi, *Mol. Phys.* **19**, 553 (1970).
- [32] T. Helgaker, W. Klopper, H. Koch, J. Noga, *J. Chem. Phys.* **106**, 9639 (1997).
- [33] J. M. L. Martin, *Chem. Phys. Lett.* **259**, 669 (1996).
- [34] D. Feller, *J. Chem. Phys.* **96**, 6104 (1992).
- [35] W. H. Press, S. A. Teukolsky, W. T. Vetterling, and B. P. flannery, *Numerical Recipe in C* (Cambridge University Press, Cambridge, 1996).
- [36] Gaussian 03, Revision D.01, Frisch, M. J. *et al.*; Gaussian, Inc., Wallingford CT, 2004.
- [37] D. C. Rapaport, *The Art of Molecular Dynamics Simulation* (Cambridge University Press, New York, 1995).
- [38] S. D. Chao and A. H.-T. Li, *J. Phys. Chem. A* **111**, 9586 (2007).
- [39] C. C. Pai, A. H.-T. Li and S. D. Chao, *J. Phys. Chem. A* **111**, 11922 (2007).
- [40] A. Halkier, W. Klopper, T. Helgaker, P. Jorgensen, P. R. Taylor, *J. Chem. Phys.* **111**, 9157 (1999).
- [41] P. Hobza and J. Sponer, *J. Am. Chem. Soc.* **124**, 11802 (2002).
- [42] A. H.-T. Li and S. D. Chao, *Phys. Rev. A* **73**, 016701 (2006).
- [43] R. J. Meier, *Chem. Phys. Lett.* **401**, 594 (2005).

Basis set	Number of basis functions	DISK (GB)	R_0 (Å)	R_m (Å)	E_b (kcal/mol)	ω (cm ⁻¹)
cc-pVDZ	68	0.16	3.62	4.06	-0.146	216.52
6-311G**	84	0.39	3.59	4.03	-0.167	232.08
6-311++G**	100	0.79	3.59	4.02	-0.180	228.87
aug-cc-pVDZ	118	1.49	3.37	3.75	-0.418	314.69
cc-pVTZ	172	6.91	3.39	3.81	-0.319	310.23
6-311++G(2df,2pd)	188	9.92	3.38	3.80	-0.335	303.47
6-311++G(3df,3pd)	222	19.45	3.35	3.73	-0.441	300.74
aug-cc-pVTZ	276	46.90	3.34	3.67	-0.491	362.35
cc-pVQZ	350	149.41	3.34	3.70	-0.433	355.73
aug-cc-pVQZ	528	781.98	3.31	3.65	-0.504	361.23
Complete basis set limit^a			3.27	3.63	-0.510	349.08

Table 1.1-1

^a Basis set limit values obtained by the numerical method [40] with the aug-cc-pVXZ (X=D, T, Q) potential data, shown in boldface.

Table 1.1-1. The basis set dependence of important potential parameters of the BSSE corrected CCSD(T) intermolecular potentials. R_0 is the distance at which the potential is zero and is obtained from a two point interpolation of the calculated data. The bond length R_m , the binding energy E_b and the intermolecular vibration frequency ω are obtained from an analysis using a quadratic polynomial function form to model the equilibrium potential well. The disk space requirements (DISK) of the CCSD(T) calculation were recorded on a single node 1-processor IBM 1350 PC cluster with distributed memory.

Extrapolation methods	DT ^a	TQ ^b	DTQ ^c	aDT ^d	aTQ ^e	aDTQ ^f
Helgaker <i>et al.</i>	-0.392(-0.387)	-0.516(-0.480)	¥NA	-0.522(-0.477)	-0.509(-0.472)	¥NA
Martin	-0.380(-0.376)	-0.499(-0.465)	¥NA	-0.517(-0.473)	-0.512(-0.470)	¥NA
Feller	¥NA	¥NA	-0.654(-0.532)	¥NA	¥NA	-0.507(-0.467)
Numerical	¥NA	¥NA	-0.570(-0.520)	¥NA	¥NA	-0.510(-0.470)

Table 1.1-2

^aBasis set limit estimation with the cc-pVXZ(X=D and T).

^bBasis set limit estimation with the cc-pVXZ(X=T and Q).

^cBasis set limit estimation with the cc-pVXZ(X=D, T, and Q).

^dBasis set limit estimation with the aug-cc-pVXZ(X=D and T).

^eBasis set limit estimation with the aug-cc-pVXZ(X=T and Q).

^fBasis set limit estimation with the aug-cc-pVXZ(X=D, T, and Q).

¥ Not available.

Table 1.1-2. Comparison the estimated CCSD(T) and MP2 (numbers in parenthesis) binding energies at the complete basis set

limit using the four extrapolation methods. The unit is *kcal/mol*.

Basis set	CCSD(T) / MP2 ^a / CCSD(T)/CBS ^b			
	R ₀ (Å)	R _m (Å)	E _b (kcal/mol)	ω (cm ⁻¹)
6-311G**	3.59/(3.59)/3.25	4.03/(4.02)/3.67	-0.167/(-0.165)/-0.472	232.08/(228.01)/366.87
6-311++G**	3.59/(3.57)/3.27	4.02/(4.01)/3.67	-0.180/(-0.176)/-0.474	228.87/(225.42)/366.25
aug-cc-pVDZ	3.37/(3.35)/3.27	3.75/(3.78)/3.63	-0.418/(-0.395)/-0.493	314.69/(323.88)/353.61
cc-pVTZ	3.39/(3.37)/3.27	3.81/(3.80)/3.67	-0.319/(-0.317)/-0.472	310.23/(304.65)/368.38
6-311++G(2df,2pd)	3.38/(3.36)/3.27	3.80/(3.78)/3.68	-0.335/(-0.331)/-0.474	303.47/(297.27)/369.00
6-311++G(3df,3pd)	3.35/(3.30)/3.30	3.73/(3.73)/3.66	-0.441/(-0.415)/-0.496	300.74/(383.20)/280.34
aug-cc-pVTZ	3.34/(3.27)/3.32	3.67/(3.70)/3.63	-0.491/(-0.453)/-0.508	362.35/(367.15)/358.00
cc-pVQZ	3.34/(3.31)/3.28	3.70/(3.71)/3.65	-0.433/(-0.411)/-0.492	355.73/(360.46)/358.07
aug-cc-pVQZ	3.31/(3.26)/3.30	3.65/(3.68)/3.63	-0.504/(-0.464)/-0.510	361.23/(356.38)/367.65
Complete basis set limit	3.27/(3.25)/3.27	3.63/(3.66)/3.63	-0.510/(-0.470)/-0.510	349.08/(362.80)/349.08

Table 1.1-3

^a The MP2 binding energy from Ref. [26].

^b The estimated CCSD(T) basis set limit binding energy using the Eq.(1).

^c A missing factor $\sqrt{2}$ to account for the reduced mass in calculating the frequency from our previous MP2 calculations [26] is included.

Table 1.1-3. Basis set dependence of the estimated potential parameters of the CCSD(T)/CBS potential using Eqs. (1) and (2).

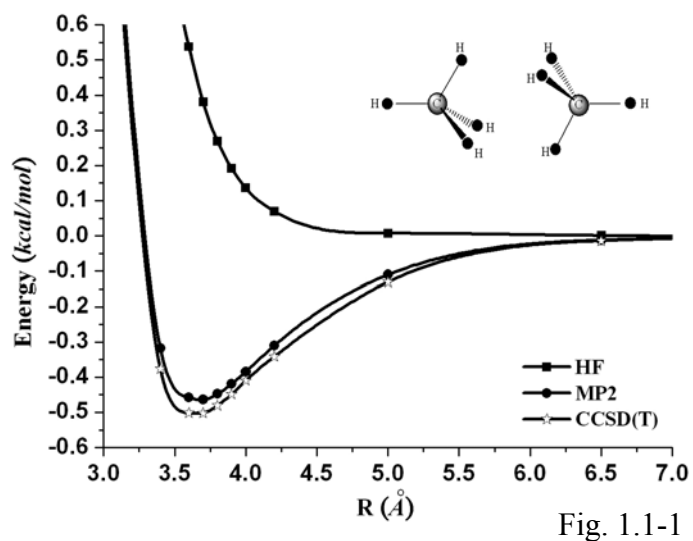


FIG. 1.1-1. The BSSE corrected HF, MP2, and CCSD(T) interaction potentials of the methane dimer using the aug-cc-pVQZ basis set.

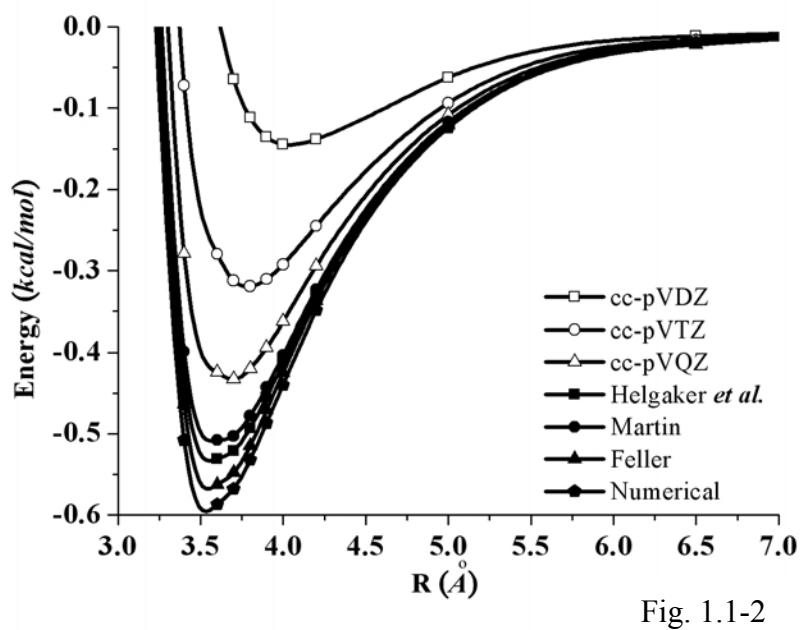


FIG. 1.1-2. The estimated CCSD(T)/CBS potential curves using the direct extrapolation scheme with the four extrapolation methods on the cc-pVXZ potential data.

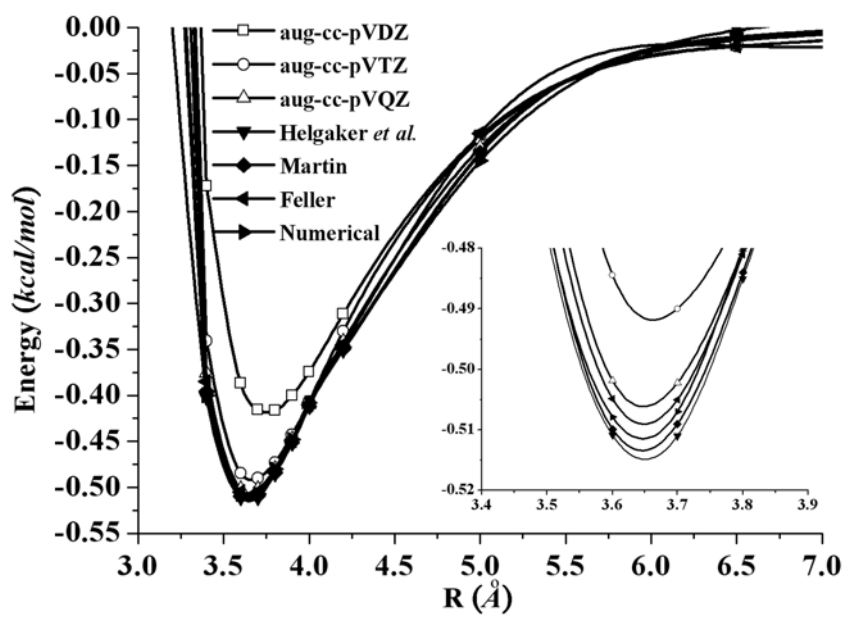


Fig. 1.1-3

FIG. 1.1-3. The estimated CCSD(T)/CBS potential curves using the direct extrapolation scheme with the four extrapolation methods on the aug-cc-pVXZ potential data.

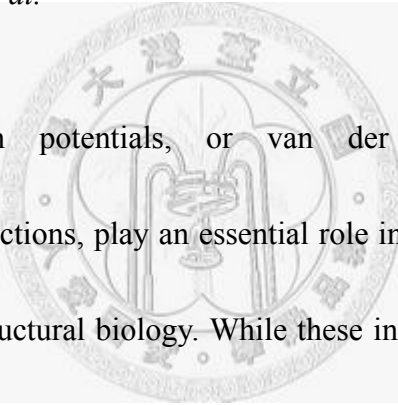
1.2 Intermolecular Potentials of the Methane Dimer Calculated with Møller-Plesset Perturbation Theory and Density Functional Theory and Comment on "Intermolecular Interaction Potential of the Methane Dimer From the Local Density Approximation"

1. Introduction

To verify the recently calculated intermolecular interaction potentials of the methane dimer within the density functional theory using the (Perdew) local density approximation (LDA) [Chen *et al.*, *Phys. Rev. A* 69, 034701 (2004)], we have performed a parallel series of calculations using the LDA/6-311++G (3df, 3pd) level of theory with selected exchange functionals (B, G96, MPW, O, PBE, PW91, S, and XA). None of the above calculated intermolecular interaction potentials from the local density approximation reproduce the results reported in the commented paper. In addition, we point out the inappropriateness of using the Lennard-Jones function to model the long-range parts of the calculated intermolecular interaction potentials, as suggested positively by Chen *et al.*

Chen *et al.* [1] recently reported the intermolecular interaction potentials of the methane dimer (CH₄)₂ within the standard density functional theory (DFT) scheme [2] using the (Perdew) local density approximation (LDA) [3], the pseudopotential [4,5], and the plane-wave expansion [6]. Their results agreed surprisingly well with those

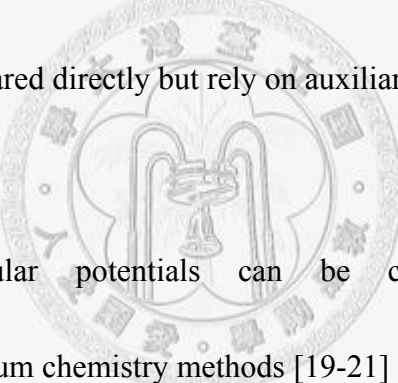
obtained by the correlation-corrected Møller-Plesset (MP2, MP3) [7] and coupled cluster (CCSD(T)) [8] methods using a large basis set [9]. Because it has been known for some time that the usual DFT based approaches, using either the LDA or the generalized gradient approximation (GGA), can not calculate the intermolecular interaction potentials of molecular dimers to such a high level of accuracy [10-12], it is important to perform a parallel series of calculations using the available implementations of commonly used exchange-correlation functionals to verify the proposed results by Chen *et al.*



Intermolecular interaction potentials, or van der Waals interactions, or non-covalent-bonded interactions, play an essential role in condensed matter physics, materials chemistry and structural biology. While these interactions are normally one or two orders of magnitude weaker than typical covalent bonds, they are crucial in determining the thermodynamic properties of molecular liquids and solids [13], the energy transfers among molecular complexes [14], and the conformational tertiary structures of macromolecules such as protein and DNA [15]. Unlike intramolecular covalent bonds, intermolecular bonds do not originate from sharing of electrons but rather arise from simultaneous electron correlation of the separated subsystems [16]. Different from stiff covalent bonds, they are relatively soft and non-rigid. Early studies of intermolecular interactions can be traced back to one century ago [17],

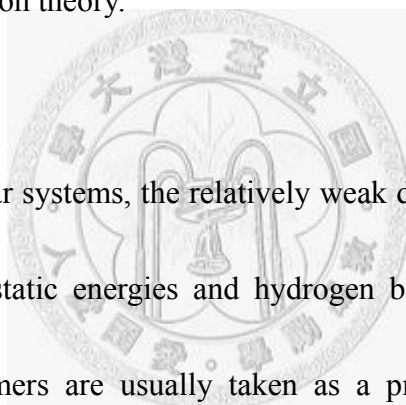
while measurements of these interactions are still challenging in the present time [18].

The main difficulty in determining intermolecular interactions experimentally resides at limited samplings of the potential energy surface. For example, experiments using the X-ray crystallography or the laser spectroscopy mainly explore the equilibrium regions of the potential, while thermodynamic measurements in the gas or liquid phase often yield isotropic potential data without the desired stereo-chemical responses. In addition, the measured potentials sensitively depend on the thermodynamic conditions. Usually two measurements carried out in different conditions cannot be compared directly but rely on auxiliary theoretical modeling.



Alternatively intermolecular potentials can be calculated in terms of correlation-corrected quantum chemistry methods [19-21] or density functional theory (DFT) [22-23]. These quantum mechanics based potentials are requested by *ab initio* molecular dynamics simulations [24] and by classical molecular simulations using force field constructions [25]. Among the components of an intermolecular interaction, the London dispersion force is the most difficult to calculate. The reason is that dispersion interactions arise from the non-local “dynamic” correlations [26]. This non-locality demands full exploration of the time-dependent perspective of quantum mechanics. Often an electron correlation-corrected method and a large basis set are

required to obtain accurate dispersion forces [27]. Also a technical note is in order. Most present implementations of quantum chemistry programs utilize Gaussian type functions to fasten the calculations of Coulomb repulsion integrals. Because Gaussian type functions are local functions, a large basis set is indispensable to perform a correlation energy calculation. Moreover, these functions do not have the correct asymptotic behavior as the intermolecular separation becomes large. Therefore, the basis set limit of the calculated potential must be estimated so as to be consistent with the conventional perturbation theory.

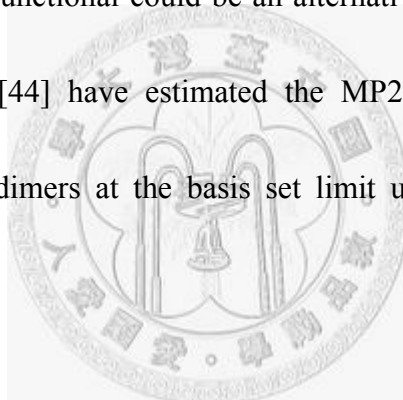


For general polar molecular systems, the relatively weak dispersion energy is masked by the competing electrostatic energies and hydrogen bond interactions. Nonpolar atomic and molecular dimers are usually taken as a prototype case to study the dispersion energy. Many previous studies on dispersion forces have focused on atomic inert gas dimers and several important conclusions have been drawn from the calculations [28]. There are, however, comparatively fewer detailed studies on whether similar conclusions can be applied to molecular dimers. Because of the extra degrees of freedom and the stereo-chemical responses, the conclusions about atomic dimers may need to be extended or modified in dealing with molecular dimers. Methane is a non-polar molecule with vanishing dipole and quadrupole moments and

the first nonvanishing electrostatic interaction is the octopole-octopole interaction. The higher order electrostatic interactions are rather weak and decay fast at large intermolecular separation. The dominant long-range attraction for the methane dimer is thus due to the London dispersion force. On the other hand, the strong repulsive force almost comes from the exchange-repulsion interaction due to the overlapping of electron clouds. Because the exchange-repulsion interactions have been incorporated in the Hartree-Fock (HF) self-consistent theory, post-HF methods such as the Møller-Plesset (MP) perturbation theory and the coupled cluster (CC) theory are often used to calculate the correlation effect. Contrasting both sets of calculation helps to delineate the relative importance of the dispersion energy in the overall intermolecular interaction. In addition, the interaction potentials of alkanes, among them methane being the smallest model, is very crucial in determining the packing morphology in solids and liquids and in lipid bilayers [29-31]. The potentials are also requested for mesoscale simulations for macromolecules [32] because many polymers contain alkyl groups as their backbone units or side chains. Therefore, the calculation of intermolecular interactions of the methane dimer is a “must” and serves as a prototype example to start to investigate the various factors affecting the calculations of these interactions.

There have been many quantum chemistry studies of intermolecular potentials of the methane dimer using correlation-corrected methods [33-44]. Szczesniak *et al.* [33] have used the MP2 method with the Sadlej basis to calculate the interaction energies for the six conformers of the methane dimer. They found that the minimum-energy conformation is the D_{3d} conformer and the dimer structure is determined by minimizing the steric repulsion between hydrogen atoms belonging to opposite subsystems. Tsuzuki *et al.* [36] have studied the basis set effects using basis sets from 6-31G* to 6-311++G (2d,2p) to calculate the interaction energies for two conformers of the methane dimer (but none of them is the D_{3d} conformer). They observed little basis set effect on the HF calculations as long as one uses a basis set larger than the 6-31G* one. The basis set effect is significant for the MP2 interaction energies and the basis set superposition error (BSSE). The dispersion energy can be seriously underestimated if a smaller (than 6-31G*) basis set has been used. They found that the BSSE uncorrected interaction energies do not systematically converge to a destined value, in contrast to those with BSSE corrections. Tsuzuki *et al.* [39, 43] studied twelve conformers and verified that the D_{3d} conformer corresponds to the minimum-energy geometry. They observed that a large basis set with multiple polarization functions is necessary to evaluate the dispersion energy accurately. They found that augmentation of the diffuse d and p functions to the 6-311G** basis set

more efficiently yields the dispersion energy. Tsuzuki *et al.* [40, 43] explored the effect of the choice of the correlation-correction methods on the calculations of intermolecular interactions. They demonstrated that the MP2 and MP3 energies are not too far away from the higher level MP4 (SDTQ) calculations, while the latter is not less expensive than the CCSD(T) calculation. They tested the DFT using the BLYP, BPW91 and B3LYP functionals but found unbound interactions while the PW91 functional underestimates only 8% of the potential well depth. They suggest that DFT with the PW91 functional could be an alternative to the *ab initio* methods. Recently, Tsuzuki *et al.* [44] have estimated the MP2 and CCSD(T) interaction energies of the n-alkane dimers at the basis set limit using Dunning's correlation consistent basis sets.



Many previous studies mainly focused on the equilibrium region of the potentials with relatively few discussions of the full potential curves. Nevertheless, to construct a reliable force field model for molecular simulations, the full intermolecular potential surfaces are required. In this paper we perform a comprehensive up-to-date study on interaction potentials of the prototype methane dimer in terms of the HF, MP2 and DFT methods to gain more understanding of this system. With current computational powers, a detailed editing of the potential data base can be obtained for small size

molecular clusters. It is thus so important to obtain general features of the calculations that we can follow to explore large scale molecular simulations via similar procedures. The purpose of this paper is twofold. First, we use the state-of-the-art methodology to obtain accurate potential energies for the methane dimer. We would like to verify or modify the previous conclusions about the basis set effects and the effect of including the BSSE on the calculation details of the intermolecular interactions. The basis set effects on repulsion exponents, equilibrium bond lengths, binding energies, and asymptotic coefficients of the calculated intermolecular potentials are thoroughly studied. This is achieved using basis sets from STO-3G [45] to aug-cc-pVQZ [46]. The full potential curves are presented in order to see the overall scope of the potential. In particular, both the BSSE corrected and uncorrected results are presented to emphasize the importance of these corrections. Second, this paper attempts to re-assess the utilities of using the available implementation of the density functional theory in determining the intermolecular interactions. From the studies of atomic dimers, it has been found that conventional DFT based on the local density approximation (LDA) and generalized gradient approximation (GGA) cannot calculate the intermolecular interactions to a satisfying level of accuracy [47]. To address the title issue, we carry out a systematic DFT study of the equilibrium binding energies and bond lengths of the methane dimer using 90 functionals. Methane is a

non-polar molecule with vanishing dipole and quadrupole moments. The first nonvanishing electrostatic interaction is the octopole-octopole interaction and all higher order interactions are weak and decay fast at large intermolecular separation. The dominant attraction for the methane dimer is thus due to the van der Waals force. Therefore, the calculation of van der Waals interactions of the methane dimer serves as a prototype study to investigate the various factors affecting the calculations of these interactions.

2. Methods and Calculations

All the calculations were performed using the Gaussian03 package suite [48] and followed a theoretical procedure similar to that employed by Tsuzuki *et al.* [9] Fig. 1.1-1 shows the calculated interaction potentials of $(\text{CH}_4)_2$ with a set of selected exchange functionals (B, G96, MPW, O, PBE, PW91, S, and XA) [49], together with the Perdew correlation functional dubbed as PL (Perdew local) [3]. Although we have used a pretty large basis set, 6-311++G (3df, 3pd), which has been shown to lead to convergent results for $(\text{CH}_4)_2$ at a chemical accuracy [50], none of the calculated intermolecular interaction potentials reproduce the results of Chen *et al.* A puzzling point in the commented paper is that there are two sets of data, one reported in their Fig. 1.2-1 and the other as numerical data in the text [1], while the latter is twice the former. Because there was no further clarification on this apparent inconsistency in

the commented paper, we present both data for comparison in Fig. 1.2-1 (open symbol-lines). Restated, neither of them can be reproduced in the present calculations.

In the case of methane dimers, a large part of the exchange-repulsion interactions can be calculated by the HF method. The calculation of electron correlation energies depends on the level of the correlation-corrected method, the size of the basis set, and the correction of the BSSE. The state-of-the-art choice of the correlation-corrected method is either the Møller-Plesset (MP_x, x=2, 3, 4) perturbation method [51] or the coupled cluster method with iterative single and double substitutions and with noniterative triple excitations [CCSD(T)] method [52]. It has been found that the MP2 results for the methane dimer are not too much different from those calculated by the much more expensive CCSD(T) as long as a large basis set has been used [43]. To study the basis set effects, we have employed comprehensive basis sets from the Slater-type orbitals fitted with Gaussian functions (STO-nG, n=3~6) [45], Pople's medium size basis sets [up to 6-311++G (3df, 3pd)] [53] to Dunning's correlation consistent basis sets (aug-cc-pVXZ, X=D, T, Q) [46]. The basis set superposition error (BSSE) was corrected by the counterpoise (CP) method of Boys and Bernardi [54]. The MP2 interaction potentials at the basis set limit have been estimated using the methods of Helgaker *et al.* [55] and Feller [56] and a numerical extrapolation scheme based on the Lagrangian formula [57].

All the HF, MP2 and DFT calculations are performed using the Gaussian 03 program package [58] on a single node 2-processor AMD 250 PC cluster with distributed memory. The equilibrium geometry of a single methane molecule was first optimized at the MP2/6-31G* level of theory. To obtain the most stable intermolecular geometry, the methane dimer has been modeled by first fixing the carbon-carbon (C-C) distance while letting the two monomers to rotate freely. By approaching the monomers from the far side with several initial choices of mutual orientation, we found the minimum-energy conformation corresponds to the D_{3d} symmetry conformer. This optimized conformer has been reached through the interplay of the steric stabilization of repulsive hydrogens in opposite monomers [33]. Subsequently the C-C distance was sampled in step 0.1 \AA for a quite large range of intermolecular separation (normally $3\sim 9 \text{ \AA}$). During the scan we allow the individual methane molecule to be fully relaxed. This means that we do not fix the monomer geometry and the methane molecule is not assumed to be rigid. Although it is not expected to see much deviation from the rigid molecule approximation, in the real condensed phase environment, stretching, bending and torsional relaxations could be important for many subtle thermodynamic properties. The inclusion of intramolecular relaxation is especially relevant to the construction of force fields for use in molecular dynamics simulations

where flexible models often work better than rigid models [59].

The density functionals used in the present work include the 90 combinations chosen among 9 exchange (B88 [60], OPTX [61], MPW [62], PBE [63], PW91 [64], TPSS [65], Slater [66], HCTH [67], XAlpha [68]) and 10 correlation (TPSS [65], PBE [63], PW91 [64], P86 [69], HCTH [67], VWN5 [70], PL [71], VWN [70], LYP [72]) functionals. We also consider several hybrid functionals of B971 [73], BB98 [74], BHandH [75], O3LYP [76], B3PW91 [77], PBE1PBE [63], MPW1PW91 [78]. The chosen functionals are selective representations of the most commonly used density functionals for van der Waals interactions in current literature. Recent studies showed that the PW91PW91 functional could yield reasonable binding energy of the methane dimer interaction [79] but the relative performance of the exchange and correlation functionals has not been systematically studied.

3. Results and Discussions

(a) Chen *et al.* also concluded that through a nonlinear fitting their calculated intermolecular potentials can be well described by the Lennard-Jones (L-J) potential function

$$V(R) = \frac{a}{R^{12}} - \frac{b}{R^6} \quad (1)$$

Because this conclusion is contrary to what has been believed that results based on the

LDA can not be used to model the long-range dispersion interaction well [16-18], the determined accuracy from their calculations remains to be verified. For the sake of comparison, in Fig. 1.2-2 we present the calculated raw data and the claimed fitting curve by Chen *et al.* using their fitting values of a and b [1]. To our great surprise, the fitting curve is anything but like the calculated raw data. To clarify this point, we perform a nonlinear fitting of their calculated data to the L-J function and obtain $a=2.09 \times 10^6 \text{ \AA}^{12} \text{ kcal/mol}$, $b=1.84 \times 10^3 \text{ \AA}^6 \text{ kcal/mol}$, and the fitting is shown in Fig.

1.1-2 As expected, although the L-J function can model the strong repulsive part quite well, there is a significant discrepancy from the calculated data for the long-range interaction part ($R > 4 \text{ \AA}$). The calculated data using the LDA often decays faster than $-1/R^6$ for the long-range part, due to the local nature of the functionals used. To demonstrate this point, we perform another nonlinear fitting using the exponential function

$$V(R) = Ae^{-\alpha R} - Be^{-\beta R} \quad (2)$$

and obtain $A=1.14 \times 10^6 \text{ kcal/mol}$, $\alpha=4.23 \text{ \AA}^{-1}$, $B=3.33 \times 10^2 \text{ kcal/mol}$, $\beta=1.71 \text{ \AA}^{-1}$. As can be seen in Fig. 1.2-2, the long-range part of the calculated data is well modeled by the fast-decaying exponential function, but not the L-J function.

(b) The intermolecular interaction potentials of the D_{3d} conformer of the methane

dimer have been calculated with the HF, the MP2 and the DFT methods. We present the respective results along with discussions and make comparisons among the results.

A. Hartree-Fock self-consistent field calculations

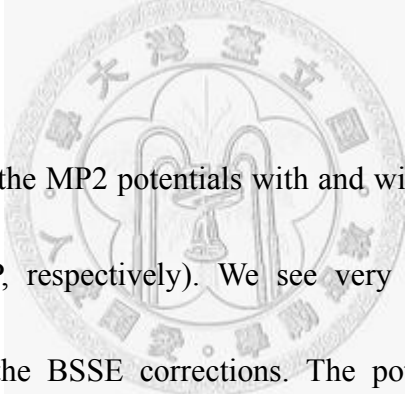
The BSSE corrected HF interaction potentials of the methane dimer using several basis sets are shown in Fig. 1.2-3. All the HF calculations yield purely repulsive potentials without minima for all the basis sets used. This can be attributed to the rather weak electrostatic interaction for the methane dimer. In the short range, the strong exchange-repulsion interaction dominates with little alternation from electrostatic and induction attractions. The HF potential is insensitive to the basis size as long as the 6-31G** basis set has been used. We can model the HF potential using the repulsive Buckingham function [80]

$$V_{HF}(R) = Ae^{-\alpha R} \quad (1)$$

where R is the C-C distance, A and α (the repulsion exponent) are the fitting parameters. The dependence of the repulsion exponent on the basis size is shown in Table 1.2-1. It is seen that the repulsion exponent converges quickly after the 6-31G** basis set being used.

B. MP2 calculations

Unlike the HF potentials, the MP2 potentials shown in Fig. 1.2-4 display clear minima and long range attractive potential tails. Because the contributions from the octopole-octopole interactions are small, the dispersion energy is mainly responsible for the attractions. Sharp differences between the HF calculations and the MP2 calculations indicate the importance of including the correlation corrections in the wave function calculations. The HF method in principle does not include the correlation effect so the attraction forces are due exclusively to the correlation effect.



In Fig. 1.2-4, we compare the MP2 potentials with and without the BSSE corrections (denoted as CP and NCP, respectively). We see very strong dependence of the interaction potentials on the BSSE corrections. The potentials without the BSSE corrections fluctuate with increasing basis size and do not systematically converge to the destined curve at the basis set limit. On the contrary, the BSSE corrected potentials systematically approach to the destined curve with increasing basis size. Therefore, it is important to consider the BSSE correction in calculating the intermolecular interactions, in particular for small basis sets.

As shown in Table 1.2-1, the basis set effect on the BSSE corrected interaction

potentials is significant. The STO-3G basis set yields very small binding energy. The interaction energy becomes more accurate as one adds polarization functions and augments diffuse functions in the Pople's basis sets. Small cc-pVDZ and cc-pVTZ basis sets lead to underestimated binding energies and it requires cc-pVQZ to saturate the result. Augmentation of the diffuse functions has significant effect on optimizing the binding energy. The cc-pVTZ basis set underestimates the energy by 30%, while the aug-cc-pVTZ basis set underestimates only 5% of the binding energy. Some subtle basis set features can also be observed. For small basis sets, adding polarization functions to the basis set does not significantly change the potential. On the other hand, augmentation of the diffuse functions has pretty significant effect. For example, the aug-cc-pVDZ energy is very close to the high level 6-311++G (3df, 3pd) and the cc-pVQZ results. These paraphrase Tsuzuki *et al.* [43] to construct a diffuse-function-augmented medium size 6-311G** basis set in their calculations. Together with diffuse functions, adding more polarization functions also improve the accuracy of the calculated potential. For example, the 6-311++G** underestimates the binding energy by 60%, while the 6-311++G (3df, 3pd) yields a binding energy by 12% lower than the MP2 energy at the basis set limit. It is understood that dispersion interactions arise from the nonlocal electron correlation effect so adding functions of extensive range help to optimize the potentials.

With the wide span of the basis sets used, the basis set dependence of important potential parameters can now be fully studied. In Table 1.2-1 we present the BSSE corrected data for the equilibrium bond length, the binding energy, and the asymptotic behavior. R_0 is the distance at which the potential is zero and can be obtained from a two point interpolation of the calculated data. The bond length R_m , the binding energy E_b and the intermolecular vibration frequency can be obtained through a harmonic modeling of the three lowest potential data near the equilibrium regions. C_6 and C_8 are the dispersion coefficients and can be obtained through a nonlinear fitting of the long-range potential data. With increasing basis size, the equilibrium bond length converges at the 6-311++G (2d,2p) basis set to a 0.1 Å accuracy, while a pretty large basis set (aug-cc-pVTZ) is required to converge the binding energy at a chemical accuracy (~ 0.01 kcal/mol). On the other hand, up to the largest basis set used, the asymptotic behavior has not yet converged to the destined C_6 value from the calculated monomer polarizability (~ 1784 kcal/mol Å⁶) [81-83]. Inclusion of the C_8 term is important if shorter range data were used for the modeling. As shown in Fig. 1.2-5, the long-range curve can be reproduced better when including the C_8 term. The slow convergence could be an indication of the inefficacy of using the MP2 method with Gaussian functions to calculate long-range interactions. Because Gaussian type

functions are local functions, a large basis set is required to obtain converged correlation energy calculations. Therefore, the basis set limit of the calculated potential must be estimated so as to be consistent with the conventional perturbation theory. Together with the nonlinear scaling of the computational cost with respect to the basis size, this is actually the main practical reason for the difficulty of obtaining dispersion interactions through *ab initio* molecular orbital methods.

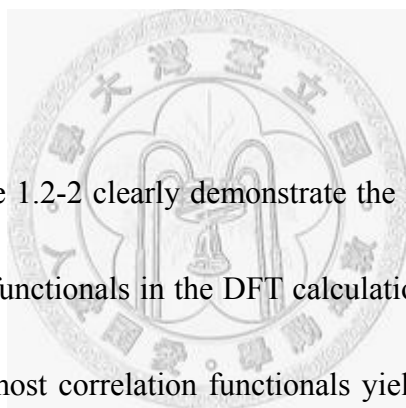
The strong basis set dependence and the slow convergence on the dispersion coefficients call for an estimation of the important potential features at the basis set limit in a calculated potential. Basis set limit of the binding energy can be approached using Dunning's basis sets with an extrapolation scheme. We consider two analytical schemes [55, 56] and a numerical scheme [57] while the results are similar. The binding energies obtained at the basis set limits (using Dunning's basis sets, aug-cc-pVXZ, X=D, T, Q) are 0.472, 0.467, and 0.470 *kcal/mol* using the methods of Helgaker *et al.* [55], Feller [56] and the numerical method [57], respectively. These values are very close to the results obtained by Tsuzuki *et al.* [44]. For the other potential parameters, we used the numerical extrapolation based on the vanishing inverse of the number of basis function [57]. These results are shown in Table 1.2-1 for comparison.

C. Density functional theory

The density functionals used in the present work include two sets. The first set fixes the exchange functional as the PW91 and changes the correlation functionals. The correlation functionals include PL [84], VWN5 [85], VWN [85], TPSS [86], PBE [87], PW91 [88], VP86 [89], P86 [89], V5LYP [90], LYP [90], HCTH93 and HCTH407 [91-93]. The second set fixes the correlation functional as the PW91 and changes the exchange functionals. The exchange functionals include HCTH93, HCTH147, HCTH407 [91-93], MPW [94], MPW1 [94], OPTX or O [95], B88 or B [96], PBE [87], Slater or S [97], and X or XA [97]. The choice of these combinations is motivated by a recent suggestion that the PW91PW91 functional yield good binding energy of the methane dimer interaction [40]. However, the role of the PW91 as an exchange versus a correlation functional has not been systematically studied. Moreover, it is not clear if the functional is reliable for use in determining other potential parameters.

Fig. 1.2-6 presents the calculated intermolecular potential curves using the PW91 as the exchange or the correlation functional. We see that the DFT calculations generally generate a diverse range of potential curves from purely unbound (BPW91) to

strongly bound (XAPW91). In Table 1.2-2 we compare the bond lengths and the binding energies calculated using the several exchange-correlation functionals with the MP2 results. We see that the PW91PW91 combination produces reasonable potential well depth while the bond length is estimated too long. The PW91VP86 functional yields good bond length and captures the attraction effect quite well, although it overestimates the binding energy by 20%. It is promising that available functionals do capture partly the correlation effects which are essential in calculating the dispersion forces.



The results shown in Table 1.2-2 clearly demonstrate the relative roles played by the exchange and correlation functionals in the DFT calculations. By fixing the PW91 as the exchange functional, most correlation functionals yield bound potentials and the binding energies are around the MP2 result (except the HCTH correlation functionals, which yield seriously overbound potentials). On the other hand, by fixing the PW91 as the correlation functional, the varying exchange functionals either overestimate (S, XA) or underestimate (HCTH, MPW, O, B, PBE) the binding energy. Previous studies on van der Waals systems [98, 99] have shown that the exchange functional plays an essential role in determining the dispersion energy while the correlation part of a density functional does not significantly affect the DFT calculations. Our results are

basically consistent with these observations, although we see appreciable effects due to the choice of the correlation functional. The performance of varying exchange functionals for a fixed correlation functional can be understood in terms of the behavior of the GGA enhancement factor $F(s)$ of the exchange functional at the large gradient-to-density ratio, denoted as s , region [100]. Following Lacks and Gordon [101], we plot the $F(s)$ versus s curve in Fig. 1.2-7. We see in Fig. 1.2-7 that the order of the magnitude of $F(s)$ at large s is B88>HCTH>OPTX>PBE>MPW>PW91. This order is essentially the order of the binding energies calculated by the corresponding functionals in Table 1.2-2. This correlation has been found in previous studies on van der Waals systems [98, 99] and serves as a useful tool in analyzing the DFT calculations. Another criterion for $F(s)$ to be satisfied is the Lieb-Oxford condition [102] which requires that $F(s) \leq 2.273$. From Fig. 1.2-7 we see that the PBE, MPW and PW91 exchange functionals obey this condition. The above analyses, together with Perdew's suggestion that the PW91 exchange functional should be used with the corresponding PW91 correlation functional [103], explain why the PW91PW91 functional outperforms other combinations of the exchange and correlation functionals in the calculations of dispersion interactions.

(c) In Table 1.2-3 we show the bond lengths using the 90 exchange-correlation

functions, displayed as the row and the column items, respectively. Roughly the bond lengths descend across the row and down the column. Compared with the MP2 result (3.73 \AA), we find the PW91VP86 function yield a value (3.73 \AA) same as the MP2 result. Table 1.2-4 presents the calculated binding energies using the 90 exchange-correlation functionals. These data are organized in a particular order as shown in Table 1.2-4. In this order, the (negative) DFT potentials descend across the row and down the column. The results clearly demonstrate the relative performance of the exchange and the correlation functionals in the DFT calculations. By fixing the PW91 as the exchange functional, for example, all correlation functionals yield bound potentials. On the other hand, by fixing the PW91 as the correlation functional, the varying exchange functionals much underestimate or overestimate the binding energy except the PW91 exchange functional. One of the combinations, PW91PW91, yields a binding energy (-0.418 kcal/mol) close to the MP2 result (-0.415 kcal/mol). Previous studies on van der Waals systems [51] have shown that the exchange functional plays an essential role in determining the binding energy while the correlation part of a density functional does not significantly affect the DFT calculations. Our results are consistent with the former observation, while we see appreciable effects due to the choice of the correlation functional. To further analyze the results, we examine the large s behavior of the GGA enhancement factors at the asymptotically low density

region.

The performance of varying the GGA exchange functionals for a fixed correlation functional can be understood in terms of the behavior of the GGA enhancement factor $F_X(s)$ of the exchange functional for the large reduced density gradient region. The exchange enhancement factor is defined by

$$F_X(s) = \frac{\epsilon_X^{GGA}}{\epsilon_X^{LDA}} \quad (1)$$

where ϵ_X^{GGA} and ϵ_X^{LDA} are the exchange potentials for the GGA and the LDA energy functionals, respectively. We plot the $F_X(s)$ versus s curve in Fig. 1.2-7. We see in Fig. 1.2-7 that the order of the magnitude of $F_X(s)$ at large s is B88 > OPTX > MPW > PBE > PW91. This order is essentially the order of the binding energies calculated by the corresponding functionals down the column in Table 1.2-4. This connection has been found in previous studies on van der Waals systems and serves as a useful tool in analyzing the DFT calculations. In the present work, we verify and extend the utilities of previous conclusions. Notice that the HCTH functional is an outlier to the previous trend. This could be due to the fact that the original set up of using an HCTH exchange functional should always work with its correlation counterpart [51].

On the other hand, the performance of varying the GGA correlation functionals for a

fixed exchange functional has not been thoroughly studied before. In calculations for chemically bonded systems or hydrogen bonded systems, the contribution of a correlation functional is often small. However, for low density and large s , the contribution of correlation energy becomes more significant [41]. In Table 1.2.4 we see that for a fixed exchange functional, it may amounts to a wide range of binding energies by varying the correlation functional. Because most GGA correlation functionals use the LDA correlation as an additive ingredient in the definition, to clearly show the nonlocal effect, an enhancement factor is defined by

$$F_C(s, r_s) = 1 - \frac{\varepsilon_C^{GGA}}{\varepsilon_C^{LDA}} \quad (2)$$

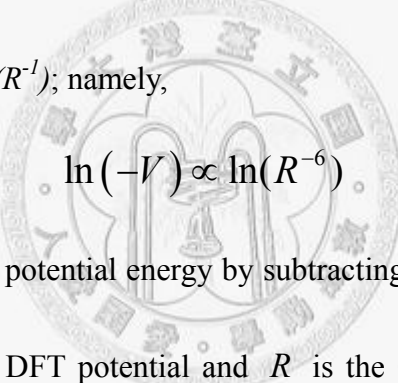
where ε_C^{GGA} and ε_C^{LDA} are the correlation potentials for the GGA and the LDA energy functionals, respectively. The correlation enhancement factor depends on s and r_s , where $r_s = (3/4\pi\rho)^{1/3}$ is the Wigner-Seitz radius. For van der Waals interactions, r_s falls in the range of 5~20. By fixing $r_s = 10$, we plot the enhancement factor $F_C(s)$ as a function of s in Fig. 1.2-8. We see in Fig. 1.2-8 that the order of the magnitude of $F_C(s)$ at medium s is TPSS > PBE > PW91 > P86 > HCTH. Interestingly, this order is essentially the order of the binding energies calculated by the corresponding functionals across the row in Table 1.2-4. These observations clearly show that the DFT potentials are correlated to the exchange and the correlation enhancement factors at the asymptotically low density region. It requires the proper match of an exchange

functional and a correlation functional to yield reasonable results. Most correlation functionals are not sensitive to the r_s for medium s range, except the P86 correlation functional. In Fig. 1.2-9, we plot the r_s dependence of the correlation enhancement factor for the P86 functional as a function of s . We see that there is a significant effect of varying r_s on the P86 functional. Therefore, one has to be more careful in making conclusions with the P86 correlation functional.

Figs. 1.2-10(a)-10(e) present the calculated potential curves by fixing 5 correlation functionals and varying the exchange functions used in this paper. Fig. 1.2-11 presents the potential curves using some hybrid functionals. We see that the DFT calculations generate a wide range of potential patterns. Some are purely repulsive (such as B88PBE), while others could be over-bounded (such as SlaterVWN). These patterns have been found before and have often been termed “unsystematic”. From our analysis, it is clear that some compensation among the respective exchange and correlation functions at the large s range of the enhancement factors must occur to yield reasonable potential well depth close to the MP2 result. For the methane case, PW91PW91 seems to achieve such appropriate compensation and thus yields a better result. Just exactly which combination should be used for a specific system is unknown *a priori*. Nevertheless, our Table 1.2-4 does show the interesting correlation

between the calculated results and the chosen functionals and should provide a useful reference for choosing such a combination.

Next we would like to discuss the asymptotic behaviors of some selective DFT potentials and compare them with those obtained from the MP2 reference potential. It is well known that a DFT potential cannot be used to model the long range tail of the van der Waals interaction. However, exactly how bad the situation is has not been systematically studied. Fig. 1.2-12 displays the linear analysis of the potential curves by plotting $\ln(-V)$ versus $\ln(R^{-1})$; namely,


$$\ln(-V) \propto \ln(R^{-6}) \quad (3)$$

where V is the (negative) potential energy by subtracting the HF potential (which is purely repulsive) from the DFT potential and R is the C-C distance. The data for $R > 5 \text{ \AA}$ has been used to perform this analysis. Notice that the MP2 potential yields a reasonably straight line. Generally DFT potentials yield erratic long range behaviors. The deviation from the straight (MP2) line indicates the inefficacy of the DFT potentials. This verifies that DFT potentials cannot be used to model the dispersion interactions, in particular at long range regions.

4. Conclusion

(a) To sum up this comment, the proposed calculated intermolecular interaction

potentials of the methane dimer by Chen *et al.* can not be reproduced using the available implementations of the LDA functionals. The calculated data can not be used to model long-range dispersion interactions of the methane dimer either. We call for a careful examination and cautious usage of the calculated potentials by Chen *et al.*

(b) We have systematically studied the calculated intermolecular potentials of the methane dimer at the most stable D_{3d} conformation using the HF, MP2 and DFT methods. A wide selection of basis sets has been employed in order to determine the basis set effects on the repulsion exponent, the binding energy, the equilibrium bond length and the asymptotic behavior of the intermolecular potentials. BSSE corrections are considered as an important factor affecting the quality of the calculated potentials.

From this study we can draw several important conclusions about using the current theoretical methods to generate the intermolecular potentials. Although only the methane dimer has been studied, these conclusions should also be useful to other molecular dimers.

(1) The HF calculations yield purely repulsive potentials for nonpolar molecular dimers. The basis size effect of the HF calculations is very small as long as the

6-31G** basis set has been used.

(2) The van der Waals bond of the methane dimer is well produced using the MP2 method. BSSE corrections must be considered to yield systematic results. Basis set effects are significant for many important parameters such as bond lengths, binding energies and dispersion coefficients. Small basis sets, especially without the augmentation of diffuse functions, could produce severe underestimation of the binding energy and overestimation of the bond length. Addition of diffuse functions and polarization functions leads to reliable binding curves.

(3) The DFT potentials display a wide range of patterns of binding curves, underestimating or overestimating the binding energy. The binding energy calculated using the PW91PW91 functional and the equilibrium bond length calculated using the PW91VP86 functional are close to the MP2 results.

From the present study we see very clearly that the HF method captures the exchange-repulsion interaction and saturates the potential curves at small basis set.

Inclusion of the correlation corrections using *ab initio* molecular orbital methods makes the calculations computationally demanding (CPU time $\sim N^4$, where N is the number of basis function). The DFT calculations are comparatively cheaper but the results are not systematic. Some functionals do capture partly the correlation effects. These observations justify the recent efforts in improving the

calculations of the intermolecular interactions using the HF or the DFT method by including explicit empirical or nonempirical dispersion energy corrections [62-78]. More works are definitely required to make the two ends (accuracy versus efficiency) meet.

(c) We have studied the DFT potentials for van der Waals interactions of the methane dimer. Weak interactions of van der Waals systems have been widely studied and discussed in various contexts and the DFT results were often termed “unsystematic”. Definitely part of the reasons can be attributed to the error cancellation between the exchange and the correlation functionals. To study their relative performance, we analyze the exchange and the correlation enhancement factors in the asymptotically low density region. Our objective is to make these results more “systematic” so that the calculated DFT potentials can be better understood. Similar to the exchange enhancement factor, the correlation enhancement factor, being useful for choosing a specific functional, should also be useful for constructing more exact functionals by “more constraint satisfaction with fewer fits”.

5. Bibliography

[1] X. R. Chen, Y. L. Bai, J. Zhu, X. D. Yang, *Phys. Rev. A* **69**, 034701(2004).

- [2] R. G. Parr and W. Yang, *Density-Functional Theory of Atoms and Molecules* (Clarendon, Oxford, 1989).
- [3] J. P. Perdew and A. Zunger, *Phys. Rev. B* **23**, 5048 (1981).
- [4] N. Troullier and J. L. Martins, *Phys. Rev. B* **43**, 1993 (1991).
- [5] L. Kleinman and D. M. Bylander, *Phys. Rev. Lett.* **48**, 1425 (1982).
- [6] M. C. Payne, M. P. Teter, D. C. Allan, T. A. Arias, and J. D. Joannopoulos, *Rev. Mod. Phys.* **64**, 1045 (1992).
- [7] C. Møller and M. S. Plesset, *Phys. Rev.* **46**, 618 (1934)
- [8] J. A. Pople, M. Head-Gordon, and K. Raghavachari, *J. Chem. Phys.* **87**, 5968 (1987).
- [9] S. Tsuzuki, T. Uchimaru, M. Mikami, and K. Tanabe, *Chem. Phys. Lett.* **287**, 202 (1998).
- [10] X. Wu, M. C. Vargas, S. Nayak, V. Lotrich and G. Scoles, *J. Chem. Phys.* **115**, 8748(2001).
- [11] H. Sabzyan, M. R. Noorbala, *J. Mol. Struct. (Theochem)* **636**, 185 (2003)
- [12] S. M. Cybulski and C. E. Seversen, *J. Chem. Phys.* **119**, 12704 (2003).
- [13] O. S. Tyagi, H. S. Bisht, and A. K. Chatterjee, *J. Phys. Chem. B* **108**, 3010 (2004).
- [14] P. Hobza and R. Zahradnik, *Intermolecular Complexes : the role of van der*

- Waals systems in physical chemistry and in the biodisciplines* (Elsevier, New York, 1988).
- [15] G. A. Jeffrey and W. Saenger, *Hydrogen Bonding in Biological Structures* (Springer-Verlag, Berlin, 1991).
- [16] A. J. Stone, *The Theory of Intermolecular Forces* (Oxford University Press, Oxford, 1996).
- [17] H. Margenau, *Rev. Mod. Phys.* **11**, 1 (1939).
- [18] A. van der Avoird, P. E. S. Wormer, and R. Moszynski, *Chem. Rev.* **94**, 1931 (1994).
- [19] A. K. Rappe and E. R. Bernstein, *J. Phys. Chem. A* **104**, 6117 (2000).
- [20] G. Chalasinski and M. M. Szczesniak, *Chem. Rev.* **100**, 4227 (2000).
- [21] R. J. Wheatley, A. S. Tulegenov, and E. Bichoutskaia, *Int. Rev. Phys. Chem.* **23**, 151 (2004).
- [22] Y. Zhao and D. G. Truhlar, *J. Chem. Theory Comput.* **1**, 415 (2005).
- [23] S. Grimme, *J. Comp. Chem.* **25**, 1463 (2004).
- [24] R. A. Friesner, *Proc. Natl. Acad. Sci.* **102**, 6648 (2005).
- [25] D. Frenkel and B. Smit, *Understanding Molecular Simulations* (Academic Press, New York, 2002).
- [26] M. Marques and E. Gross, *Annual Rev. Phys. Chem.* **55**, 427 (2004)

- [27] C. E. Dykstra, G. Frenking, K. S. Kim, and G. E. Scuseria, *Theory and Applications of Computational Chemistry : The first forty years* (Elsevier, Amsterdam, 2005).
- [28] A. Ruzsinszky, J. P. Perdew, and G. I. Csonka, *J. Phys. Chem. A* **109**, 11015 (2005).
- [29] M. D. Malinsky, K. L. Kelly, G. C. Schatz, and R. P. van Duyne, *J. Am. Chem. Soc.* **123**, 1471 (2001).
- [30] G. Y. Liu, S. Xie, and Y. L. Qian, *Acc. Chem. Res.* **23**, 457 (2000).
- [31] W. Rawicz, K. C. Olbrich, T. McIntosh, D. Needham, E. Evans, *Biophys. J.* **79**, 328 (2000).
- [32] S. D. Chao, J. D. Kress, and A. Redondo, *J. Chem. Phys.* **122**, 234912 (2005).
- [33] M. M. Szczesniak, G. Chalasinski, S. M. Cybulski, and S. Scheiner, *J. Chem. Phys.* **93**, 4243 (1990).
- [34] R. L. Rowley and T. Pakkanen, *J. Chem. Phys.* **110**, 3368 (1999).
- [35] D. E. Williams and D. J. Craycroft, *J. Phys. Chem.* **91**, 6365 (1987).
- [36] S. Tsuzuki and K. Tanabe, *J. Phys. Chem.* **95**, 2272 (1991)
- [37] J. J. Novoa, M. -H. Whangho, and J. M. Williams, *J. Chem. Phys.* **94**, 4835 (1991)
- [38] D. H. Gay, H. Dai, and D. R. Beck, *J. Chem. Phys.* **95**, 9106 (1991).

- [39] S. Tsuzuki, T. Uchimaru, K. Tanabe, and S. Kuwajima, *J. Phys. Chem.* **98**, 1830 (1994).
- [40] S. Tsuzuki and H. P. Luthi, *J. Chem. Phys.* **114**, 3949 (2001).
- [41] J. Nagy, D. F. Weaver, and V. H. Smith, *Mol. Phys.* **85**, 1179 (1995).
- [42] E. Fraschini and A. J. Stone, *J. Comput. Chem.* **19**, 847 (1998).
- [43] S. Tsuzuki, T. Uchimaru, and K. Tanabe, *Chem. Phys. Lett.* **287**, 202 (1998).
- [44] S. Tsuzuki, K. Honda and T. Uchimaru, M. Mikami, *J. Chem. Phys.* **124**, 114304
- [45] A. Szabo, N. S. Ostlund, *Modern Quantum Chemistry. Introduction to Advanced Electronic Structure Theory* (Dover, New York, 1996).
- [46] T. H. Dunning, Jr., *J. Chem. Phys.* **90**, 1007 (1989).
- [47] K. Burke, J. P. Perdew, and Y. Wang, in *Electronic Density Functional Theory: Recent Progress and New Directions*, Ed. J. F. Dobson, G. Vignale, and M. P. Das (Plenum, 1998).
- [48] M. J. Frisch, G. W. Trucks, H. B. Schlegel *et al.*, Gaussian 03, Revision B.04 (Gaussian Inc., Pittsburgh, 2003).
- [49] Gaussian 03 User's Reference and IOps Reference (Gaussian Inc., Pittsburgh, 2003).
- [50] S. Tsuzuki, T. Uchimaru, M. Mikami, and K. Tanabe, *J. Phys. Chem. A.* **102**, 2091 (1998).

- [51] C. Møller and M. S. Plesset, *Phys. Rev.* **46**, 618 (1934).
- [52] J. A. Pople, M. Head-Gordon, and K. Raghavachari, *J. Chem. Phys.* **87**, 5968 (1987).
- [53] R. Krishnan, J. S. Binkley, R. Seeger, J. A. Pople, *J. Chem. Phys.* **72**, 650 (1980)
- [54] S. F. Boys and F. Bernardi, *Mol. Phys.* **19**, 553 (1970).
- [55] T. Helgaker, W. Klopper, H. Koch, J. Noga, *J. Chem. Phys.* **106**, 9639 (1997).
- [56] D. Feller, *J. Chem. Phys.* **96**, 6104 (1992).
- [57] W. H. Press, S. A. Teukolsky, W. T. Vetterling, and B. P. flannery, *Numerical Recipe in C* (Cambridge University Press, Cambridge, 1996).
- [58] Gaussian 03, Revision C.02, Frisch, M. J. *et al.* Gaussian, Inc., Wallingford CT, 2004.
- [59] D. C. Rapaport, *The Art of Molecular Dynamics Simulation* (Cambridge University Press, New York, 1995).
- [60] A. D. Becke, *Phys. Rev. A* **38**, 3098 (1988).
- [61] N. C. Handy and A. J. Cohen, *Mol. Phys.* **99**, 403 (2001).
- [62] C. Adamo and V. Barone, *J. Chem. Phys.* **108**, 664 (1998).
- [63] J. P. Perdew, K. Burke, and M. Ernzerhof, *Phys. Rev. Lett.* **77**, 3865 (1996).
- [64] K. Burke, J. P. Perdew, and Y. Wang, in *Electronic Density Functional Theory: Recent Progress and New Directions*, Ed. J. F. Dobson, G. Vignale, and M. P. Das

(Plenum, 1998).

[65] J. Tao, J. P. Perdew, V. N. Staroverov, and G. E. Scuseria, *Phys. Rev. Lett.* **91**,

146401 (2003).

[66] W. Kohn and L. J. Sham, *Phys. Rev.* **140**, A1133 (1965).

[67] A. D. Boese and N. C. Handy, *J. Chem. Phys.* **114**, 5497; see also the supp.

material: EPAPS Document No. E-JCPA6-114-301111 (2001).

[68] J. C. Slater, *Quantum Theory of Molecular and Solids. Vol. 4: The Self-Consistent*

Field for Molecular and Solids (McGraw-Hill, New York, 1974).

[69] J. P. Perdew, *Phys. Rev. B* **33**, 8822 (1986).

[70] S. H. Vosko, L. Wilk, and M. Nusair, *Can. J. Phys.* **58**, 1200 (1980).

[71] J. P. Perdew and A. Zunger, *Phys. Rev. B* **23**, 5048 (1981).

[72] C. Lee, W. Yang, and R. G. Parr, *Phys. Rev. B* **37**, 785 (1988).

[73] F. A. Hamprecht, A. J. Cohen, D. J. Tozer, and N. C. Handy, *J. Chem. Phys.* **109**,

6264 (1998).

[74] H. L. Schmider and A. D. Becke, *J. Chem. Phys.* **108**, 9624 (1998).

[75] A. D. Becke, *J. Chem. Phys.* **98**, 1372 (1993).

[76] A. J. Cohen and N. C. Handy, *Mol. Phys.*, **99**, 607 (2001).

[77] A. D. Becke, *J. Chem. Phys.* **98**, 5648 (1993).

[78] C. Adamo and V. Barone, *J. Chem. Phys.* **108**, 664 (1998).

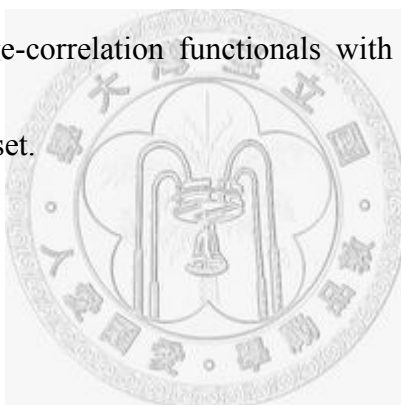
- [79] A. H.-T. Li and S. D. Chao, *J. Chem. Phys.* **125**, 094312 (2006).
- [80] F. Jensen, *Introduction to Computational Chemistry* (Wiley, New York, 1999).
- [81] M. A. Spackman, *J. Chem. Phys.* **94**, 1295 (1991).
- [82] Q. Wu and W. Yang, *J. Chem. Phys.* **116**, 515 (2002).
- [83] A. D. Becke and E. R. Johnson, *J. Chem. Phys.* **122**, 154104 (2005).
- [84] J. P. Perdew and A. Zunger, *Phys. Rev. B* **23**, 5048 (1981).
- [85] S. H. Vosko, L. Wilk, and M. Nusair, *Can. J. Phys.* **58**, 1200 (1980).
- [86] J. Tao, J. P. Perdew, V. N. Staroverov, and G. E. Scuseria, *Phys. Rev. Lett.* **91**, 146401 (2003).
- [87] J. P. Perdew, K. Burke, and M. Ernzerhof, *Phys. Rev. Lett.* **77**, 3865 (1996).
- [88] K. Burke, J. P. Perdew, and Y. Wang, in *Electronic Density Functional Theory: Recent Progress and New Directions*, edited by J. F. Dobson, G. Vignale, and M. P. Das Plenum, New York, 1998.
- [89] J. P. Perdew, *Phys. Rev. B* **33**, 8822 (1986).
- [90] C. Lee, W. Yang, and R. G. Parr, *Phys. Rev. B* **37**, 785 (1988).
- [91] F. A. Hamprecht, A. J. Cohen, D. J. Tozer, and N. C. Handy, *J. Chem. Phys.* **109**, 6264 (1998).
- [92] A. D. Boese, N. L. Doltsinis, N. C. Handy, and M. Sprik, *J. Chem. Phys.* **112**, 1670 (2000).

- [93] A. D. Boese and N. C. Handy, *J. Chem. Phys.* **114**, 5497; see also the supplementary material: EPAPS Document No. E (2001).
- [94] C. Adamo and V. Barone, *J. Chem. Phys.* **108**, 664 (1998).
- [95] N. C. Handy and A. J. Cohen, *Mol. Phys.* **99**, 403 (2001).
- [96] A. D. Becke, *Phys. Rev. A* **38**, 3098 (1988).
- [97] J. C. Slater, *Quantum Theory of Molecular and Solids. Vol. 4: The Self-Consistent Field for Molecular and Solids* (McGraw-Hill, New York, 1974).
- [98] T. A. Wesolowski, O. Parisel, Y. Ellinger, and J. Weber, *J. Phys. Chem. A* **101**, 7818 (1997).
- [99] Y. Zhang, W. Pan, and W. Yang, *J. Chem. Phys.* **107**, 7921 (1997).
- [100] G. E. Scuseria and V. N. Staroverov, Chap. 24 in C. E. Dykstra, G. Frenking, K. S. Kim, and G. E. Scuseria (Ed.), *Theory and Applications of Computational Chemistry : The first forty years* (Elsevier, Amsterdam, 2005).
- [101] D. J. Lacks and R. G. Gordon, *Phys. Rev. A* **47**, 4681 (1993).
- [102] E. H. Lieb and S. Oxford, *Int. J. Quam. Chem.* **19**, 427 (1981).
- [103] J. Tao and J. P Perdew, *J. Chem. Phys.* **122**, 114102 (2005).

Table captions

TABLE 1.2-1. The basis set dependence of important potential parameters using the BSSE corrected HF and MP2 intermolecular potentials. R_0 is the distance at which the potential is zero and R_m is the equilibrium bond length. The CPU time of the MP2 calculation was recorded on a single node 2-processor AMD 250 PC cluster with distributed memory.

TABLE 1.2-2. Comparison of the bond lengths and the binding energies calculated using the several exchange-correlation functionals with the MP2 results using the 6-311++G (3df,3pd) basis set.



Basis set	MP2		HF		MP2						
	Number of basis function	CPU Time (hour)	A ^a (kcal/mol)	α^a (\AA^{-1})	R ₀ (\AA)	R _m (\AA)	E _b (kcal/mol)	ω (cm^{-1})	1 term ^b	2 terms ^c	
									C ₆	C ₆	C ₈
STO-3G	9	0.25	219400	3.62	4.36	4.75	-0.009	42.99	189.03	136.04	1596.61
3-21G	34	0.28	83319	3.29	4.05	4.50	-0.047	78.39	641.57	419.58	6477.70
6-31G	34	0.28	104302	3.36	3.99	4.45	-0.053	73.33	676.57	438.12	6957.93
6-311G	50	0.37	113764	3.39	3.91	4.36	-0.064	83.45	747.23	486.94	8437.88
3-21G**	58	0.38	83602	3.30	3.85	4.31	-0.078	101.15	832.07	556.44	10586.51
6-311G*	60	0.48	115208	3.40	3.73	4.16	-0.104	108.73	951.51	454.57	8356.77
cc-pVDZ	68	0.68	120594	3.41	3.63	4.05	-0.150	130.17	1174.71	684.90	11986.23
6-31G**	70	0.57	108646	3.39	3.73	4.19	-0.101	108.73	941.68	544.89	11028.72
6-311G**	84	1.17	115208	3.40	3.59	4.02	-0.165	161.64	1207.04	640.12	14790.89
6-311+G**	92	1.57	115057	3.40	3.58	4.01	-0.174	159.31	1245.15	673.37	15081.38
6-311++G**	100	2.42	115298	3.40	3.57	4.01	-0.176	159.31	1259.19	671.72	15584.98
aug-cc-pVDZ	118	3.22	123739	3.42	3.35	3.78	-0.395	369.19	1995.05	764.34	22587.36
6-311++G(2d,2p)	134	5.62	114025	3.40	3.38	3.80	-0.315	217.47	1674.00	812.170	21662.07
6-311++G(3d,3p)	168	12.22	112605	3.40	3.33	3.75	-0.401	278.15	1964.62	1456.53	9860.58
cc-pVTZ	172	13.35	113006	3.40	3.37	3.80	-0.317	215.83	1880.25	1446.17	10119.20
6-311++G(2df,2pd)	188	20.35	113940	3.40	3.36	3.78	-0.331	209.88	1697.49	1437.55	10518.06
6-311++G(3df,3pd)	222	22.63	112373	3.40	3.30	3.73	-0.415	270.57	1979.52	1593.49	7987.79
aug-cc-pVTZ	276	82.70	112320	3.40	3.27	3.70	-0.453	260.45	2048.04	1442.32	11755.28
aug-cc-pVQZ	528	941.83	111828	3.40	3.26	3.68	-0.464	250.34	2029.20	1053.08	18021.33
Basis set limit			113458	3.40	3.25	3.66	-0.470	256.54	---	---	---

^a Fit to the formula $V_{HF}(R) = Ae^{-\alpha R}$.

^b Fit to the formula $V_{disp}(R) = -\frac{C_6}{R^6}$, C_6 in unit (kcal/mol \AA^6), using data $R > 5.0 \text{\AA}$.

^c Fit to the formula $V_{disp}(R) = -\frac{C_6}{R^6} - \frac{C_8}{R^8}$, C_8 in unit (kcal/mol \AA^8), using data $R > 4.0 \text{\AA}$.

Functional	6-311++G(3df,3pd)	
	Bond length (\AA)	Binding Energy (<i>kcal/mol</i>)
PW91PL	4.19	-0.360
PW91VWN5	4.19	-0.358
PW91VWN	4.14	-0.387
PW91TPSS	4.05	-0.376
PW91PBE	4.04	-0.379
PW91PW91	3.99	-0.418
PW91VP86	3.73	-0.572
PW91P86	3.72	-0.577
PW91V5LYP	3.80	-0.669
PW91LYP	3.80	-0.669
PW91HCTH93	3.56	-1.444
PW91HCTH407	3.52	-3.367
HCTH93PW91	5.93	-0.003
HCTH147PW91	5.82	-0.006
HCTH407PW91	5.93	-0.004
MPWPW91	4.83	-0.071
MPW1PW91	4.80	-0.050
OPW91	5.23	-0.021
BPW91	Unbound	---
PBEPW91	4.04	-0.167
SPW91	3.08	-2.483
XAPW91	2.97	-2.671
MP2	3.73	-0.415

Table 1.2-2

		<i>Correlation functional</i>									
		VWN5	PL	TPSS	PBE	PW91	VWN	P86	VP86	LYP	HCTH
<i>Exchange functional</i>	B88	U	U	U	U	U	U	U	U	U	3.62
	HCTH	5.85	5.85	5.93	5.93	5.93	5.83	6.14	6.14	5.90	3.92
	OPTX	5.20	5.20	5.24	5.23	5.24	4.93	5.30	5.30	4.83	3.81
	MPW	4.77	4.77	4.84	4.84	4.83	4.73	4.69	4.69	4.26	3.57
	TPSS	4.40	4.40	4.42	4.41	4.40	4.35	4.03	4.03	3.98	3.52
	PBE	4.26	4.25	4.08	4.06	4.04	4.21	3.72	3.72	3.79	3.53
	PW91	4.19	4.19	4.05	4.04	3.99	4.14	3.72	3.73	3.80	3.52
	Slater	3.33	3.99	3.10	3.07	3.08	3.31	2.99	3.00	3.13	NA [‡]
	XAlpha	3.26	3.26	3.54	3.52	2.97	3.24	3.49	3.00	3.07	3.15

[‡] Not available

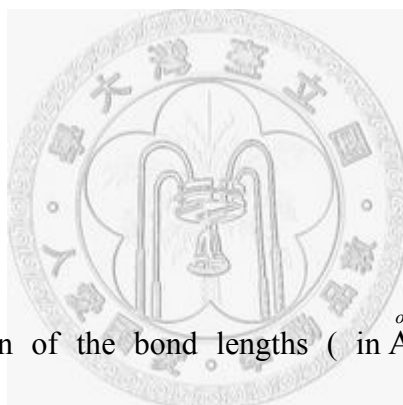


Table 1.2-3

TABLE 1.2-3 Comparison of the bond lengths (in Å) calculated with the 90 exchange-correlation functionals using the 6-311++G (3df, 3pd) basis set. As a reference, the MP2 bond length calculated at this basis set is 3.73 Å [22]. The better DFT results of errors within 10% as compared to the MP2 result are marked in black boldface.

		<i>Correlation functional</i>									
		VWN5	PL	TPSS	PBE	PW91	VWN	P86	VP86	LYP	HCTH
<i>Exchange functional</i>	B88	1.206	1.206	1.090	1.075	1.054	1.130	0.802	0.801	0.718	-1.749
	HCTH	-0.007	-0.007	-0.003	-0.003	-0.004	-0.008	0.000	0.000	-0.006	-0.668
	OPTX	-0.030	-0.030	-0.020	-0.020	-0.021	-0.032	-0.007	-0.006	-0.039	-1.582
	MPW	-0.085	-0.085	-0.070	-0.070	-0.071	-0.096	-0.057	-0.056	-0.150	-2.559
	TPSS	-0.087	-0.087	-0.074	-0.074	-0.077	-0.105	-0.118	-0.116	-0.250	-2.753
	PBE	-0.149	-0.150	-0.157	-0.158	-0.167	-0.174	-0.358	-0.353	-0.457	-3.174
	PW91	-0.358	-0.360	-0.376	-0.379	-0.418	-0.387	-0.577	-0.572	-0.669	-3.367
	Slater	-1.173	-1.184	-2.330	-2.445	-2.483	-1.287	-3.436	-3.416	-2.884	NA [‡]
	XAlpha	-1.290	-1.302	-2.500	-2.634	-2.671	-1.415	-3.702	-0.364	-3.119	-5.838

[‡] Not available

Table 1.2-4

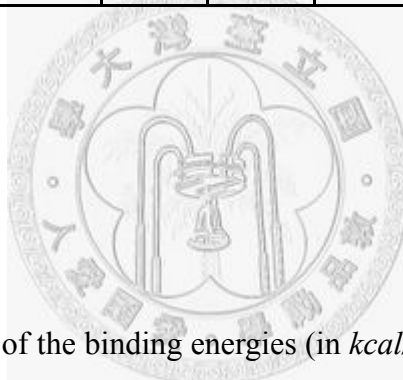


TABLE 1.2-4 Comparison of the binding energies (in *kcal/mol*) calculated with the 90 exchange-correlation functionals using the 6-311++G (3df, 3pd) basis set. As a reference, the MP2 binding energy calculated at this basis set is -0.415 kcal/mol [22]. Positive values represent unbound dimer structures and the energies are calculated at $R=3.73 \text{ \AA}$. The better DFT results of errors within 10% as compared to the MP2 result are marked in black boldface.

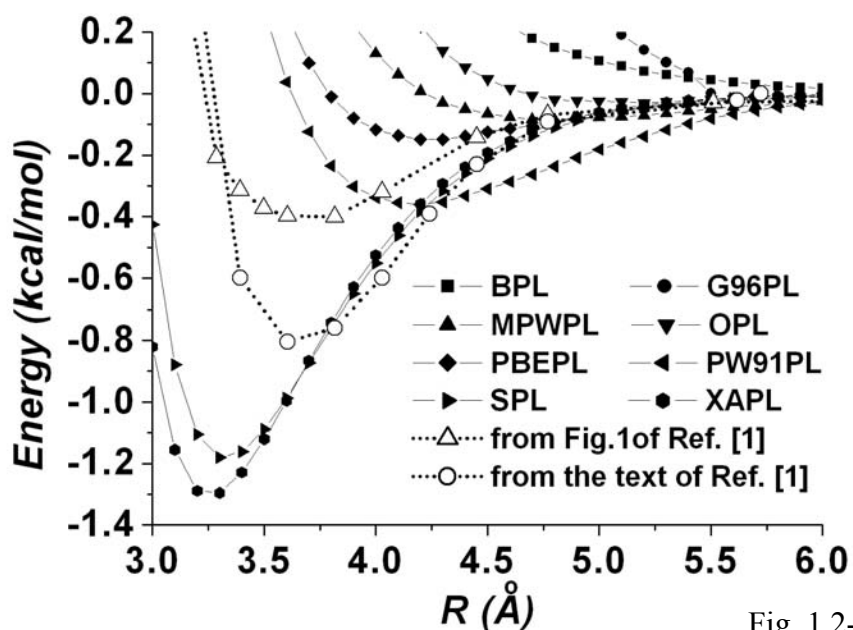


Fig. 1.2-1

FIG. 1.2-1. The calculated intermolecular interaction potentials using a series of exchange-correlation functionals. The open symbol-lines are the two sets of data taken from Fig. 1.2-1 and the text of Ref. [1], respectively. The filled symbol-lines are calculated in the present work using a combination of the selected exchange functionals with the Perdew correlation functional.

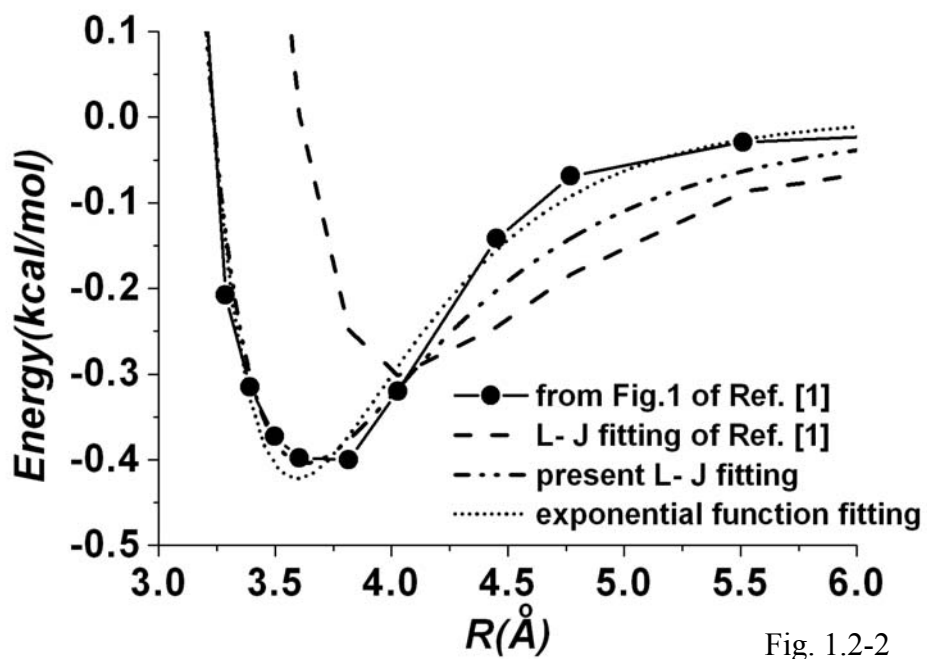
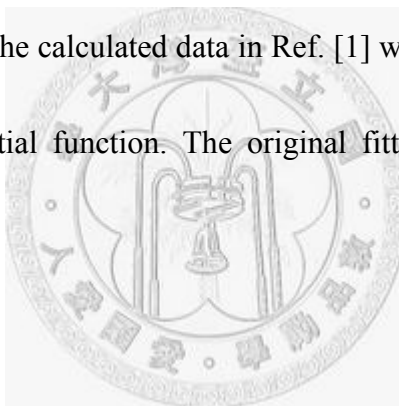


FIG. 1.2-2 Comparison of the calculated data in Ref. [1] with the fittings using the L-J function and the exponential function. The original fitting by Chen *et al.* is also presented for comparison.



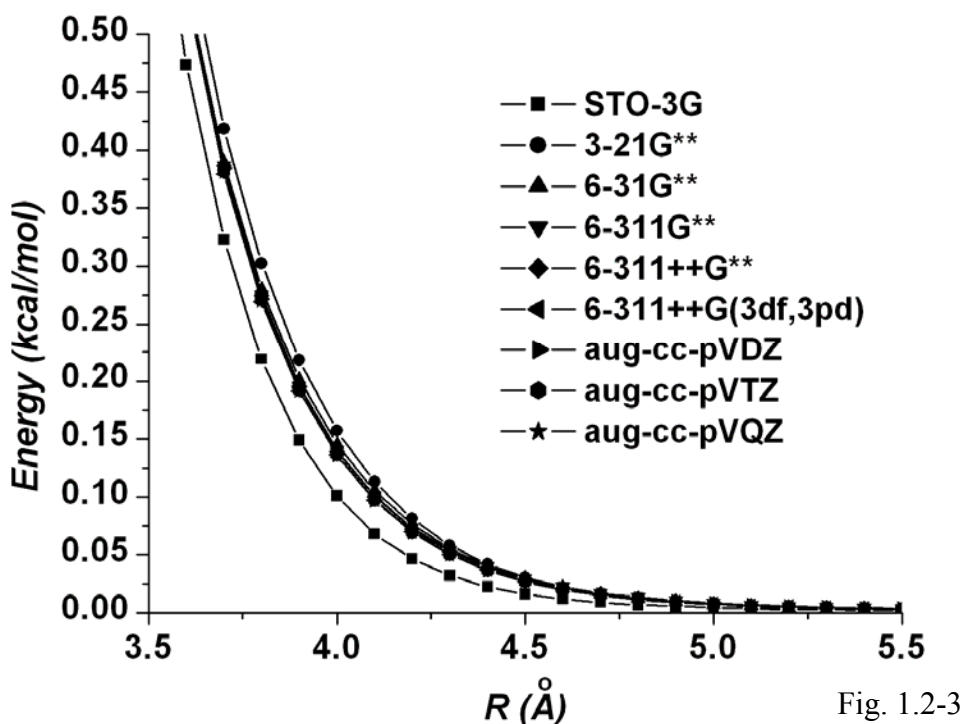


Fig. 1.2-3

FIG. 1.2-3. The BSSE corrected HF interaction potentials of the methane dimer using several basis sets.

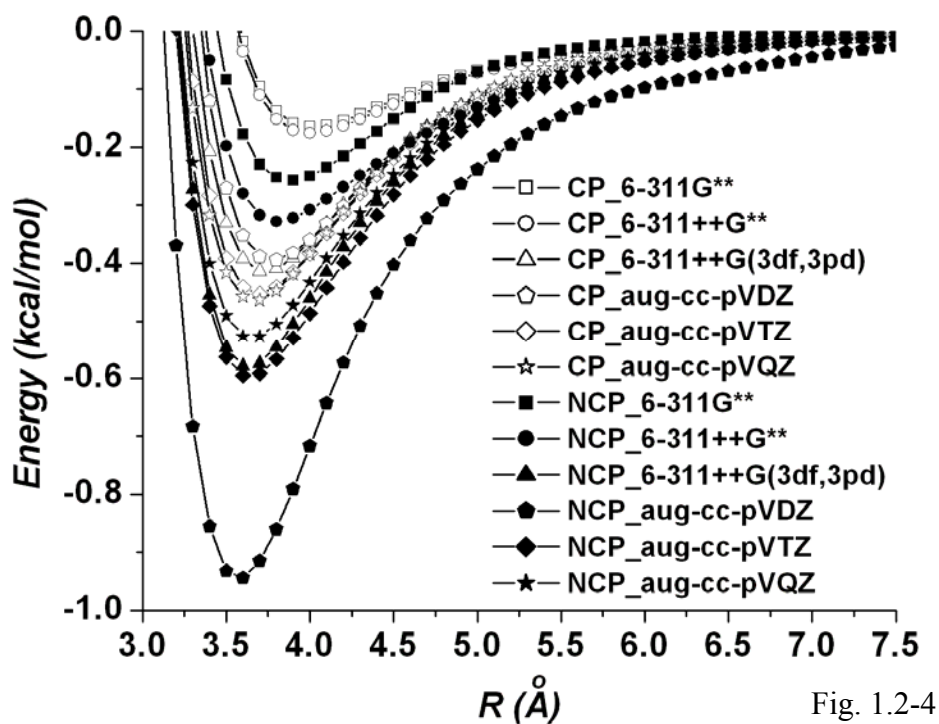


Fig. 1.2-4

FIG. 1.2-4. The BSSE corrected (CP) and uncorrected (NCP) MP2 potentials of the methane dimer using a series of basis sets.

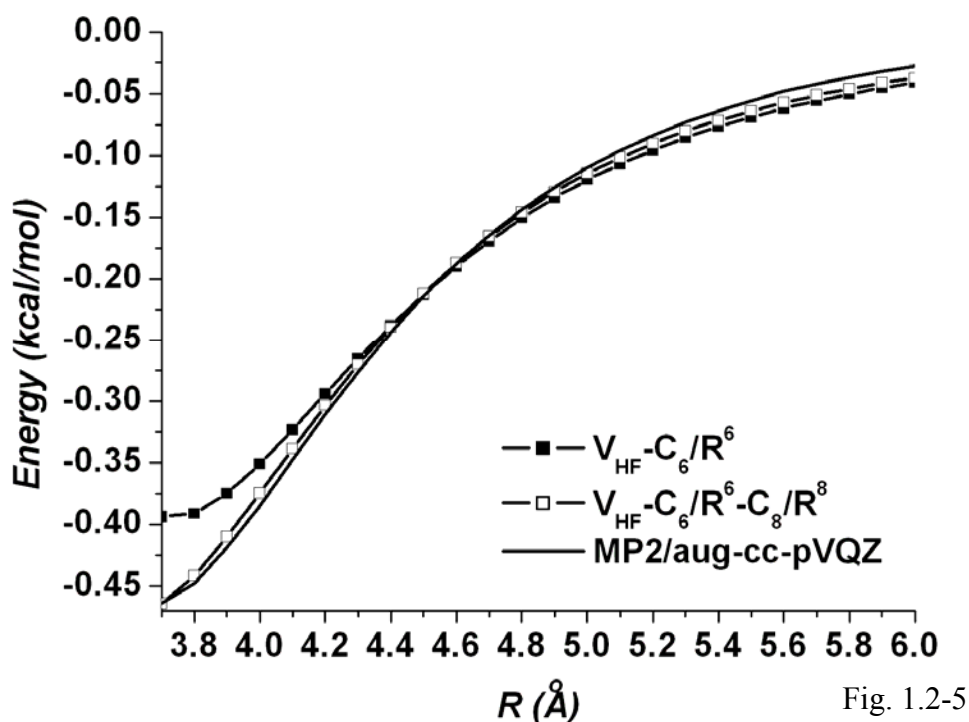


FIG. 1.2-5. Comparison of the BSSE corrected MP2 potential curve calculated at the aug-cc-pVQZ basis set and the sum of the HF potential and the long range dispersion potentials.

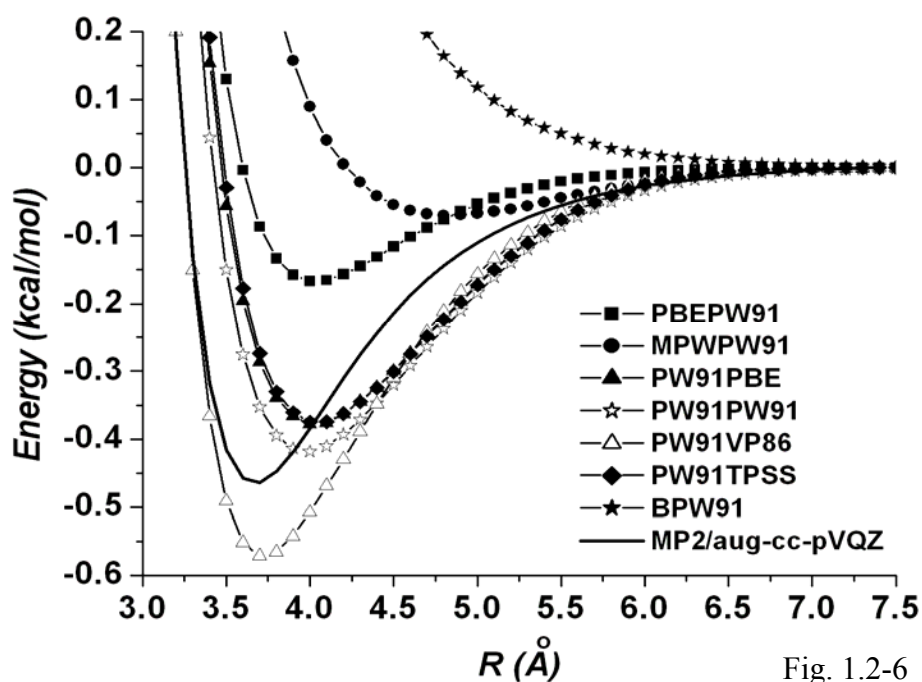


FIG. 1.2-6. The BSSE corrected DFT intermolecular potential curves using the PW91 as the exchange or correlation functional.

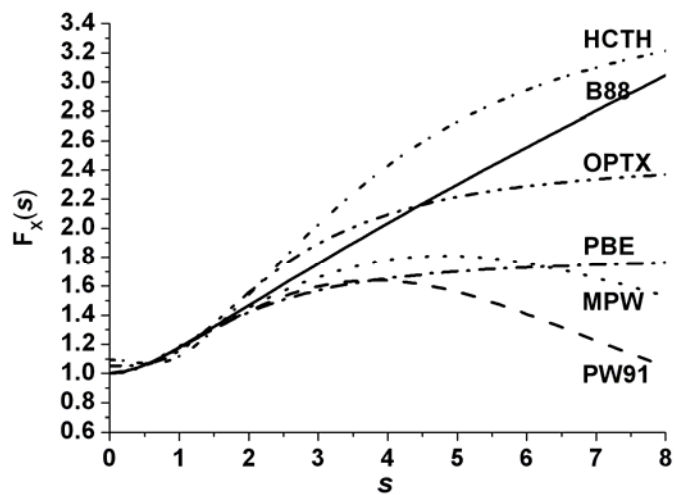


Fig. 1.2-7

FIG. 1.2-7 The GGA exchange enhancement factor as a function of s for the B88, HCTH, OPTX, MPW, PBE, and PW91 exchange functionals.

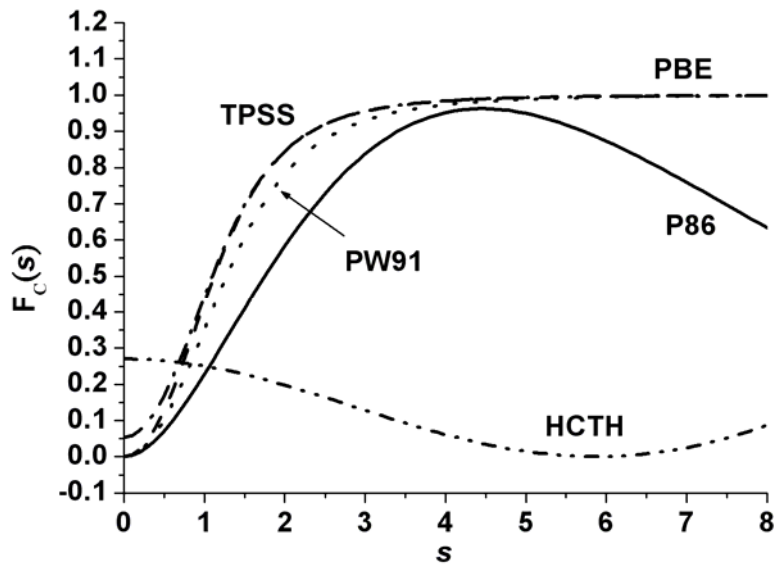


Fig. 1.2-8

FIG. 1.2-8 The GGA correlation enhancement factor as a function of s for the TPSS, PBE, PW91, P86, and HCTH correlation functionals. Here $r_s = 10$.

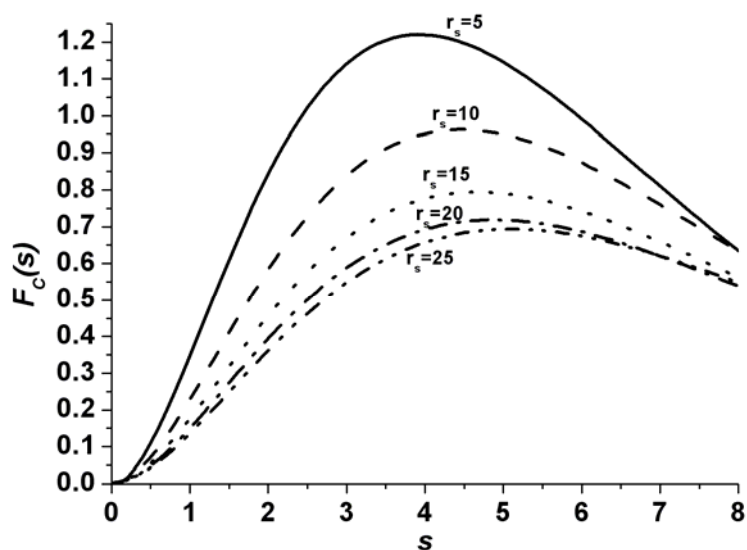


Fig. 1.2-9

FIG. 1.2-9 The r_s dependence of the GGA correlation enhancement factor as a function of s for the P86 correlation functional.

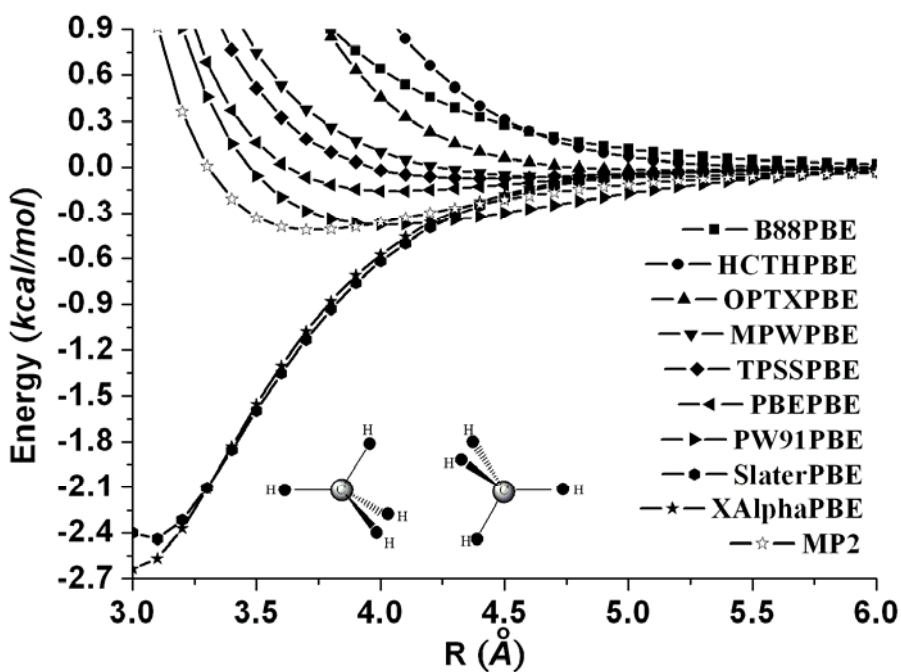
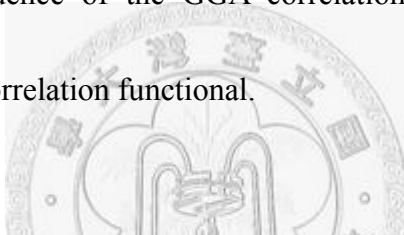


Fig. 1.2-10(a)

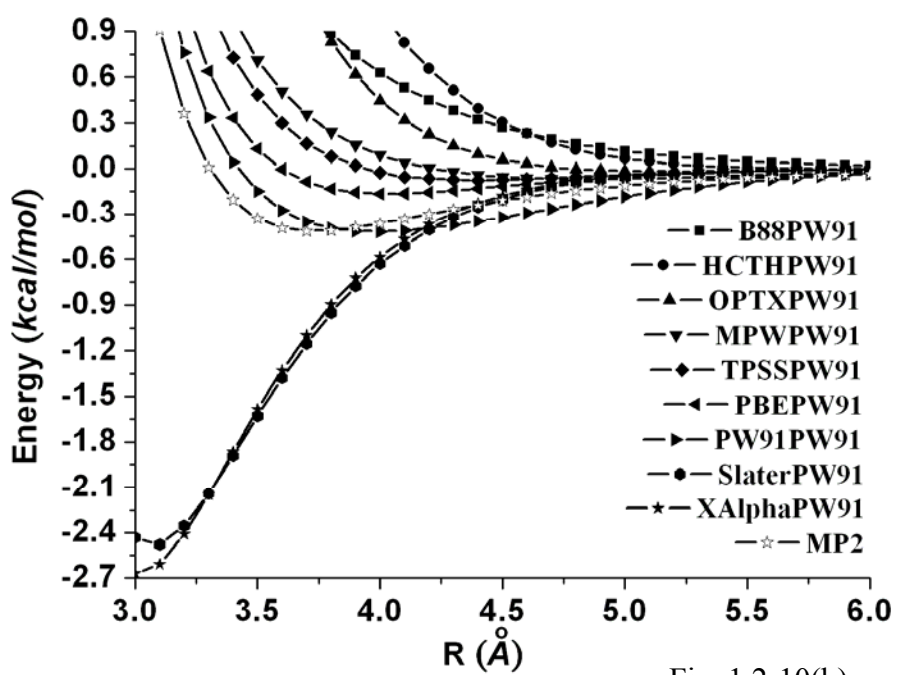


Fig. 1.2-10(b)

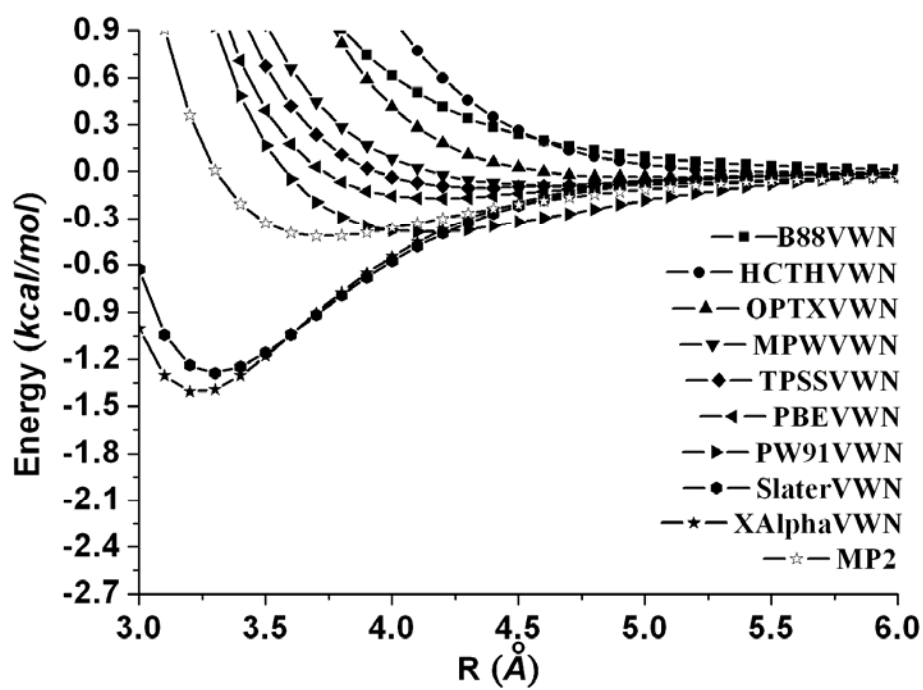


Fig. 1.2-10(c)

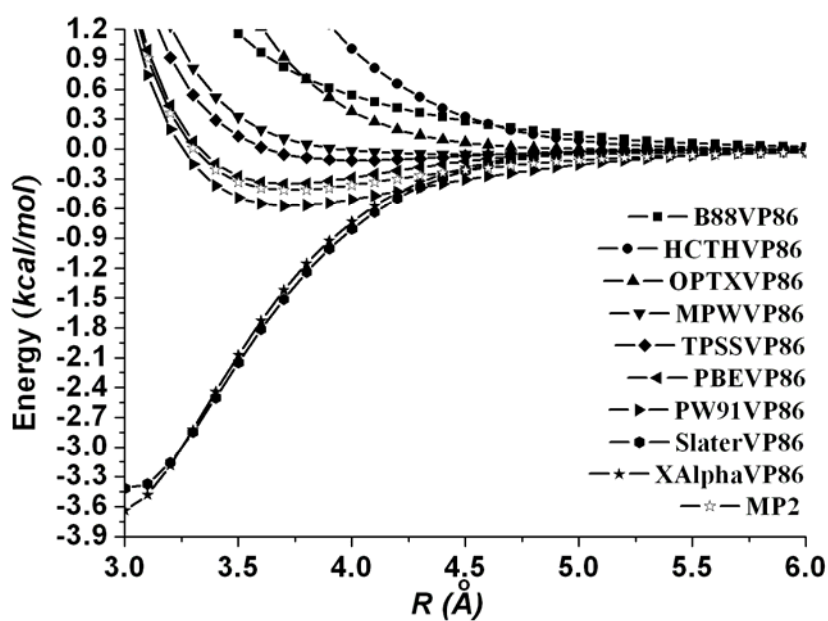


Fig. 1.2-10(d)

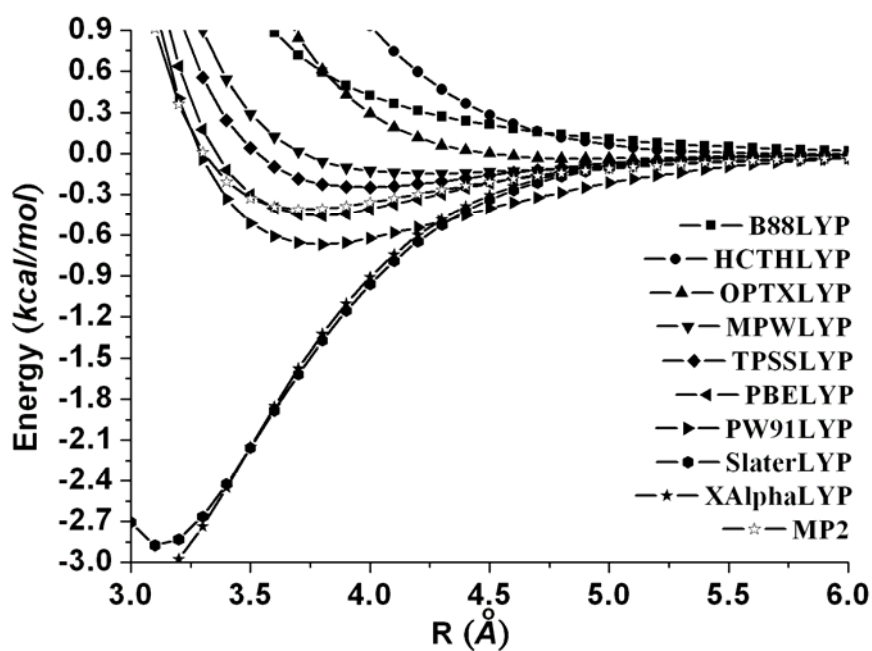


Fig. 1.2-10(e)

FIG. 1.2-10 The BSSE corrected potential curves with varying exchange functionals by fixing (a) PBE, (b) PW91, (c) VWN, (d) VP86 and (e) LYP correlation functionals, respectively. The MP2 potential curve is also shown as a reference.

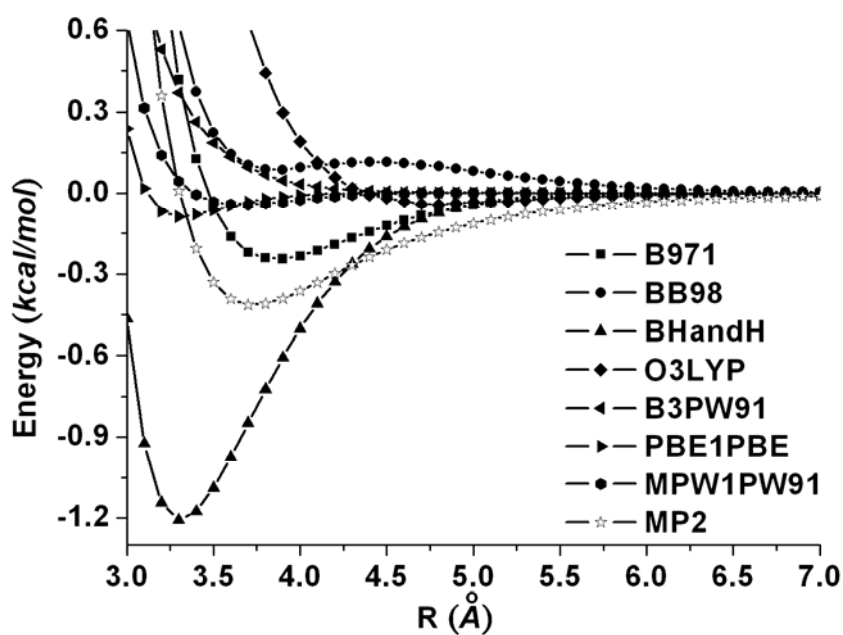


Fig. 1.2-11

FIG. 1.2-11 The BSSE corrected potential curves selective using several hybrid functionals.

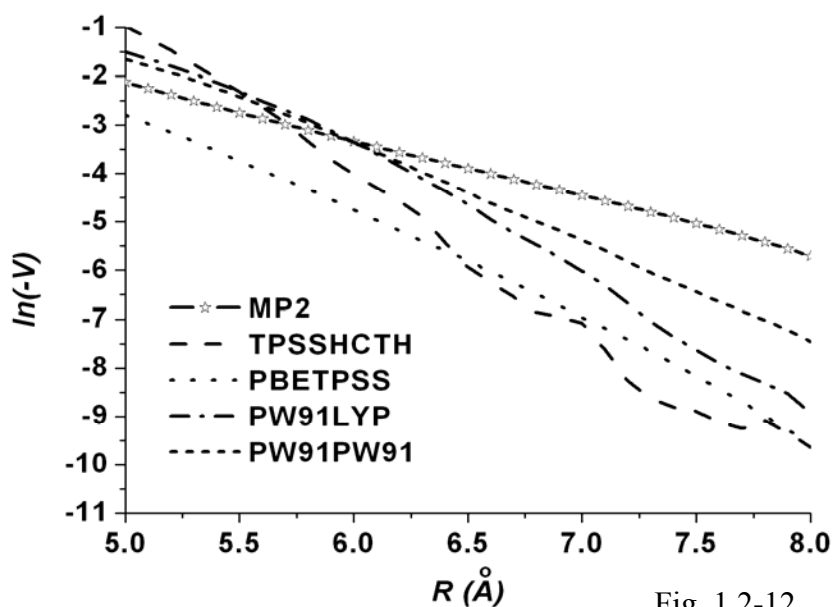
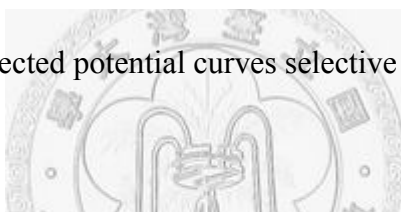


Fig. 1.2-12

FIG. 1.2-12 The asymptotic behavior of selective DFT potentials versus the MP2 potential via a analysis of the long-range data.

1.3 Molecular Dynamics Simulations of Fluid Methane Properties Using *Ab Initio* Intermolecular Interaction Potentials

1. Introduction

The interaction potentials of hydrocarbons are crucial in determining the packing stability in solids and fluids and in biological soft matters [1-4]. Methane is a prototype system of hydrocarbon interactions and thus has attracted intense theoretical studies on the interaction potentials of the methane dimer [5-20, 22-23]. These potentials are required in a molecular simulation to calculate bulk properties of fluids [21]. Most previous investigations of fluid methane properties used empirical force fields together with molecular dynamics (MD) or Monte Carlo simulations. However, none of them can be universally applied to reproducing experiments quantitatively. For recent reviews on the performance of several popular empirical force fields, see Nagy *et al.* [22] and Hayes *et al.* [23].

Recently, intermolecular potential energy surfaces (PESs) from first-principles calculations, or *ab initio* force fields, have been developed to simulate fluid methane properties [23-27]. Gay *et al.* [24] obtained the PES using the Møller-Plesset (MP_x, x=2-4) perturbation theory with the Sadlej basis set for six conformers and a 5-site (at the carbon and the hydrogen positions) potential function was used to fit the

calculated data. Using the PES they could reproduce the experimental second virial coefficients for the temperature range of 110-623 K. Palmer and Anchelll [25] obtained the PES using the MP2/6-31+G* theory for 7 conformers and a 5-site potential function was used in the data fitting. Their MD simulations using the PES reproduced some experimental thermodynamic properties (pressure, enthalpy etc.) at a single state point. In a series of papers, Tsuzuki *et al.* [9, 26] have calculated the interaction energies for 12 conformers using up to the MP3/aug (df, pd) 6-311G** level of theory with a total of 132 configuration points calculated. They used a 5-site model to fit the potential data where the four hydrogen sites were relocated toward the carbon atom. Their MD simulations reproduced some thermodynamic properties and the self-diffusion coefficient at a single state point. Rowley and Pakkanen [27] have used the MP2/6-311+G (2df, 2pd) theory to calculate the potential energies for 11 conformers and their PES was based on a 5-site model. They further improved the accuracy of the PES by including some potential data calculated at the MP4/6-311+G (2df, 2pd) theory in the fitting procedure. However, no simulation results compared with experiments were provided in this work. Hayes *et al.* [23] have calculated the interaction energies for 10 conformers at the MP2/aug (df, pd)-6-311G** level of theory, resulting in a total of 130 configuration points calculated. They further improved the accuracy of the PES by including 78 potential data calculated at the

MP4/aug (df, pd) 6-311G** theory for selected conformers. They used a 5-site model, where the four hydrogen sites were relocated toward the carbon atom, to fit the potential data. Their MD simulations reproduced some thermodynamic properties at more than a single state point.

These previous works are either inaccurate enough in the potential data or are not validated against a wider enough range of experimental data. Currently, no *ab initio* PES so far has been calculated at a spectroscopic accuracy while at the same time can reproduce the structural and transport properties of fluid methane. Moreover, previous modeling procedures used brute-force fittings without utilizing the physical understanding of the potential anisotropy. Our data modeling is based on an analyzed hydrogen-hydrogen repulsion mechanism to explain the relative stability of different conformers [6]. In this paper we construct an *ab initio* PES using a high level theory, up to MP2/aug-cc-pVQZ, for 12 conformers. Using well-establish extrapolation formulas the potential data at the complete basis set (CBS) limit can achieve a CCSD(T)/aug-cc-pVQZ level of quality. We determine the accuracy of the constructed *ab initio* PES using MD simulations and the results are compared with experiments. Quantitative agreements with the measured radial distribution functions (RDFs) and the self-diffusion coefficients for a wide range of thermodynamic

conditions provide proper justification on the validity of this PES.

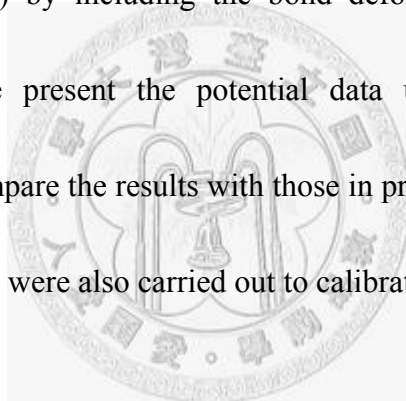
The paper is organized as follows. In Section II, we describe the details of these calculations. In Section III the results are presented and discussed. A summary and a brief perspective are given in Section IV.

2. Methods and Calculations

All the calculations were performed using the Gaussian 03 program package [28] on a single node AMD PC cluster with distributed memory. The isolated methane molecule was first optimized at the CCSD(T)/aug-cc-pVTZ theory and was found to be at the tetrahedral configuration (T_d symmetry) with the C-H bond length of 1.085 Å. The 12 symmetric conformers chosen to sample the orientational response are depicted in Fig.

1.3-1. Because of the high symmetry of the dimer configuration, the angular sampling should be wide enough to model the rotational dynamics in normal thermodynamic conditions. The MP2 method [29] has been used to treat the correlation effect. Pople's medium size basis sets [up to 6-311++G (3df, 3pd)] [30] and Dunning's correlation consistent basis sets (cc-pVXZ and aug-cc-pVXZ, X=D, T, Q) [31] were employed in the calculations. The basis set superposition errors (BSSEs) were corrected by the counterpoise (CP) method of Boys and Bernardi [32]. Subsequently the

carbon-carbon (C-C) distance, denoted as R , was sampled for a large range of 3~9 Å, with 61 configuration points for each conformer. A total of 732 configuration points were actually sampled and the energies calculated. During the scan we first fixed the monomer geometry (rigid monomer assumption) and the conformer symmetry. Next, to check the validity of the rigid monomer assumption, we repeat the above procedure while allowing the monomer carbon-hydrogen (C-H) bonds to relax during the scan. However, we found very little effect (normally less than 0.01 kcal/mol in the energy difference, see Fig. 1.3-2) by including the bond deformation. Therefore, in the following discussions we present the potential data under the rigid monomer assumption in order to compare the results with those in previous studies. Single point CCSD(T) [33] calculations were also carried out to calibrate the MP2 potentials.



The MD simulations were performed in a rectangular cell with the periodic boundary conditions imposed on the three coordinate directions. A total of 256 methane molecules were initially arranged in a face-centered-cubic lattice with a relative configuration like the E conformer. A canonical ensemble (NVT) was used with the temperature control by rescaling the center-of-mass velocities every 1000 time steps. Equations of motion were solved using the velocity-Verlet algorithm with the time step of 1 fs. The system was checked equilibrium after running 20 ps and another 200

ps period (the longest run being up to 1 *ns*) was allowed for data collection. The cut-off radius was set to be half of the box size to avoid long range correlations. The simulated thermodynamic conditions cover a density range of 10-28 *mol/L* and a temperature range of 112-525 *K*, where the experimental data are available.

3. Results and Discussions

A. *Ab initio* calculations

In Fig. 1.3-3 we show the MP2 potentials for the twelve conformers using the aug-cc-pVQZ basis set. We see that the potentials become deeper when there are more inner hydrogen atom contacts between the monomers. It is found that the minimum-energy conformation corresponds to the D_{3d} symmetry configuration (the J conformer), which is consistent with most previous studies. This optimized conformer has been explained in terms of the interplay of the steric stabilization of repulsive hydrogen atoms in opposite monomers [6]. It is interesting to analyze the oriental responses from the repulsive and the attractive components of the potentials separately. Methane is a non-polar molecule and the first nonvanishing electrostatic interaction is the octopole-octopole interaction, which is rather weak and decays fast at large intermolecular separation. The dominant long-range attraction for the methane dimer is thus due to the London dispersion force. On the other hand, the strong

repulsive force almost comes from the exchange-repulsion interaction which can be calculated by the Hatree-Fock (HF) self-consistent theory [34]. Contrasting the HF and the MP2 potentials thus helps to delineate the relative importance of the dispersion energy in the overall intermolecular interactions. In Fig. 1.3-4 we show the HF potentials and the MP2 potentials subtracting the corresponding HF potentials, dubbed as MP2-HF, for the twelve conformers. All the HF potentials are repulsive due to the exchange-repulsion interactions [18]. The MP2-HF potentials largely represent the dispersion curves which are purely attractive. We see larger variations for the repulsive components as compared to the attractive components. For example, at $R=3.8 \text{ \AA}$, the HF potentials (MP2-HF potentials) vary from 0.274 kcal/mol (-0.722 kcal/mol) for the J conformer to 4.405 kcal/mol (-1.992 kcal/mol) for the A conformer. That is to say, compared to the others, the J conformer has actually the weakest attractive but also the weakest repulsive parts. Therefore, it is actually due to the stronger variation in the repulsive interactions, but not due to the stronger attraction as would be intuitively expected, that the J conformer is the most stable methane dimer.

In Table 1.3-1 we present the basis set dependence of several important potential quantities extracted from the MP2 potentials at a series of basis sets. R_0 is the distance at which the potential is zero and can be obtained from a two point interpolation of the

calculated data. The bond length R_m , the binding energy E_b and the intermolecular vibration frequency ω can be obtained through a harmonic modeling of the three lowest potential data near the equilibrium regions. With increasing basis size, the equilibrium bond length converges at the aug-cc-pVDZ basis set to a 0.1 Å accuracy, while a pretty large basis set, aug-cc-pVTZ, is required to converge the binding energy at a spectroscopic accuracy (~ 0.01 kcal/mol). The strong basis set dependence and the slow convergence on the binding energy call for an estimation of the potential features at the complete basis set (CBS) limit. The CBS binding energies can be obtained by an extrapolation scheme with Dunning's basis sets. We consider the methods of Helgaker *et al.* [35], Martin [36], Feller [37] and a numerical extrapolation scheme based on the 3-term Lagrange formula [38] and the MP2/CBS results are listed in Table 1.3-2. We see that using the aug-cc-pVXZ data, the four extrapolation methods yield similar CBS values.

To calibrate the MP2 potentials, we perform single point CCSD(T) calculations at several key structures using the aug-cc-pVQZ basis set. In Table 1.3-3 we show the MP2 and the CCSD(T) potentials of the methane dimer using the aug-cc-pVQZ basis set for the J conformer. The MP2 potential energies near the potential minimum are generally accurate up to 0.05 kcal/mol, as compared to the CCSD(T) energies. The

MP2 interaction potentials at the complete basis set (CBS) limit were estimated using the above four extrapolation methods [35-38] and are shown in Table 1.3-3. We see that the MP2/CBS potential data are very close to (namely, within 0.05 *kcal/mol*) the CCSD(T) potential data.

The full CBS potential curves can also be obtained using a direct extrapolation on the potential data calculated at a series of basis sets for each sampled C-C distance. It is found that the CBS potential curves obtained by the methods of Helgaker *et al.* [35] and Martin [36] are more self-consistent than those using the method of Feller [37], in particular if the cc-pVXZ potential data were used to perform extrapolation. In Fig. 1.3-5 we present the CBS potential curves obtained from the extrapolation method of Helgaker *et al.* [35], using the aug-cc-pVXZ (X=T, Q) potential data.

B. Analytical site-site pair potential model

Representing the potential data by an analytical PES is a not a trivial task but requires the physical understanding of the potential anisotropy. In Fig. 1.3-3 we see strong orientation dependence of the calculated potentials. The high anisotropy of the methane interactions was often ignored in simplified empirical force fields [12]. A closer look at the potential curves reveals interesting interplay among the contact

atoms of methane dimer. First we notice that for the A~F conformers, the A and B, the C and D, and the E and F potential curves are numerically identical, respectively (hence we show only one respective curve of them in Fig. 1.3-3). This indicates that the inner hydrogen-hydrogen (H-H) interactions play a major role, as compared with the outer H-H interactions, in determining the overall interaction energies. Next we observe that the G and H potential curves are almost identical (see Table 1.3-1), which indicates that some compensation among the inner 3-2 hydrogen atoms occurs to allow possible binding configurations. The inner H-H interactions contribute largely the overall binding energies and allow two degenerate 3-2 configurations; namely, the G and H conformers. Due to the large carbon-carbon (C-C) bond distances for these conformers and the possible shielding from the hydrogen atoms, the C-C interactions should play a relatively minor role also, which echoes previous studies [6, 8, 12, 27].

The same reasoning can be used to comprehend the relative stability of the I and J conformers. For the J conformer, the inner 3-3 hydrogen atoms manage to “avoid” each other to reach a more favorable stabilization over the I conformer where the hydrogen atoms “head on”. Similar arguments apply to the K and L conformers also.

We see that the energy curve for the E/F conformer is a little bit lower than what we expected from the above simple model. This is because the E/F conformer is a favorable configuration for the electrostatic octopole-octopole interactions. Therefore,

we conclude that the inner H-H interactions are the major components contributing to the potential anisotropy.

Based on the above observations, an analytical 4-site model was proposed to represent the *ab initio* data. The sites are associated with the hydrogen atoms and this model uses only two parameters. The 4-site model is schematically depicted in Fig. 1.3-6.

This model is very simple and is more suitable for the development of coarse-grained potentials [39-40]. The site-site interaction is represented by a Lennard-Jones (L-J) function.

$$U(r_{ij}) = 4\varepsilon \left[\left(\frac{\sigma}{r_{ij}} \right)^{12} - \left(\frac{\sigma}{r_{ij}} \right)^6 \right] \quad (1)$$

where the indices i and j denote the hydrogen atoms in separated monomers, respectively, and r_{ij} represents the hydrogen-hydrogen distance for a pair of i and j hydrogens. In this model only σ and ε are the potential parameters to be determined.

The total dimer energy is thus

$$U_{total}(R; \Omega) = 4\varepsilon \sum_i \sum_j \left[\left(\frac{\sigma}{r_{ij}} \right)^{12} - \left(\frac{\sigma}{r_{ij}} \right)^6 \right] \quad (2)$$

The total energy as a function of R for different conformer designated by Ω is used to fit the calculated potential data through a nonlinear fitting using the normal Broyden-Fletcher-Goldfarb-Shanno (BFGS) procedure [38]. No bias weights were put on specific configurations except that we excluded the largest repulsive energy points in the regression to prevent their dominance in the least-squares cost function [23]. However, this latter constraint could effectively put more weight on deeper wells. The fitting parameters we obtained are $\sigma=2.67\text{\AA}$ and $\varepsilon=0.054\text{ kcal/mol}$. In Fig. 1.3-7 we present the fitting curves and the *ab initio* data. The *ab initio* data used in the fitting and the fit data are presented in Table 1.3-4. The deviation of the fit data from the *ab initio* data ABS_{per} and ABS_{err} represent the root mean square errors in Table 1.3-5. Notice that the order of the potential data has been correctly represented by the fitting curves, which reflects the above physical arguments. Using Eq. (2) we can generate the six-dimension PES as shown in Fig. 1.3-8. It is seen that the PES reproduces the global features of the *ab initio* potential data reasonably well.

C. Molecular dynamics simulations

We evaluate the PES by running molecular dynamics simulations on it. We calculate the atom-atom radial distribution functions (RDFs) at a specific experimental condition, which is a phase point far from the triple point but close to the melting line.

The RDFs are given by the definition [41-42]

$$g_{\alpha\beta}(r) = \frac{n(r)}{\rho 4\pi r^2 \Delta r} \quad (3)$$

where $g_{\alpha\beta}(r)$ is the radial distribution function for the α - β atom pair, $n(r)$ is the mean number of atoms in a shell of radius r and thickness Δr surrounding the atom, and ρ is the mean density for total system. The calculation of $g_{\alpha\beta}(r)$ consists of about 10000 trials, with each by selecting an α atom as the origin and counting the β atoms within the spherical shells of thickness $\Delta r=0.02\sigma$ using the histogram method. Fig. 1.3-9 presents the simulated atom-atom radial distribution functions for temperature $T=150\text{ K}$ and density $\rho=28.06\text{ mol/L}$ (0.449 g/cm^3). As we can see from the comparison with the experimental data [43], the overall agreement is satisfactory. The peak and valley positions are accurately reproduced for the three RDFs. The peak heights are systematically overestimated partly due to the PES being modeled too deep. On the other hand the close-contact distances are perfectly reproduced which verifies the proper modeling of the strong repulsion parts of the PES.

We have also calculated the self-diffusion coefficients with a wide range of

thermodynamic conditions. The self-diffusion coefficients can be calculated using the Green-Kubo formula [41]

$$D = \frac{1}{3N} \int_0^{\infty} \left\langle \sum_i^N \bar{v}_i(t) \cdot \bar{v}_i(0) \right\rangle dt \quad (4)$$

where \bar{v}_i is the velocity vector of particle i and the statistical average is the velocity autocorrelation functions (VAFs). In Fig. 1.3-10 we show the VAFs for several phase conditions considered in this paper. We see that the VAFs exhibit both gaseous and liquid behaviors. In Table 1.3-4 and in Fig. 1.3-11 we present the comparison of the calculated self-diffusion coefficients with experiments from different research groups [44-45]. In Fig. 1.3-12 and Fig. 1.3-13, we see that to a very wide range of thermodynamic conditions, MD simulations with the *ab initio* PES are capable of reproducing the experimental data within the estimated experimental uncertainties.

4. Conclusion

To simulate fluid methane properties, we have constructed an *ab initio* PES based on a high level, MP2/aug-cc-pVQZ, quantum chemistry calculation of the potential data. The potential data achieve a CCSD(T)/aug-cc-pVQZ level of quality by extrapolating them to the complete basis set (CBS) limit values. The potentials exhibit significant anisotropy, which is analyzed and considered in the 4-site model used to fit the

potential data. We determine the accuracy of the constructed *ab initio* PES using MD simulations and the results are compared with experiments. Quantitative agreements with the observed radial distribution functions (RDFs) and the self-diffusion coefficients have been obtained for a wide range of thermodynamic conditions.

The main source of errors of the constructed PES comes from the analytical representation of the *ab initio* potential data. Our 4-site model is so far the simplest one which is based on the analysis of the strong anisotropy of the calculated potential data. The potential curves for the 12 conformers are treated equally without bias. Certainly this model can be improved in many ways such as by including the C-C and C-H interactions, possibly in combination with rescaled hydrogen sites. The electrostatic terms can also be included for better modeling the E and F conformers. However, these possible extensions should keep the total number of the adjustable parameters as low as possible. Overdosed potential parameters might pose implicit overweight on a particular configuration and thus yield a high sensitivity on the choice of the conformers included in the fitting. Because of the simplicity of the current model, one should be cautious in extending its application to larger alkanes before a better modeling is obtained.

5. Bibliography

- [1] G. Y. Liu, S. Xie, and Y. L. Qian, *Acc. Chem. Res.* **23**, 457 (2000).
- [2] W. Rawicz, K. C. Olbrich, T. McIntosh, D. Needham, and E. Evans, *Biophys. J.* **79**, 328 (2000).
- [3] M. D. Malinsky, K. L. Kelly, G. C. Schatz, and R. P. van Duyne, *J. Am. Chem. Soc.* **123**, 1471 (2001).
- [4] V. R. Cooper, T. Thonhauser, A. Puzder, E. Schroeder, B. I. Lundqvist, and D. C. Langreth, *J. Am. Chem. Soc.* **130**, 1304 (2008).
- [5] D. E. Williams and D. J. Craycroft, *J. Phys. Chem.* **91**, 6365 (1987).
- [6] M. M. Szczesniak, G. Chalasinski, S. M. Cybulski, and S. Scheiner, *J. Chem. Phys.* **93**, 4243 (1990).
- [7] S. Tsuzuki and K. Tanabe, *J. Phys. Chem.* **95**, 2272 (1991)
- [8] J. J. Novoa, M. -H. Whangho, and J. M. Williams, *J. Chem. Phys.* **94**, 4835 (1991)
- [9] S. Tsuzuki, T. Uchimaru, K. Tanabe, and S. Kuwajima, *J. Phys. Chem.* **98**, 1830 (1994).
- [10] J. Nagy, D. F. Weaver, and V. H. Smith, *Mol. Phys.* **85**, 1179 (1995).
- [11] S. Tsuzuki, T. Uchimaru, and K. Tanabe, *Chem. Phys. Lett.* **287**, 202 (1998).
- [12] E. Fraschini and A. J. Stone, *J. Comput. Chem.* **19**, 847 (1998).
- [13] S. Tsuzuki and H. P. Luthi, *J. Chem. Phys.* **114**, 3949 (2001).

- [14] C. Diedrich, A. Luchow, and S. Grimme, *J. Chem. Phys.* **123**, 184106 (2005).
- [15] S. Tsuzuki, K. Honda and T. Uchimaru, and M. Mikami, *J. Chem. Phys.* **124**, 114304 (2006).
- [16] P. Jurecka, J. Sponer, J. Cerny, and P. Hobza, *Phys. Chem. Chem. Phys.* **8**, 1985 (2006).
- [17] S. Tsuzuki, K. Honda and T. Uchimaru, and M. Mikami, *J. Chem. Phys.* **124**, 114304 (2006).
- [18] A. H.-T. Li and S. D. Chao, *J. Chem. Phys.* **125**, 094312 (2006).
- [19] A. H.-T. Li and S. D. Chao, *Phys. Rev. A* **73**, 016701 (2006).
- [20] T. Takatani and C. D. Sherrill, *Phys. Chem. Chem. Phys.* **9**, 6106 (2007).
- [21] D. Frenkel and B. Smit, *Understanding Molecular Simulations* (Academic Press, New York, 2002).
- [22] J. Nagy, D. F. Weaver, and V. H. Smith, *J. Phys. Chem.* **99**, 8058 (1995).
- [23] J. M. Hayes, J. C. Greer, and D. A. Morton-Blake, *J. Comp. Chem.* **25**, 1953 (2004).
- [24] D. H. Gay, H. Dai, and D. R. Beck, *J. Chem. Phys.* **95**, 9106 (1991).
- [25] B. J. Palmer and J. L. Anchell, *J. Phys. Chem.* **99**, 12239 (1995).
- [26] S. Tsuzuki, T. Uchimaru, and K. Tanabe, *Chem. Phys. Lett.* **287**, 327 (1998).
- [27] R. L. Rowley and T. Pakkanen, *J. Chem. Phys.* **110**, 3368 (1999).

- [28] Gaussian 03, Revision D.01, Frisch, M. J. *et al.*; Gaussian, Inc., Wallingford CT, 2004.
- [29] C. Møller and M. S. Plesset, *Phys. Rev.* **46**, 618 (1934).
- [30] R. Krishnan, J. S. Binkley, and R. Seeger and J. A. Pople, *J. Chem. Phys.* **72**, 650 (1980)
- [31] T. H. Dunning, Jr., *J. Chem. Phys.* **90**, 1007 (1989).
- [32] S. F. Boys and F. Bernardi, *Mol. Phys.* **19**, 553 (1970).
- [33] J. A. Pople, M. Head-Gordon, and K. Raghavachari, *J. Chem. Phys.* **87**, 5968 (1987).
- [34] A. Szabo and N. S. Ostlund, *Modern Quantum Chemistry. Introduction to Advanced Electronic Structure Theory* (Dover, New York, 1996).
- [35] T. Helgaker, W. Klopper, H. Koch, and J. Noga, *J. Chem. Phys.* **106**, 9639 (1997).
- [36] J. M. L. Martin, *Chem. Phys. Lett.* **259**, 669 (1996).
- [37] D. Feller, *J. Chem. Phys.* **96**, 6104 (1992).
- [38] W. H. Press, S. A. Teukolsky, W. T. Vetterling, and B. P. Flannery, *Numerical Recipe in C* (Cambridge University Press, Cambridge, 1996).
- [39] S. D. Chao, J. D. Kress, and A. Redondo, *J. Chem. Phys.* **120**, 5558 (2004).
- [40] S. D. Chao, J. D. Kress, and A. Redondo, *J. Chem. Phys.* **122**, 234912 (2005).

- [41] D. C. Rapaport, *The Art of Molecular Dynamics Simulation* (Cambridge University Press, New York, 1995).
- [42] F. Jensen, *Introduction to Computational Chemistry* (Wiley, New York, 1999).
- [43] G. Straub, A. Bassen, H. Zweier, H. Bertagnolli, K. Todheide, A. K. Soper, and J. Turner, *Phys. Rev. E* **53**, 3505 (1996).
- [44] R. Dawson, F. Khoury, and R. Kobayashi, *AIChE J.* **16**, 725 (1970).
- [45] K. R. Harris and N. J. Trappeniers, *Physica A.* **104**, 262 (1980).



	Basis set	R_0 (Å)	R_m (Å)	E_b (kcal/mol)	ω (cm ⁻¹)
A	6-311++G(3df,3pd)	4.43	4.86	-0.135	178.54
	aug-cc-pVDZ	4.48	4.92	-0.128	197.40
	aug-cc-pVTZ	4.40	4.84	-0.143	223.21
	aug-cc-pVQZ	4.40	4.85	-0.143	223.87
B	6-311++G(3df,3pd)	4.43	4.86	-0.135	178.46
	aug-cc-pVDZ	4.48	4.92	-0.128	197.32
	aug-cc-pVTZ	4.40	4.84	-0.143	223.16
	aug-cc-pVQZ	4.40	4.85	-0.143	223.83
C	6-311++G(3df,3pd)	3.94	4.38	-0.260	258.46
	aug-cc-pVDZ	3.99	4.44	-0.236	281.74
	aug-cc-pVTZ	3.91	4.35	-0.279	316.21
	aug-cc-pVQZ	3.91	4.35	-0.284	246.51
D	6-311++G(3df,3pd)	3.94	4.39	-0.260	258.38
	aug-cc-pVDZ	3.99	4.44	-0.236	281.65
	aug-cc-pVTZ	3.91	4.35	-0.279	316.11
	aug-cc-pVQZ	3.91	4.35	-0.285	246.42
E	6-311++G(3df,3pd)	3.72	4.16	-0.332	278.14
	aug-cc-pVDZ	3.78	4.22	-0.298	302.45
	aug-cc-pVTZ	3.68	4.12	-0.361	339.23
	aug-cc-pVQZ	3.69	4.10	-0.369	261.31
F	6-311++G(3df,3pd)	3.72	4.16	-0.333	277.85
	aug-cc-pVDZ	3.78	4.22	-0.298	302.28
	aug-cc-pVTZ	3.68	4.12	-0.362	338.75
	aug-cc-pVQZ	3.69	4.10	-0.369	260.90

TABLE 1.3-1

	Basis set	R_0 (Å)	R_m (Å)	E_b (kcal/mol)	ω (cm ⁻¹)
G	6-311++G(3df,3pd)	3.49	3.93	-0.343	336.05
	aug-cc-pVDZ	3.54	3.98	-0.315	281.42
	aug-cc-pVTZ	3.46	3.89	-0.373	321.83
	aug-cc-pVQZ	3.45	3.88	-0.392	409.38
H	6-311++G(3df,3pd)	3.49	3.93	-0.341	337.19
	aug-cc-pVDZ	3.54	3.98	-0.314	282.51
	aug-cc-pVTZ	3.46	3.89	-0.371	322.99
	aug-cc-pVQZ	3.46	3.88	-0.390	410.82
I	6-311++G(3df,3pd)	3.36	3.78	-0.375	320.17
	aug-cc-pVDZ	3.40	3.83	-0.351	344.56
	aug-cc-pVTZ	3.32	3.74	-0.411	393.15
	aug-cc-pVQZ	3.32	3.74	-0.424	302.08
J	6-311++G(3df,3pd)	3.31	3.73	-0.414	383.78
	aug-cc-pVDZ	3.35	3.78	-0.395	323.88
	aug-cc-pVTZ	3.27	3.70	-0.453	367.15
	aug-cc-pVQZ	3.26	3.68	-0.464	356.38
K	6-311++G(3df,3pd)	3.77	4.21	-0.241	264.72
	aug-cc-pVDZ	3.81	4.25	-0.224	223.25
	aug-cc-pVTZ	3.74	4.17	-0.262	254.58
	aug-cc-pVQZ	3.74	4.15	-0.272	318.44
L	6-311++G(3df,3pd)	3.61	4.06	-0.319	268.66
	aug-cc-pVDZ	3.66	4.11	-0.294	289.26
	aug-cc-pVTZ	3.58	4.03	-0.345	328.33
	aug-cc-pVQZ	3.56	4.01	-0.357	319.84

Table 1.3-1. The basis set dependence of important potential quantities extracted from the MP2 potentials for the 12 conformers. R_0 is the distance at which the potential is zero, R_m is the equilibrium bond length, E_b is the binding energy, and ω is the harmonic frequency.

TABLE 1.3-1 (Cont.)

Extrapolation methods	DT^a	TQ^b	DTQ^c	aDT^d	aTQ^e	aDTQ^f
Helgaker et al.	-0.387	-0.480	¥NA	-0.477	-0.472	¥NA
Martin	-0.376	-0.465	¥NA	-0.473	-0.470	¥NA
Feller	¥NA	¥NA	-0.532	¥NA	¥NA	-0.467
Numerical	¥NA	¥NA	-0.520	¥NA	¥NA	-0.470

^aBasis set limit estimation with the cc-pVXZ(X=D and T).

^bBasis set limit estimation with the cc-pVXZ(X=T and Q).

^cBasis set limit estimation with the cc-pVXZ(X=D, T, and Q).

^dBasis set limit estimation with the aug-cc-pVXZ(X=D and T).

^eBasis set limit estimation with the aug-cc-pVXZ(X=T and Q).

^fBasis set limit estimation with the aug-cc-pVXZ(X=D, T, and Q).

¥ Not available.

Table 1.3-2. The MP2/CBS binding energies using the four extrapolation methods.

TABLE 1.3-2

$R(\text{\AA})$	MP2 (<i>kcal/mol</i>)	MP2 _{CBS} (<i>kcal/mol</i>)				CCSD(T)(<i>kcal/mol</i>)
		Helgaker <i>et al.</i>	Martin	Feller	Numerical	
3.0	1.444	1.351	1.370	1.397	1.329	1.386
3.4	-0.318	-0.344	-0.339	-0.329	-0.345	-0.376
3.6	-0.458	-0.472	-0.469	-0.463	-0.470	-0.502
3.7	-0.464	-0.473	-0.472	-0.470	-0.471	-0.502
3.8	-0.448	-0.455	-0.453	-0.450	-0.452	-0.480
3.9	-0.419	-0.423	-0.422	-0.420	-0.419	-0.448
4.0	-0.384	-0.385	-0.385	-0.384	-0.381	-0.410
4.2	-0.311	-0.310	-0.310	-0.311	-0.305	-0.342
5.0	-0.110	-0.105	-0.106	-0.114	-0.097	-0.130
6.5	-0.012	-0.006	-0.007	-0.019	-0.002	-0.014
9.0	-0.000	-0.000	-0.000	-0.000	-0.000	-0.000

Table 1.3-3. Comparison of the MP2/aug-cc-pVQZ and MP2/CBS potential data with the CCSD(T)/aug-cc-pVQZ data for the J conformer.

TABLE 1.3-3

Density (mol/L)	Temperature (K)	D (EXP) ^a (10 ⁻⁹ m ² /s)	D (MD) (10 ⁻⁹ m ² /s)
10	207	68±7	58.8
10	279	87±9	76.8
10	360	100±10	90.0
10	525	---	112.4
18.5	183	27±3	22.4
18.5	225	32±3	25.7
18.5	306	45±5	31.8
18.5	381	53±5	37.0
25.27	124	7.6±1	6.50
23.26	145	12.1±1	10.17
20.88	162	19±2	15.3
26.5	112	5.4±0.5 ^b	4.76

a. Experimental data from Ref. [43]

b. Experimental data from Ref. [44,45]

Table 1.3-4 Comparison of the experimental (EXP) and molecular dynamics (MD) self-diffusion coefficients for a wide range of thermodynamic conditions.

TABLE 1.3-4

Orientations														
	A	B	C	D	E	F	G	H	I	J	K	L	Mean	σ
ABSper^t	0.206	0.207	0.067	0.067	0.031	0.032	0.022	0.019	0.023	0.022	0.025	0.009	0.061	0.067
ABSper	0.031	0.031	0.022	0.020	0.023	0.020	0.032	0.027	0.038	0.030	0.034	0.025	0.028	0.006
ABSper	0.237	0.237	0.089	0.087	0.054	0.052	0.054	0.046	0.060	0.053	0.059	0.035	0.089	0.068
ABSper^t	Joseph M. Hayes, James C. Greer, David A. Morton-Blaks, <i>J. Comput. Chem.</i> , 25, 1953 (2004)												0.15	0.13
ABSper													0.15	0.04
ABSper													0.15	0.05
Orientations														
	A	B	C	D	E	F	G	H	I	J	K	L	Mean	
ABSerr	0.019	0.019	0.040	0.040	0.013	0.014	0.020	0.020	0.012	0.009	0.041	0.004	0.021	
ABSerr	Joseph M. Hayes, James C. Greer, David A. Morton-Blaks, <i>J. Comput. Chem.</i> , 25, 1953 (2004)												0.113	

$$ABSper = \frac{1}{N} \sum_{i=1}^N \left| \frac{E_{FF} - E_{ai}}{E_{ai}} \right|$$

$$ABSerr = \frac{1}{N} \sum_{i=1}^N |E_{FF} - E_{ai}|$$

Table 1.3-5. The deviation of the fit data from the *ab initio* data. *ABSper*

and *ABSerr* represent the root mean square errors.

TABLE 1.3-5

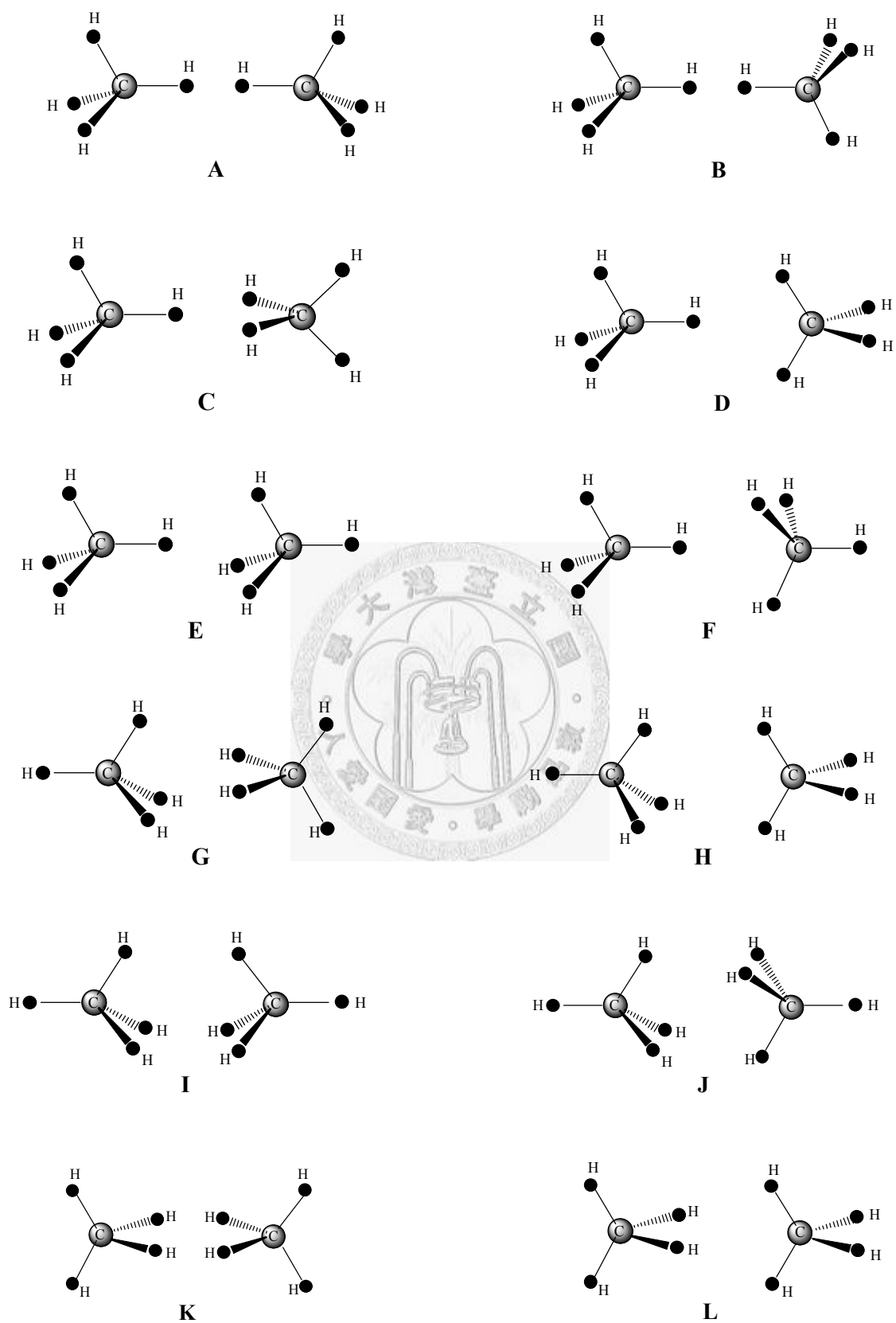


Fig. 1.3-1

FIG. 1.3-1. The twelve symmetric conformers of the methane dimer considered in this paper. We designate each conformer by a representative capital letter from A~L.

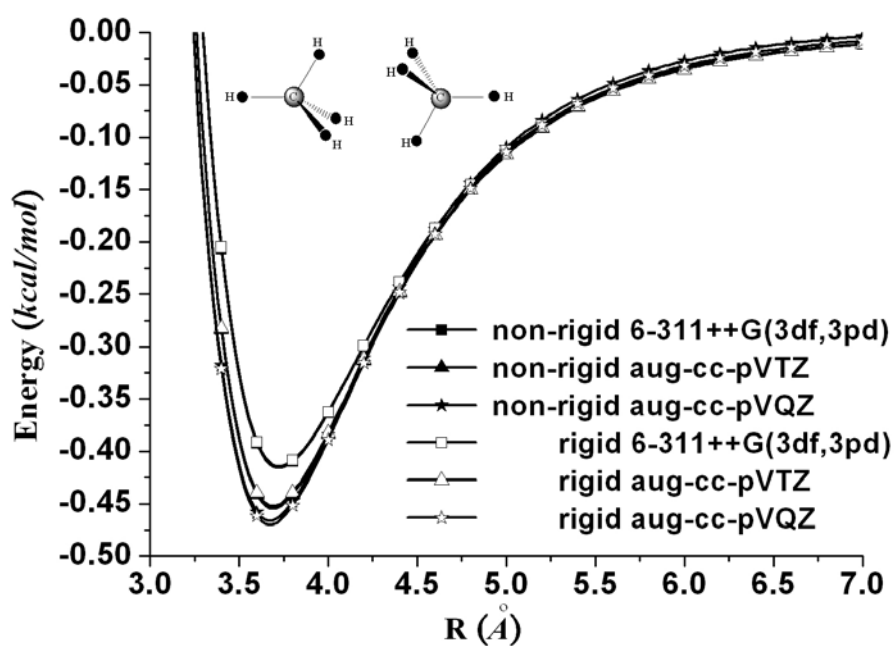


Fig. 1.3-2

FIG. 1.3-2. Comparison of the potentials with (rigid) and without (non-rigid) the rigid monomer assumption for the J conformer. Basis set dependence is also shown as a reference.

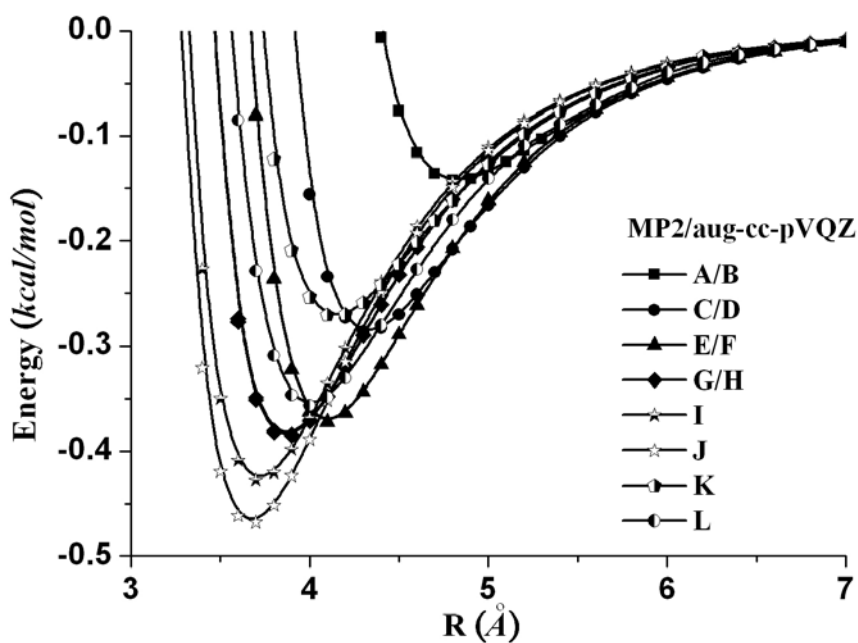


Fig. 1.3-3

FIG. 1.3-3. The MP2/aug-cc-pVQZ potentials of the methane dimer for the 12 conformers. The A and B, the C and D, the E and F, and the G and H potential curves are numerically identical, respectively, so we show only one respective curve of them; A/B, C/D, E/F and G/H, respectively.

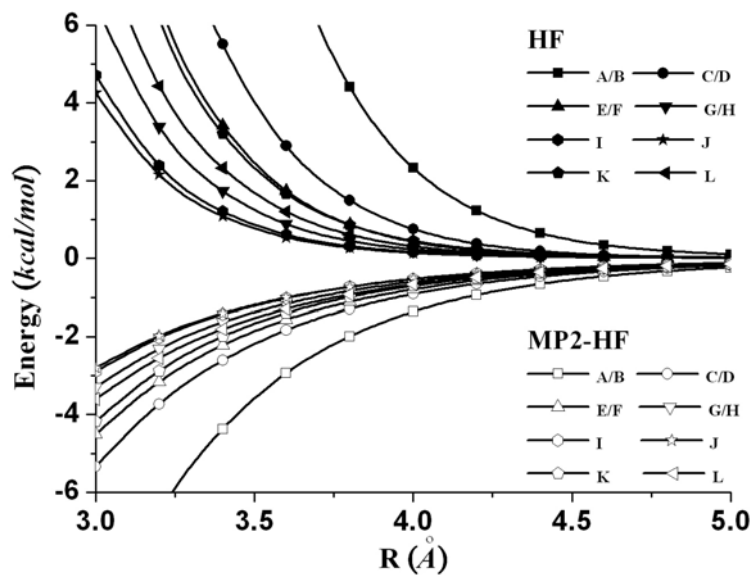


Fig. 1.3-4

FIG. 1.3-4. Comparison of the HF (repulsive) and MP2-HF (attractive) potentials for the 12 conformers.

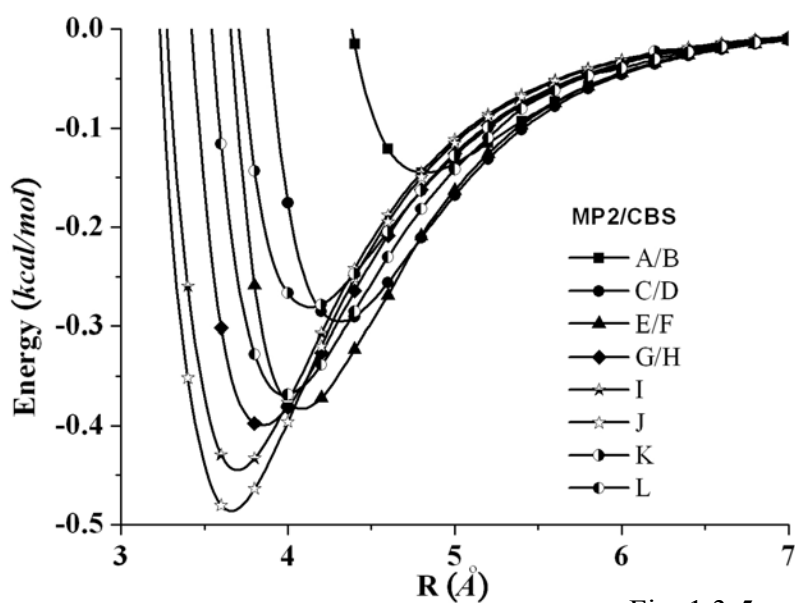
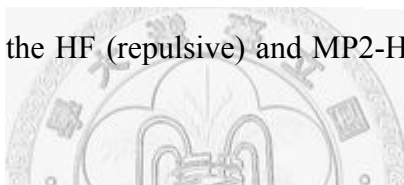


Fig. 1.3-5

FIG. 1.3-5. The MP2/CBS potential curves using the extrapolation method of Halgaker et al. [35].

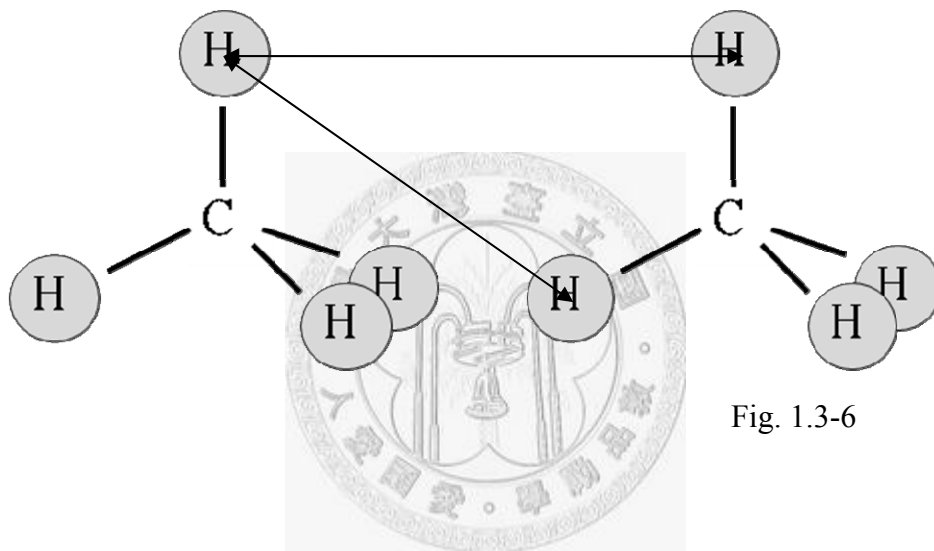


Fig. 1.3-6

FIG. 1.3-6. A schematic plot of the 4-site model where the sites are located at the hydrogen positions only.

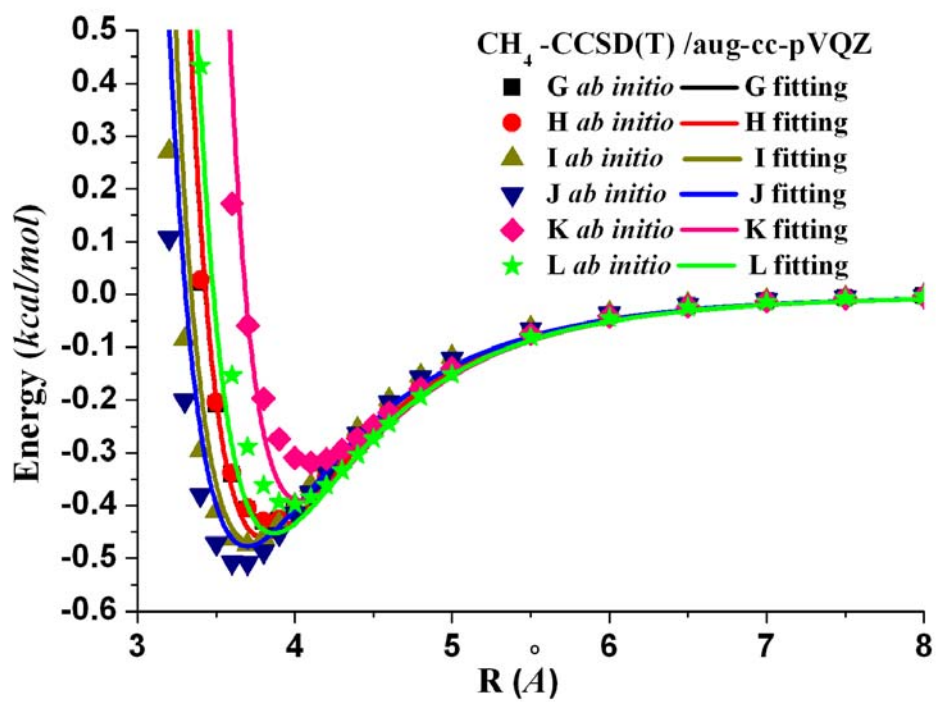
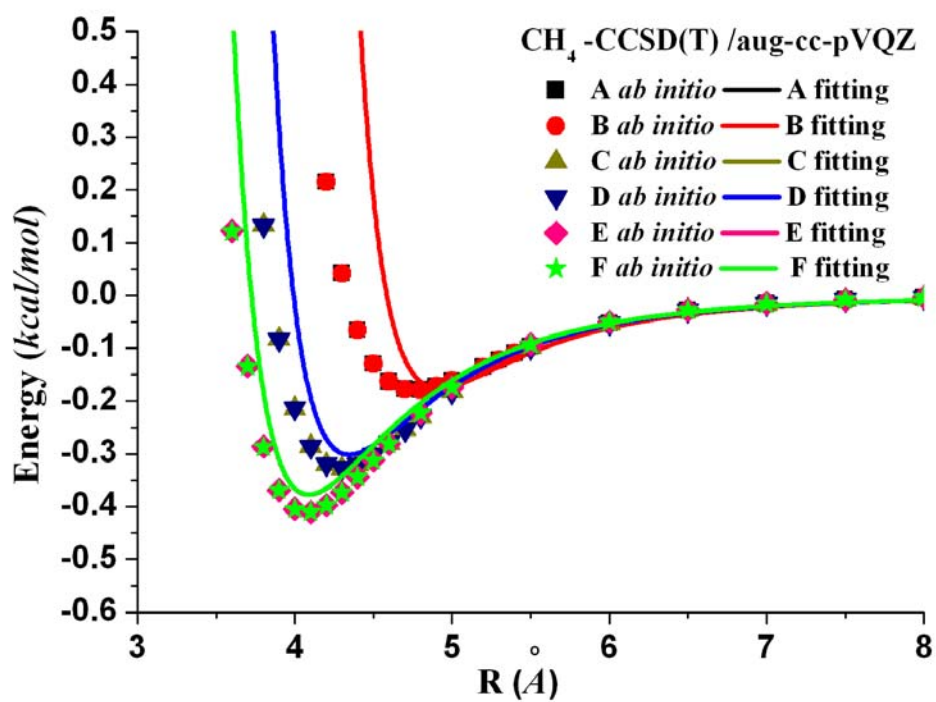


Fig. 1.3-7

FIG. 1.3-7. Comparison of the fitting curves and the calculated potential data.

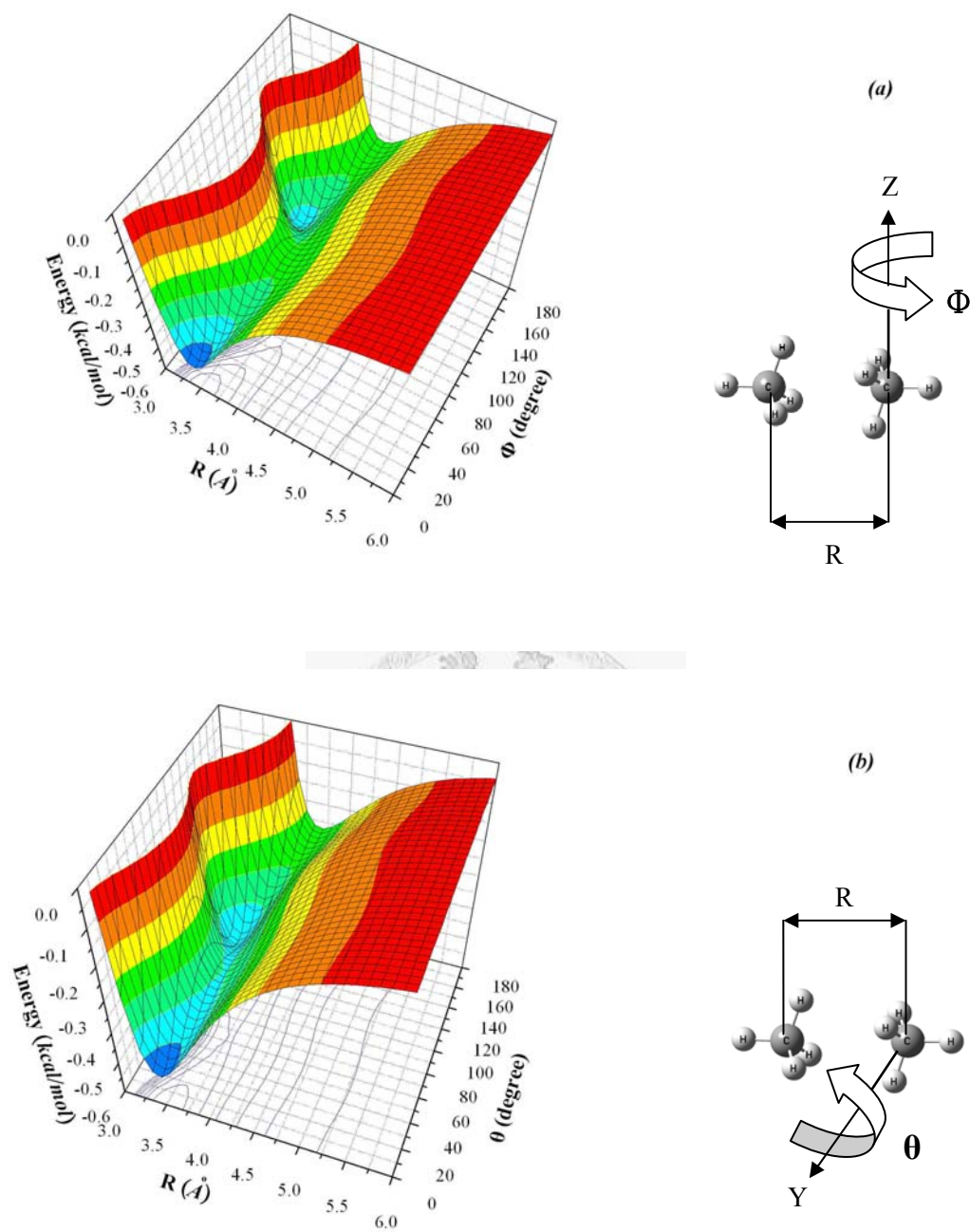
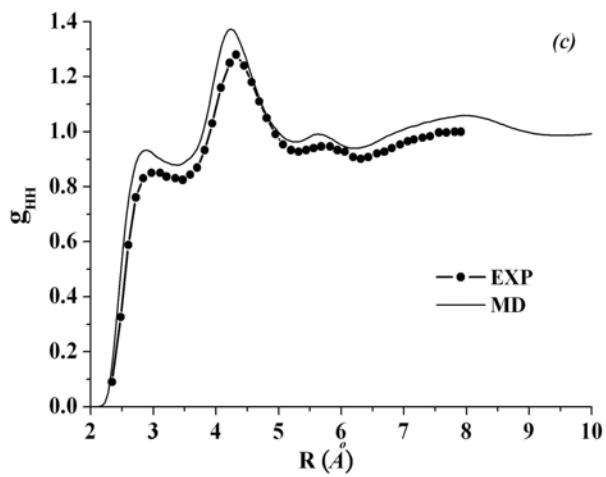
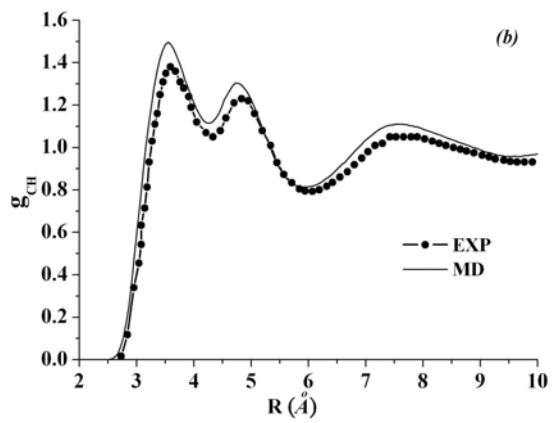
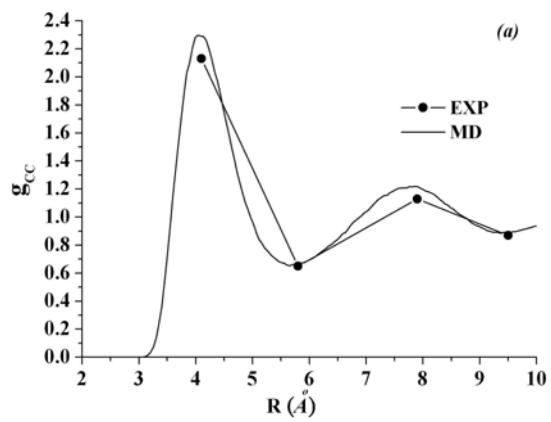


Fig. 1.3-8

FIG. 1.3-8. The six-dimension PES. (a) The PES as a function of R and the rotation angle Φ with respect to the Z axis. (a) The PES as a function of R and the rotation angle Θ with respect to the Y axis.



(d)

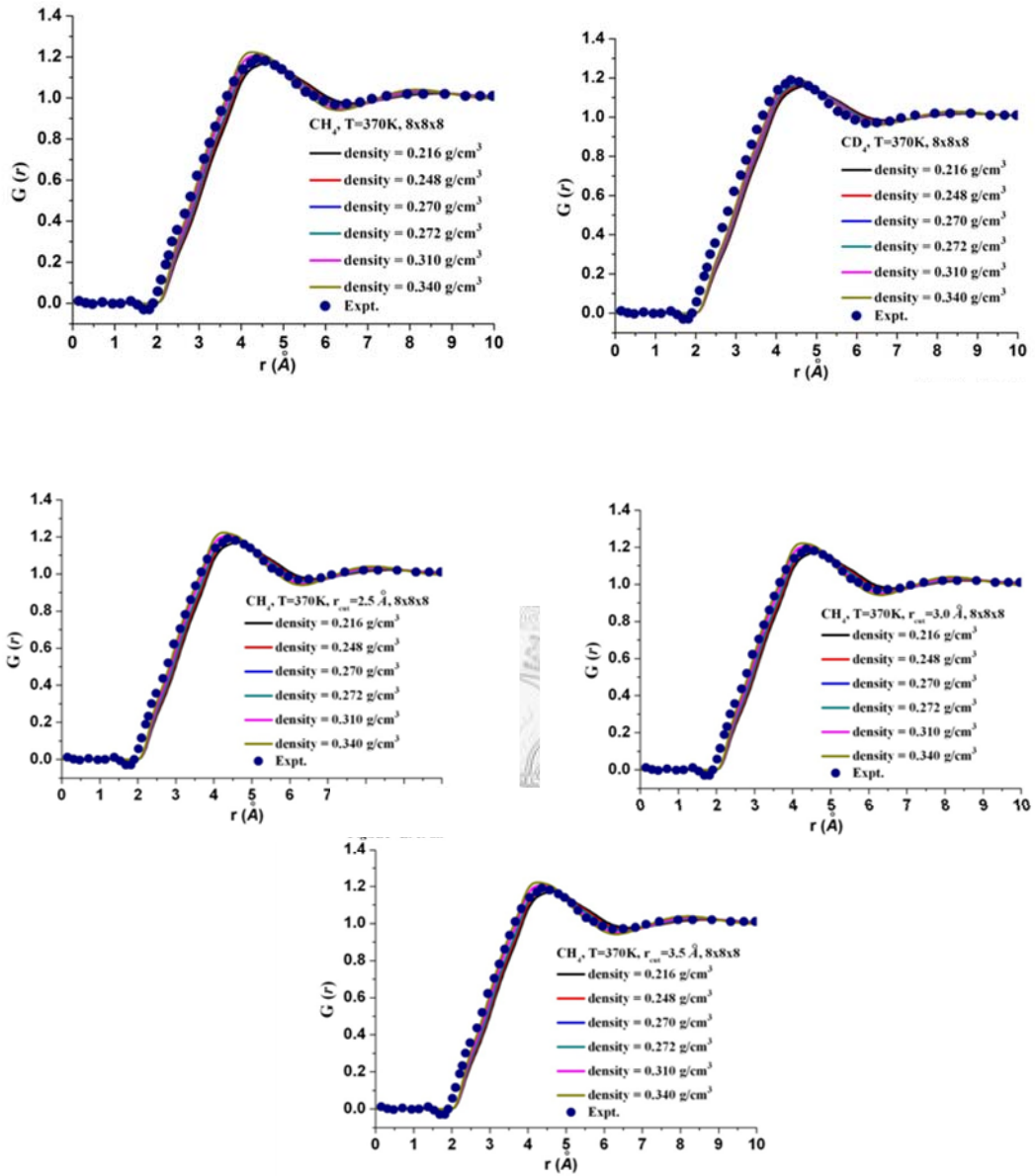


Fig. 1.3-9

FIG. 1.3-9. Comparison of the experimental (EXP) and the molecular dynamics (MD) radial distribution functions (RDFs) as a function of R . (a) The carbon-carbon RDFs g_{CC} . (b) The carbon-hydrogen RDFs g_{CH} . (c) The hydrogen-hydrogen RDFs g_{HH} . (d) The RDFs $g(r)$ of CH_4 and CD_4 in different r_{cut} .

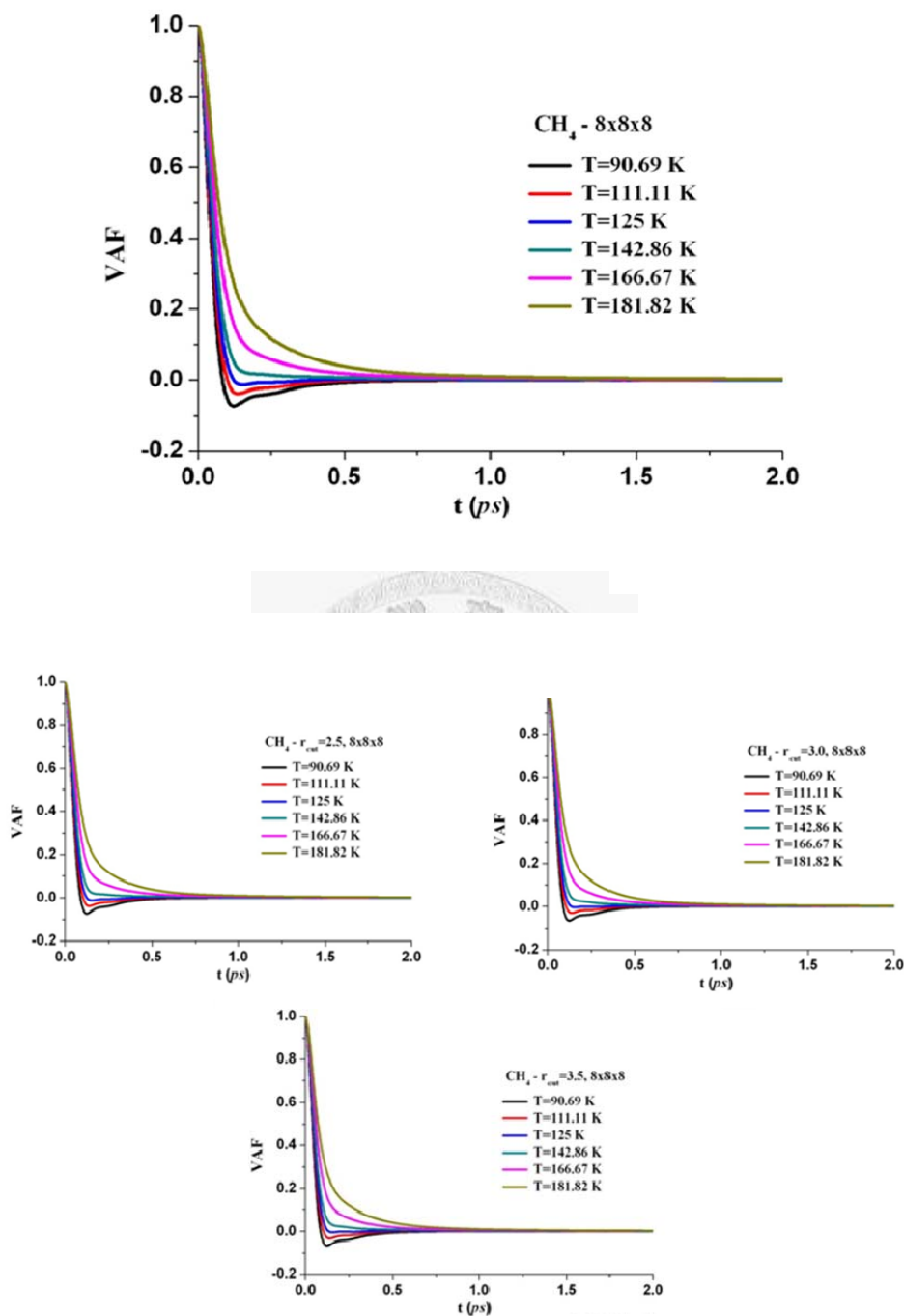


Fig. 1.3-10

FIG. 1.3-10. Velocity autocorrelation functions as a function of time for several experimental conditions. Here T denotes the temperature and ρ denotes the number density.

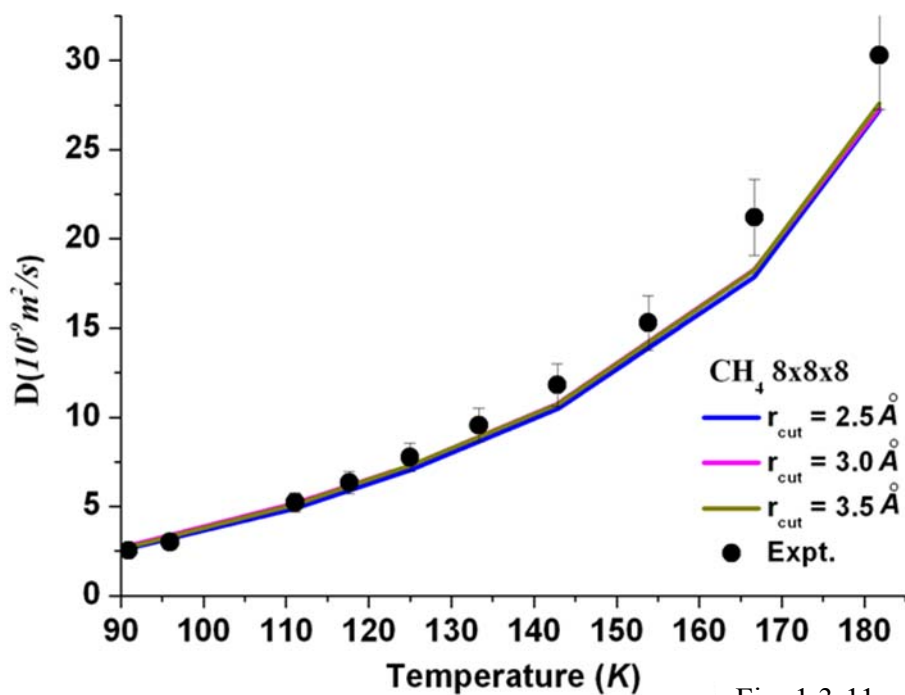
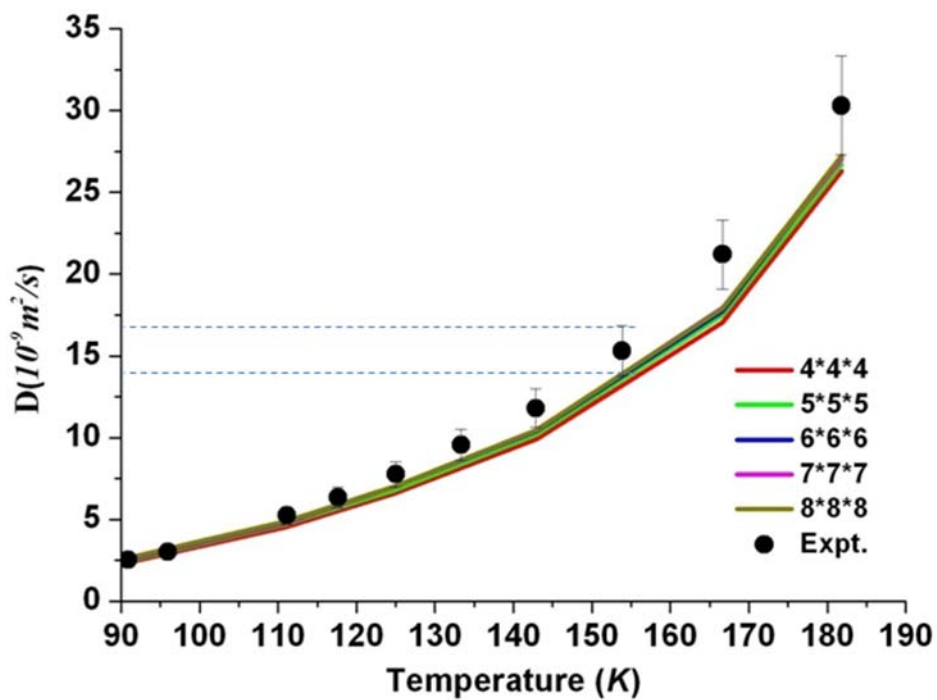


Fig. 1.3-11

FIG. 1.3-11. The diffusion coefficient as a function of temperature for different cell sizes and r_{cut} .

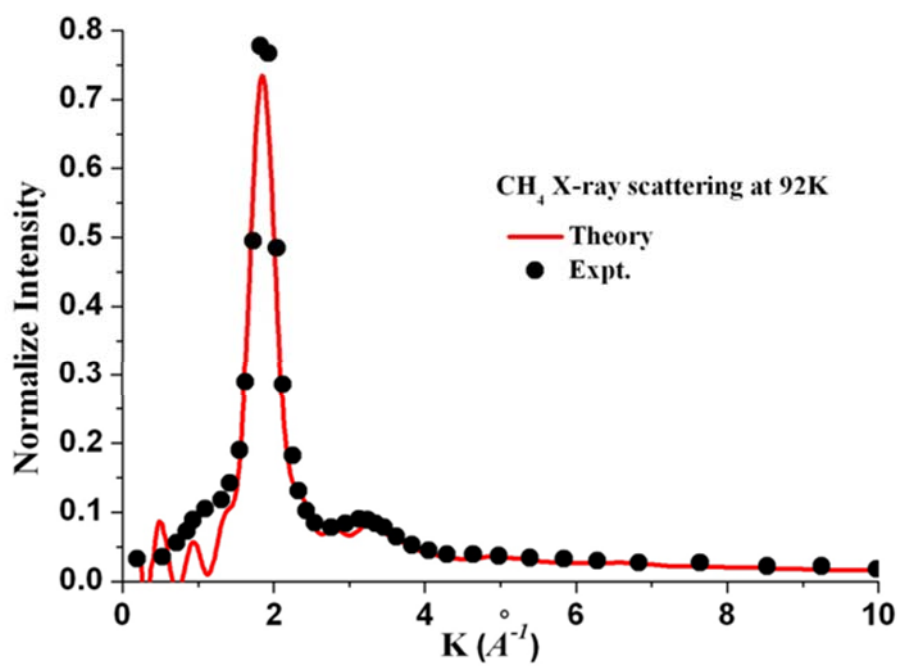


Fig. 1.3-12

FIG. 1.3-12. Comparison of the experimental (EXP) and the molecular dynamics (MD) X-ray scattering as a function of K .

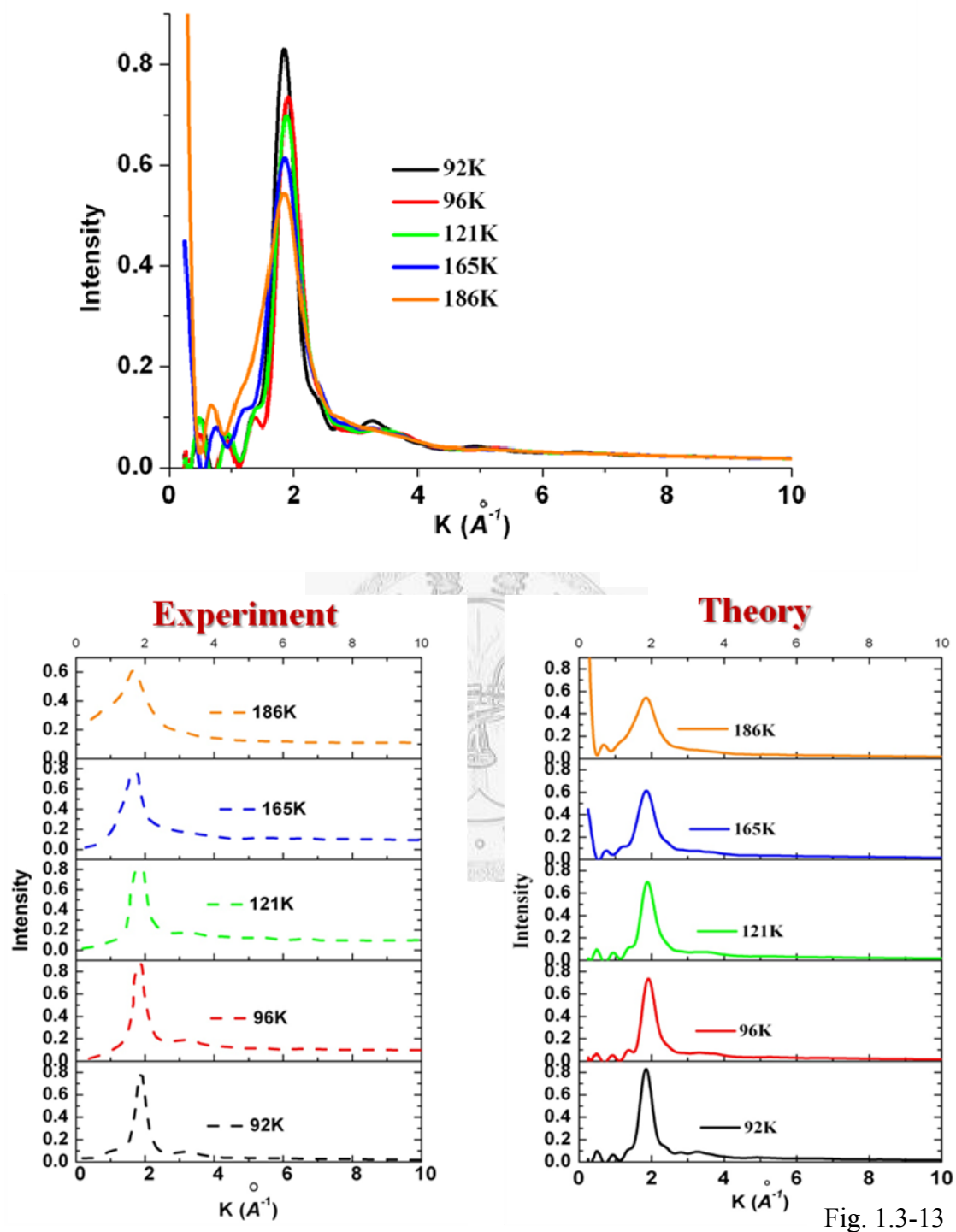


Fig. 1.3-13

FIG. 1.3-13. Comparison of the experimental (EXP) and the molecular dynamics (MD) thermal effect as a function of K .

Chapter 2 Theoretical Studies on the Silane Dimers

2.1 Intermolecular Potentials of the Silane Dimer Calculated with Hartree-Fock Theory, Møller-Plesset Perturbation Theory, and Density Functional Theory

1. Introduction

Accurate determination of intermolecular interaction potentials, or van der Waals interactions, is important in the studies of condensed matter physics, materials chemistry, and structural biology. These interactions are crucial in understanding and predicting the thermodynamic properties of molecular liquids and solids [1], the energy and charge transfers among molecular complexes [2], and the conformational tertiary structures of macromolecules such as protein and DNA [3]. Intermolecular bonds do not originate from sharing of electrons but rather arise from simultaneous electron correlation of the separated subsystems [4] and they are relatively soft and non-rigid as compared to intramolecular covalent bonds. Studies of intermolecular interactions abound [5], but measurements of these interactions are still challenging now [6]. The main difficulty in determining intermolecular interactions experimentally resides at limited samplings of the potential energy surface. For example, experiments using the X-ray crystallography or the laser luminescence spectroscopy mainly explore the equilibrium regions of the potential surface, while thermodynamic measurements in the fluid or solid phase often yield isotropic

potential data without the desired stereo-chemical responses. Moreover, the extracted potentials from experiments sensitively depend on the thermodynamic conditions such as temperature and pressure. Usually two measurements carried out in different conditions cannot be compared directly but rely on auxiliary theoretical modeling.

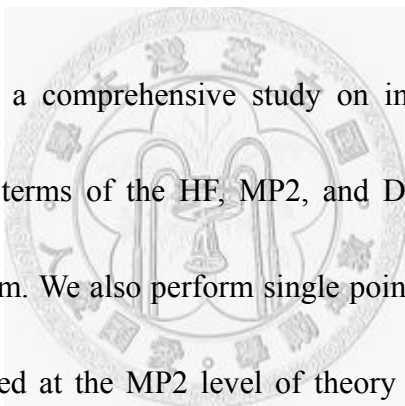
It is now well recognized that intermolecular potentials can be calculated in terms of correlation-corrected quantum chemistry methods [7-9] or density functional theory (DFT) [10-11] with improved generalized gradient approximation (GGA) functionals.

These calculations are normally done with the supermolecular scheme in which the intermolecular potential is defined as the total energy difference between the supermolecule and the isolated subsystems. In practice, the London dispersion force is the most difficult to calculate due partly to its small magnitude. Because the Hartree-Fock (HF) self-consistent method cannot calculate the dispersion force, an electron correlation-corrected method and a large basis set are required to obtain accurate dispersion forces [12]. We note that many computational chemistry programs utilize Gaussian type functions to fasten the calculations of Coulomb repulsion integrals. Because Gaussian type functions are local functions, a large basis set is indispensable to calculate the correlation energy. Moreover, these functions do not have the correct asymptotic behavior of the atomic orbitals. Therefore, the basis set

limit of the calculated potential must be estimated so as to be consistent with the conventional perturbation theory based on separated molecules.

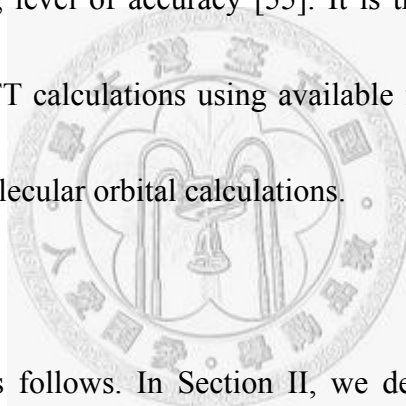
Because the dispersion energy is relatively weak, nonpolar atomic and molecular dimers are usually taken as a prototype case to study the dispersion energy. There have been many studies on atomic inert gas dimers which serve as a stepstone to study more complex potential landscapes of molecular dimers [13]. However, there are comparatively fewer studies on molecular dimer systems. Thanks to the extra degrees of freedom and the stereo-chemical responses, new insights may need to be developed in dealing with molecular dimers. In a previous study [14], we have thoroughly calculated the interaction potentials of the methane dimer. Methane is a non-polar molecule with a leading nonvanishing octopole-octopole interaction and the dominant long-range attraction is thus due to the London dispersion force. Therefore, the study of the methane dimer is a good starting point to investigate the various factors affecting the calculations of the dispersion force, such as the level of the theory, the basis set dependence, and the inclusion of the basis set superposition error (BSSE) corrections. Silane, due to its structural similarity to the methane, is another candidate to perform a prototype study. Besides, silane is a commonly used chemical in semi-conductor engineering processes such as the low-pressure vapor deposited

thin-film fabrication process in a microelectromechanical system (MEMS) [49]. High pressure silane crystals could be a good system to demonstrate the insulator-conductor transition in modern solid state physics [15]. Although the interaction potentials of the methane dimer have been studied extensively, there have been relatively few *ab initio* studies on the interaction potentials of the structurally similar silane dimer. In fact, it is the case that only until very recently a reasonably well designed quantum chemistry study of the intermolecular interactions of the silane dimer was reported [16].



In this paper we perform a comprehensive study on interaction potentials of the prototype silane dimer in terms of the HF, MP2, and DFT methods to gain better understanding of this system. We also perform single point CCSD(T) calculations for the key structures calculated at the MP2 level of theory to calibrate the correlation effect. The purpose of this paper is to use the state-of-the-art methodology to obtain accurate potential energies for the silane dimer. We would like to study the effect of including the BSSE on the calculated intermolecular interactions. The basis set effects on repulsion exponents, equilibrium bond lengths, binding energies, and asymptotic coefficients of the calculated intermolecular potentials are thoroughly studied. This is achieved using basis sets from STO-3G [17] to aug-cc-pVQZ [19] with the basis number from 26 to 536, respectively. The full potential curves are presented in order

to see the overall scope of the potential. In particular, both the BSSE corrected and uncorrected results are presented to emphasize the importance of these corrections. Moreover, in this paper we will assess the utilities of using the available implementation of the density functional theory in determining the intermolecular interactions. From the studies of atomic dimers, it has been found that conventional exchange-correlation functionals based on the local density approximation (LDA) and generalized gradient approximation (GGA) cannot calculate the intermolecular interactions to a satisfying level of accuracy [55]. It is thus desirable to investigate that to what extent the DFT calculations using available functionals can serve as an alternative for *ab initio* molecular orbital calculations.



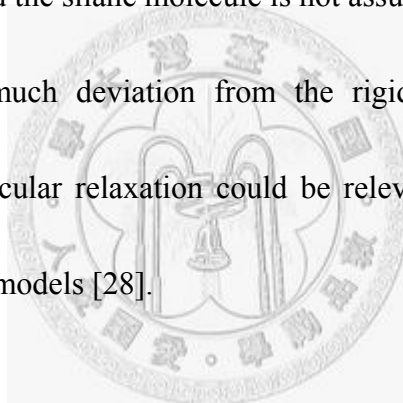
The paper is organized as follows. In Section II, we describe the details of these calculations. In Section III, the results are presented and discussed. A summary is given in Section IV.

2. Methods and Calculations

Similar to the methane dimer, a large part of the exchange-repulsion interactions of the silane dimer can be calculated by the HF method. The calculation of electron correlation energies depends on the level of the correlation-corrected method, the size

of the basis set, and the correction of the BSSE. The state-of-the-art choice of the correlation-corrected method is either the Møller-Plesset (MP_x, x=2,3,4) perturbation method [20] or the coupled cluster method with iterative single and double substitutions and with noniterative triple excitations [CCSD(T)] method [21]. Many studies showed that the MP2 results for alkane dimers would not be too much different from those calculated by the much more expensive CCSD(T) method as long as a large basis set has been used [22]. To calibrate the correlation effect, several single point CCSD(T) calculations for the key structures calculated at the MP2 level of theory have been performed. To study the basis set effects, we have employed comprehensive basis sets from the Slater-type orbitals fitted with Gaussian functions (STO-nG, n=3~6) [17], Pople's medium size basis sets [up to 6-311++G (3df, 3pd)] [18] to Dunning's correlation consistent basis sets (aug-cc-pVXZ, X=D, T, Q) [19]. The basis set superposition error (BSSE) was corrected by the counterpoise (CP) method of Boys and Bernardi [23]. The MP2 interaction potentials at the basis set limit have been estimated using the methods of Martin [56], Helgaker *et al.* [24] and Feller [25] and a numerical extrapolation scheme based on the Lagrangian formula [26]. The other potentials parameters at the basis set limit are estimated using the numerical extrapolation.

All the HF, MP2, and DFT calculations are performed using the Gaussian 03 program package [27] on a single node two-processor AMD 250 PC cluster with distributed memory. The equilibrium geometry of a single silane molecule was first optimized at the MP2/6-311++G (3df,3pd) level of theory. Subsequently the Si-Si distance was sampled in a step of 0.1 Å for a quite large range of intermolecular separation (normally 3~9 Å), resulting in a total of 61 configuration points. During the scan we allow the individual silane molecule to be fully relaxed. This means that we do not fix the monomer geometry and the silane molecule is not assumed to be rigid. Although it is not expected to see much deviation from the rigid molecule approximation, inclusion of the intramolecular relaxation could be relevant to molecular dynamics simulations using flexible models [28].



From a previous energy dissection method [57], it is found that for a general tetrahedral molecule (such as methane and silane) either the D_{3d} or the C_{3v} conformer would be possibly the most stable conformer. We have thus first calculated the potential interaction energies for these two conformers at the MP2/aug-cc-pVTZ level of theory. In Fig. 2.1-1 we show the comparison of the potential curves for the D_{3d} and the C_{3v} conformers. As can be seen, the D_{3d} conformer is more stable than the C_{3v} one. Therefore, we will focus on the D_{3d} conformer in this paper.

3. Results and Discussions

The intermolecular interaction potentials of the D_{3d} conformer of the silane dimer have been calculated with the HF, MP2, and DFT methods. We present the results respectively along with discussions and make comparisons among the results.

A. Hartree-Fock self-consistent field calculations

The BSSE corrected HF interaction potentials of the silane dimer using several basis sets are shown in Fig. 2.1-2. The HF calculations yield purely repulsive potentials without minima for all the basis sets used. This can be attributed to the rather weak electrostatic interaction for the silane dimer. In the short range, the strong exchange-repulsion interaction dominates with little alternation from the electrostatic and induction attractions. The HF potential is insensitive to the basis size as long as the 6-31G** basis set has been used. We can model the HF potential using the repulsive Buckingham function [29]

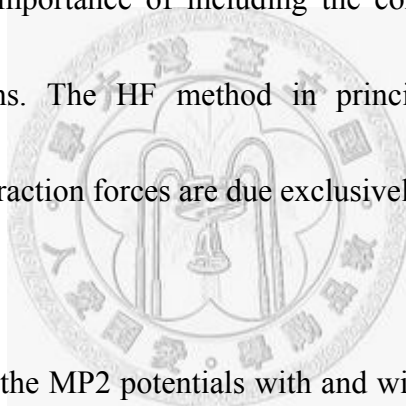
$$V_{HF}(R) = Ae^{-\alpha R} \quad (1)$$

where R is the Si-Si distance, A and α (the repulsion exponent) are the fitting parameters. The dependence of the repulsion exponent on the basis size is shown in Table 2.1-1. It is seen that the repulsion exponent converges quickly after the 6-31G**

basis set being used.

B. MP2 calculations

Unlike the HF potentials, the MP2 potentials shown in Fig. 2.1-3 display clear minima and long-range attractive potential tails. Because the contributions from the electrostatic interactions are small, the dispersion energy is mainly responsible for the attractions. The sharp differences between the HF calculations and the MP2 calculations indicate the importance of including the correlation corrections in the wave function calculations. The HF method in principle does not include the correlation effect so the attraction forces are due exclusively to the correlation effect.

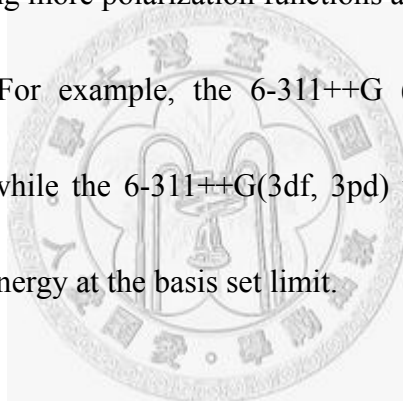


In Fig. 2.1-3, we compare the MP2 potentials with and without the BSSE corrections (denoted as CP and NCP, respectively). We see very strong dependence of the interaction potentials on the BSSE corrections. The potentials without the BSSE corrections fluctuate with increasing basis size and do not systematically converge to the expected curve at the basis set limit. On the contrary, the BSSE corrected potentials systematically approach to the expected curve with increasing basis size. Therefore, the BSSE correction must be considered in calculating the intermolecular interactions, in particular for small basis sets.

The strong basis set dependence and the slow convergence on the dispersion coefficients require an estimation of the important potential features at the basis set limit in a calculated potential. Basis set limit of the binding energy can be approached using Dunning's basis sets with an extrapolation scheme. We consider three analytical schemes [56, 24, 25] and a numerical scheme [26] while the results are similar. The binding energies obtained at the basis set limit (using Dunning's basis sets, aug-cc-pVXZ, X=D, T, Q) are 0.597, 0.601, 0.590, and 0.603 *kcal/mol* using the methods of Martin [56], Helgaker *et al.* [24] and Feller [25] and the numerical method [26], respectively. For the other potential parameters, we used the numerical extrapolation based on the vanishing inverse of the number of basis function [26]. These results are shown in Table I for comparison.

As shown in Table 2.1-1, the basis set effect on the BSSE corrected interaction potentials is significant. The STO-3G basis set yields a very small binding energy. The interaction energy becomes more accurate as one adds polarization functions and augments diffuse functions in the Pople's basis sets. Small cc-pVDZ and cc-pVTZ basis sets lead to underestimated binding energies and it requires cc-pVQZ to obtain a result with an accuracy of 0.1 *kcal/mol*. Augmentation of the diffuse functions has

significant effect on optimizing the binding energy. The cc-pVTZ basis set underestimates the energy by 40%, while the aug-cc-pVTZ basis set underestimates only 9% of the binding energy. Some subtle basis set features can also be observed. For small basis sets, adding polarization functions to the basis set does not significantly change the potential. On the other hand, augmentation of the diffuse functions has pretty significant effect. For example, the aug-cc-pVDZ energy is very close to the high level 6-311++G (3df, 3pd) and the cc-pVQZ results. Together with the diffuse functions, adding more polarization functions also improve the accuracy of the calculated potential. For example, the 6-311++G (2d,2p) underestimates the binding energy by 50%, while the 6-311++G(3df, 3pd) yields a binding energy by 25% lower than the MP2 energy at the basis set limit.



With the wide span of the basis sets used, the basis set dependence of important potential parameters can now be fully studied. In Table 2.1-1 we present the BSSE corrected data for the equilibrium bond length, the binding energy, and the asymptotic behavior. R_0 is the distance at which the potential is zero and can be obtained from a two point interpolation of the calculated data. The bond length R_m , the binding energy E_b and the intermolecular vibration frequency ω can be obtained through a harmonic modeling of the three lowest potential data near the equilibrium regions. C_6 and C_8 are

the dispersion coefficients and can be obtained through a nonlinear fitting of the long-range potential data. With increasing basis size, the equilibrium bond length converges at the 6-311++G(3d,3p) basis set to a 0.2 Å accuracy, while a pretty large basis set (aug-cc-pVTZ) is required to converge the binding energy at a chemical accuracy (~ 0.05 kcal/mol). On the other hand, up to the largest basis set used, the asymptotic behavior has not yet converged to the expected C_6 value from the calculated monomer polarizability (~ 4734.47 kcal/mol Å⁶) [30-32]. It is well known that the long range interactions can be represented by an infinite series involving higher order terms C_8 , C_{10} , etc. Inclusion of the higher order term is important if shorter range data were used for the modeling. For example, as shown in Fig. 2.1-4, the long-range curve can be reproduced better by including the C_8 term. Similar to our previous study on the methane dimer [14], we attribute the slow convergence partly to the inefficacy of using the MP2 method with Gaussian functions to calculate long-range interactions. Therefore, the basis set limit of the calculated potential must be estimated so as to be consistent with the conventional perturbation theory. Together with the nonlinear scaling of the computational cost with respect to the basis size, this is actually the main practical reason for the difficulty of obtaining dispersion interactions through *ab initio* molecular orbital methods. Also notice that the magnitude of the vibration frequency ($\omega \sim 294$ cm⁻¹ calculated with MP2/aug-cc-pVQZ)

can contribute significantly to the zero-point-energy correction of the binding energy.

This anharmonicity in the intermolecular vibrational motion should be taken into account in analyzing spectra involving van der Waals complexes [58].

To calibrate the correlation effect, we perform single point CCSD(T) calculations at several key structures (one at the repulsion region, three at the minimum region, and one at the asymptotic long range region) using the basis set up to aug-cc-pVTZ. As shown in Table 2.1-2, the MP2 results are generally accurate up to 0.1 *kcal/mol*, as compared to those calculated with the CCSD(T) method. The basis set limits of the binding energy have also been obtained using several analytical and numerical extrapolation methods. The results using different extrapolation methods are close to each other within the 0.1 *kcal/mol* accuracy. The same level of accuracy has also been found before for the methane dimer case [22].

C. Density functional theory

We have examined the basis set effect on the DFT potentials in a similar manner as in the HF and MP2 calculations (see Fig. 2.1-5). We found that in general the DFT potentials converge at a larger basis set than the HF potentials but at a smaller basis set than the MP2 potentials. Therefore, only the 6-311++G (3df,3pd) basis set is used

to obtain the DFT potentials which are compared to the MP2 potentials calculated at the same basis set.

The density functionals used in the present work include the 108 combinations chosen among 9 exchange (B88 [33], OPTX [34], MPW [35], PBE [36], PW91 [37], TPSS [38], Slater [39], HCTH [40], and XAlpha [41]) and 12 correlation (TPSS [38], PBE [36], PW91 [37], P86 [42], HCTH [40], VWN5 [43], PL [44], VWN [43], LYP [45], HCTH93 [46], and HCTH147 [46]) functionals. We intend to examine the relative performance of the chosen exchange and correlation functionals in determining the interaction potentials for the silane dimer. The chosen functionals are selective representations of the most commonly used density functionals for van der Waals interactions in current literature. Our previous studies showed that several functionals could yield reasonable binding energies of the methane dimer interaction [14]. In this study we would like to check the applicability of these functionals for the silane dimer.

In Table 2.1-3 we show the bond lengths from the calculated DFT potentials using the 108 exchange-correlation functionals, displayed as the row and the column items, respectively. Roughly the bond lengths descend across the row and down the column.

Compared with the MP2 result (4.25 Å), we find the TPSSHCTH and MPWHCTH93 functionals yield a value (4.22 Å) close to the MP2 result. Other candidates are marked in boldface in Table III. Table IV presents the calculated binding energies using the 108 exchange-correlation functionals in a particular order. In this order, the (negative) DFT potentials descend across the row and down the column. The results clearly demonstrate the relative performance of the exchange and the correlation functionals in the DFT calculations. By fixing the PW91 as the exchange functional, for example, all correlation functionals yield bound potentials. On the other hand, by fixing the PW91 as the correlation functional, the varying exchange functionals much underestimate or overestimate the binding energy. One of the combinations, OPTXHCTH147, yields a binding energy (-0.443 kcal/mol) close to the MP2 result (-0.454 kcal/mol). Other candidates yielding better results include the PBEVP86, PBEP86, PW91TPSS, PW91PBE, and PW91PW91 functionals. Previous studies on van der Waals systems [47] have shown that the exchange functional plays an essential role in determining the binding energy while the correlation part of a density functional does not significantly affect the DFT calculations. Our results are consistent with the former observation, while we see appreciable effects due to the choice of the correlation functional. It is also found that the calculated binding

energies are related to the large reduced density gradient, $s = \frac{|\nabla\rho|}{2(3\pi)^{1/3}\rho^{4/3}}$, ρ

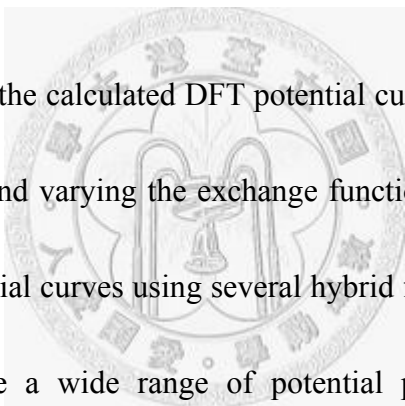
being the density, of the GGA enhancement factor [47]. However, for dispersion interactions, a large s actually means a low density because the electron overlapping is relatively small. To further analyze the calculated results, we examine the large s behavior of the GGA enhancement factors at the low density region.

The performance of varying the GGA exchange functionals for a fixed correlation functional has been related to the behavior of the GGA enhancement factor $F_X(s)$ of the exchange functional for the large reduced density gradient region [47]. On the other hand, the performance of varying the GGA correlation functionals for a fixed exchange functional has not been well recognized. For low density and large s , the contribution of correlation energy becomes significant [36]. In Table IV we see that for a fixed exchange functional, it may amounts to a wide range of binding energies by varying the correlation functional. Because most GGA correlation functionals use the LDA correlation as an additive ingredient in the definition, to clearly show the nonlocal effect, an enhancement factor is defined by

$$F_C(s, r_s) = 1 - \frac{\varepsilon_C^{GGA}}{\varepsilon_C^{LDA}} \quad (2)$$

where ε_C^{GGA} and ε_C^{LDA} are the correlation potentials for the GGA and the LDA energy functionals, respectively. The correlation enhancement factor depends on s and r_s , where $r_s = (3/4\pi\rho)^{1/3}$ is the Wigner-Seitz radius. For van der Waals interactions, r_s

falls in the range of 5~20. By fixing $r_s = 10$, we plot the enhancement factor $F_C(s)$ as a function of s in Fig. 2.1-6. We see in Fig. 2.1-6 that the order of the magnitude of $F_C(s)$ at medium s is TPSS > PBE > PW91 > P86 > HCTH. Interestingly, this order is essentially the order of the binding energies calculated by the corresponding functionals across the row in Table 2.1-4. These observations clearly show that the DFT binding energies are correlated to the exchange and the correlation enhancement factors at the low density region.



Figs. 2.1-7(a)-7(e) present the calculated DFT potential curves by fixing 5 correlation functionals, respectively, and varying the exchange functions used in this paper. Fig. 2.1-7(f) presents the potential curves using several hybrid functionals. We see that the DFT calculations generate a wide range of potential patterns. Some are purely repulsive (such as B88PBE), while others could be over-bounded (such as XAlphaVP86). These diverse patterns have been found before and have often been termed “unsystematic”. From our analysis, it is clear that some compensation among the respective exchange and correlation functions must occur to yield a reasonable potential well depth close to the MP2 result. For the silane case, OPTXHCTH147 seems to achieve such appropriate compensation and thus yields a better result. However, exactly which combination should be used for a specific system is unknown

a priori. It is hoped that the interesting correlation between the calculated results and the exchange and the correlation enhancement factors shown in Table 2.1-4 can provide a useful reference for choosing such a combination.

Finally we would like to discuss the asymptotic behaviors of some selective DFT potentials and compare them with those obtained from the MP2 reference potential. It is often iterated that a DFT potential cannot be used to model the long-range tail of the van der Waals interaction. However, exactly how bad the situation is for a specific DFT potential has not been systematically studied due partly to insufficient long-range potential data. Fig. 8 displays the linear analysis of the potential curves by plotting $\ln(-V)$ versus $\ln(R)$, where V is the (negative) potential energy by subtracting the HF potential (which is purely repulsive) from the DFT potential and R is the Si-Si distance. The data for $R > 5\text{\AA}$ have been used to perform this analysis. Notice that the MP2 potential yields a straight line. Generally the DFT potentials yield erratic long-range behaviors. The deviation from the straight (MP2) line indicates the inefficacy of the DFT potentials. This verifies that DFT potentials calculated using most of the LDA and GGA functionals cannot be used to model the dispersion interactions, in particular at long-range regions [48]. In this regard, one might resort to other recent approaches to calculate the long-range dispersion interactions [50-54].

4. Conclusion

In this paper we have systematically studied the calculated intermolecular potentials of the silane dimer at D_{3d} conformation using the HF, MP2, and DFT methods. A wide selection of basis sets has been employed in order to determine the basis set effects on the repulsion exponent, the binding energy, the equilibrium bond length, and the asymptotic behavior of the intermolecular potentials. BSSE corrections are considered as an important factor affecting the quality of the calculated potentials.

From this study and our previous studies [14, 48], we can draw several useful conclusions about using the current theoretical methods to generate the intermolecular potentials of nonpolar molecular dimers.

- (4) The HF calculations yield purely repulsive potentials for nonpolar molecular dimers. This is due to the small electrostatic interactions. The basis size effect of the HF calculations is very small as long as the 6-31G** basis set has been used. The HF method can be used to calculate the exchange-repulsion interactions.
- (5) The potential energy minima can be well produced using the MP2 method. The BSSE corrections must be considered to yield systematic results. Basis set effects are significant for many important potential parameters such as bond lengths,

binding energies, and dispersion coefficients. Small basis sets, especially without the augmentation of diffuse functions, could produce a severe underestimation of the binding energy and an overestimation of the bond length.

(6) The DFT potentials display a diverse range of patterns of potential curves, underestimating or overestimating the binding energy. Some functionals do capture partly the correlation effects. For the silane dimer, the binding energies calculated using the OPTXHCTH147, PBEVP86, PBEP86, PW91TPSS, PW91PBE, and PW91PW91 functionals and the equilibrium bond lengths calculated using the MPWHCTH93, TPSSHCTH, PBEVP86, PBEP86, PW91TPSS, PW91PBE, and PW91PW91 functionals are close to the respective MP2 results. The calculated binding energies can be correlated to the asymptotic behaviors of the exchange and the correlation enhancement factors at the low density region. The long-range DFT potential data cannot be used to model dispersion interaction.

5. Bibliography

- [1] I. G. Kaplan, *Intermolecular Interaction* (Wiley, New York, 2006).
- [2] H.-A. Wagenknecht (Ed.), *Charge transfer in DNA: from mechanism to application* (Wiley-VCH, Weinheim, 2005).

- [3] W. Binder (Ed.), *Hydrogen Bonded Polymers* (Springer-Verlag, Berlin, 2007).
- [4] A. J. Stone, *The Theory of Intermolecular Forces* (Oxford University Press, Oxford, 1996).
- [5] K. Szalewicz, K. Patkowski, and B. Jeziorski, *Struct. Bond.* **116**, 43 (2005).
- [6] A. van der Avoird, P. E. S. Wormer, and R. Moszynski, *Chem. Rev.* **94**, 1931 (1994).
- [7] A. K. Rappe and E. R. Bernstein, *J. Phys. Chem. A.* **104**, 6117 (2000).
- [8] G. Chalasinski and M. M. Szczesniak, *Chem. Rev.* **100**, 4227 (2000).
- [9] R. J. Wheatley, A. S. Tulegenov, and E. Bichoutskaia, *Int. Rev. Phys. Chem.* **23**, 151 (2004).
- [10] Y. Zhao and D. G. Truhlar, *J. Chem. Theory Comput.* **1**, 415 (2005).
- [11] S. Grimme, *J. Comp. Chem.* **25**, 1463 (2004).
- [12] C. E. Dykstra, G. Frenking, K. S. Kim, and G. E. Scuseria (Ed.), *Theory and Applications of Computational Chemistry : The first forty years* (Elsevier, Amsterdam, 2005).
- [13] A. Ruzsinszky, J. P. Perdew, and G. I. Csonka, *J. Phys. Chem. A.* **109**, 11015 (2005).
- [14] A. H.-T. Li and S. D. Chao, *J. Chem. Phys.* **125**, 094312 (2006).
- [15] C. J. Pickard and R. J. Needs, *Phys. Rev. Lett.* **97**, 045504 (2006).

- [16] Y. Sakiyama, S. Takagi and Y. Matsumoto, *Phys. Fluids*. **16**, 1620 (2004).
- [17] A. Szabo and N. S. Ostlund, *Modern Quantum Chemistry. Introduction to Advanced Electronic Structure Theory* (Dover, New York, 1996).
- [18] R. Krishnan, J. S. Binkley, R. Seeger, and J. A. Pople, *J. Chem. Phys.* **72**, 650 (1980).
- [19] T. H. Dunning, Jr., *J. Chem. Phys.* **90**, 1007 (1989).
- [20] C. Møller and M. S. Plesset, *Phys. Rev.* **46**, 618 (1934).
- [21] J. A. Pople, M. Head-Gordon, and K. Raghavachari, *J. Chem. Phys.* **87**, 5968 (1987).
- [22] S. Tsuzuki, K. Honda, T. Uchimaru, and M. Mikami, *J. Chem. Phys.* **124**, 114304 (2006).
- [23] S. F. Boys and F. Bernardi, *Mol. Phys.* **19**, 553 (1970).
- [24] T. Helgaker, W. Klopper, H. Koch, and J. Noga, *J. Chem. Phys.* **106**, 9639 (1997).
- [25] D. Feller, *J. Chem. Phys.* **96**, 6104 (1992).
- [26] W. H. Press, S. A. Teukolsky, W. T. Vetterling, and B. P. Flannery, *Numerical Recipe in C* (Cambridge University Press, Cambridge, 1996).
- [27] M. J. Frisch, G. W. Trucks, H. B. Schlegel *et al.*, Gaussian 03, Revision C.02, Gaussian, Inc., Wallingford CT, 2004.

- [28] D. C. Rapaport, *The Art of Molecular Dynamics Simulation* (Cambridge University Press, New York, 1995).
- [29] F. Jensen, *Introduction to Computational Chemistry* (Wiley, New York, 1999).
- [30] M. A. Spackman, *J. Chem. Phys.* **94**, 1295 (1991).
- [31] Q. Wu and W. Yang, *J. Chem. Phys.* **116**, 515 (2002).
- [32] A. D. Becke and E. R. Johnson, *J. Chem. Phys.* **122**, 154104 (2005).
- [33] A. D. Becke, *Phys. Rev. A* **38**, 3098 (1988).
- [34] N. C. Handy and A. J. Cohen, *Mol. Phys.* **99**, 403 (2001).
- [35] C. Adamo and V. Barone, *J. Chem. Phys.* **108**, 664 (1998).
- [36] J. P. Perdew, K. Burke, and M. Ernzerhof, *Phys. Rev. Lett.* **77**, 3865 (1996).
- [37] K. Burke, J. P. Perdew, and Y. Wang, in *Electronic Density Functional Theory: Recent Progress and New Directions*, Ed. J. F. Dobson, G. Vignale, and M. P. Das (Plenum, 1998).
- [38] J. Tao, J. P. Perdew, V. N. Staroverov, and G. E. Scuseria, *Phys. Rev. Lett.* **91**, 146401 (2003).
- [39] W. Kohn and L. J. Sham, *Phys. Rev.* **140**, A1133 (1965).
- [40] A. D. Boese and N. C. Handy, *J. Chem. Phys.* **114**, 5497; see also the supplementary material: EPAPS Document No. E-JCPA6-114-301111 (2001).
- [41] J. C. Slater, *Quantum Theory of Molecular and Solids. Vol. 4: The Self-Consistent*

Field for Molecular and Solids (McGraw-Hill, New York, 1974).

- [42] J. P. Perdew, *Phys. Rev. B* **33**, 8822 (1986).
- [43] S. H. Vosko, L. Wilk, and M. Nusair, *Can. J. Phys.* **58**, 1200 (1980).
- [44] J. P. Perdew and A. Zunger, *Phys. Rev. B* **23**, 5048 (1981).
- [45] C. Lee, W. Yang, and R. G. Parr, *Phys. Rev. B* **37**, 785 (1988).
- [46] A. D. Boese, N. L. Doltsinis, N. C. Handy, and M. Sprik, *J. Chem. Phys.* **112**, 1670 (2000).
- [47] Y. Zhang, W. Pan, and W. Yang, *J. Chem. Phys.* **107**, 7921 (1997).
- [48] A. H.-T. Li and S. D. Chao, *Phys. Rev. A* **73**, 016701 (2006).
- [49] Y. Sakiyama, S. Takagi, and Y. Matsumoto, *J. Chem. Phys.* **122**, 234501 (2005).
- [50] Y. Andersson, D. C. Langreth, and B. I. Lundqvist, *Phys. Rev. Lett.* **76**, 102 (1996).
- [51] J. F. Dobson and B. P. Dinte, *Phys. Rev. Lett.* **76**, 1780 (1996).
- [52] W. Kohn, Y. Meir, and D. E. Makarov, *Phys. Rev. Lett.* **80**, 4153 (1998).
- [53] A. J. Misquitta, B. Jeziorski, and K. Szalewicz, *Phys. Rev. Lett.* **91**, 033201 (2003).
- [54] A. Hebelmann, G. Jansen, and M. Schütz, *J. Chem. Phys.* **122**, 014103 (2005).
- [55] K. Burke, J. P. Perdew, and Y. Wang, in *Electronic Density Functional Theory: Recent Progress and New Directions*, edited by J. F. Dobson, G. Vignale, and M.

P. Das (Plenum, New York, 1998)

[56] J.M.L. Martin, *Chem. Phys. Lett.* **259**, 669 (1996).

[57] M. M. Szczesniak, G. Chalasinski, S. M. Cybulski, and S. Scheiner, *J. Chem. Phys.* **93**, 4243 (1990).

[58] J. Tao and J. P. Perdew, *J. Chem. Phys.* **122**, 114102 (2005).

[59] *Gaussian 03 User's Reference and IOps Reference* (Gaussian Inc., Pittsburgh, 2003).



Table captions

TABLE 2.1-1. The basis set dependence of important potential parameters using the BSSE corrected HF and MP2 intermolecular potentials. R_0 is the distance at which the potential is zero and R_m is the equilibrium bond length. The CPU time of the MP2 calculation was recorded on a single node two-processor AMD 250 PC cluster with distributed memory.

TABLE 2.1-2. Comparison of the binding energies using the BSSE corrected MP2 and CCSD(T) intermolecular potentials calculated at several basis sets. The basis set limits of the binding energies using the extrapolation methods of Helgaker *et al.* [24], Martin [56], and a numerical method [26] are shown for comparison.

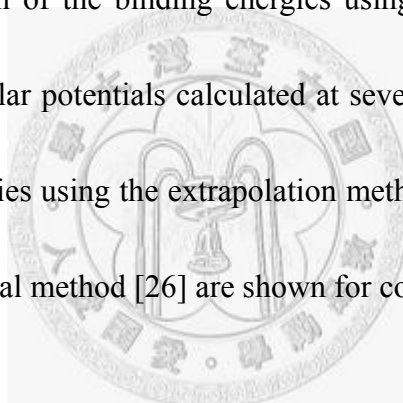


TABLE 2.1-3. Comparison of the bond lengths (in \AA) calculated with the 108 exchange-correlation functionals using the 6-311++G (3df,3pd) basis set. As a reference, the MP2 bond length calculated at this basis set is 4.25\AA . The better DFT results of errors within 10% as compared to the MP2 result are marked in black boldface.

TABLE 2.1-4. Comparison of the binding energies (in kcal/mol) calculated with the

108 exchange-correlation functionals using the 6-311++G (3df, 3pd) basis set. As a reference, the MP2 binding energy calculated at this basis set is -0.454 kcal/mol .

Positive values represent unbound dimer structures and the energies are calculated at $R = 4.25 \text{ \AA}$. The better DFT results of errors within 10% as compared to the MP2 result are marked in black boldface.



Basis set	MP2		HF		MP2						
	Number of basis function	CPU Time (h)	A ^a (kcal/mol)	α^a (\AA^{-1})	R ₀ (\AA)	R _m (\AA)	E _b (kcal/mol)	ω (cm^{-1})	1 term ^b	2 terms ^c	
									C ₆	C ₆	C ₈
STO-3G	26	1.55	122104.69	2.94	5.98	6.73	-0.001	5.18	317.02	448.94	3203.81
3-21G	42	1.42	58783.30	2.66	4.75	5.22	-0.037	69.61	1941.38	628.66	54171.60
6-31G	42	1.49	54009.26	2.64	4.67	5.14	-0.050	87.08	1908.43	660.34	49972.43
3-21G*	54	1.50	55908.20	2.69	4.55	5.05	-0.058	88.28	2108.34	848.16	49176.41
6-31G*	54	1.57	53175.77	2.68	4.55	5.04	-0.062	90.25	2062.71	833.95	47916.34
6-311G*	76	1.56	55354.29	2.67	4.51	5.02	-0.060	81.01	2207.05	930.44	49690.29
cc-pVDZ	76	2.12	49043.50	2.65	4.17	4.66	-0.166	122.98	3351.38	1728.99	55937.64
6-31G**	78	1.78	52290.93	2.68	4.45	4.94	-0.077	101.20	2223.41	964.67	47740.30
6-311G**	100	1.92	53132.34	2.68	4.31	4.80	-0.100	104.08	2685.28	1324.22	49936.37
6-311++G**	116	2.98	51820.70	2.67	4.29	4.79	-0.105	103.66	2763.58	1297.37	53976.66
aug-cc-pVDZ	126	4.97	51371.83	2.67	3.83	4.32	-0.435	232.04	5246.08	3221.51	63124.55
6-311++G(2d,2p)	150	5.41	49711.75	2.67	3.91	4.40	-0.285	180.64	4077.60	2292.74	57950.76
cc-pVTZ	180	15.86	48247.93	2.66	3.84	4.31	-0.353	212.96	4516.86	2598.04	60292.92
6-311++G(3d,3p)	184	14.08	49624.69	2.67	3.82	4.30	-0.410	222.38	4869.69	2797.09	65087.98
6-311++G(2df,2pd)	204	21.20	48903.09	2.67	3.86	4.33	-0.320	208.82	4248.72	2419.41	57507.36
6-311++G(3df,3pd)	238	43.37	51326.84	2.68	3.77	4.25	-0.454	260.87	5074.31	2956.27	64289.42
aug-cc-pVTZ	284	137.05	50474.57	2.68	3.70	4.17	-0.551	244.49	5529.30	3291.79	65493.19
cc-pVQZ	358	232.25	48247.94	2.66	3.72	4.19	-0.489	241.42	5119.50	2688.24	71369.18
aug-cc-pVQZ	536	1167.03	49979.36	2.68	3.67	4.14	-0.580	293.89	5556.37	3266.28	67621.33
basis set limit			49317.50	2.68	3.65	4.12	-0.603	378.80	---	---	---

^a Fit to the formula $V_{HF}(R) = Ae^{-\alpha R}$, ^b Fit to the formula $V_{disp}(R) = -\frac{C_6}{R^6}$, C₆ in unit (kcal/mol \AA^6), using data R > 4.6 \AA .

^c Fit to the formula $V_{disp}(R) = -\frac{C_6}{R^6} - \frac{C_8}{R^8}$, C₈ in unit (kcal/mol \AA^8), using data R > 5 \AA .

Table 2.1-1

Binding Energies						
	cc-pVDZ(76)^a	cc-pVTZ(180)	cc-pVQZ(358)	aug-cc-pVDZ(126)	aug-cc-pVTZ(284)	aug-cc-pVQZ(536)
MP2	-0.166	-0.353	-0.489	-0.435	-0.551	-0.580
CCSD(T)	-0.170	-0.378	-0.559	-0.480	-0.632	NA [‡]
Basis set limit estimation						
Method	DT^d	TQ^e	DTQ^f	aDT^g	aTQ^h	aDTQⁱ
Helgaker <i>et al.</i>	-0.432 ^b (-0.466) ^c	-0.588 (-0.691)	NA	-0.543 (-0.696)	-0.601	NA
Martin	-0.419 (-0.451)	-0.567 (-0.663)	NA	-0.592 (-0.685)	-0.597	NA
Numerical	-0.490 (-0.530)	-0.627 (-0.742)	-0.663 (-0.799)	-0.644 (-0.753)	-0.613	-0.603

^a Number of basis function in parentheses.

^b MP2 basis set limit estimation.

^c CCSD(T) basis set limit estimation in parentheses.

^d Basis set limit estimation with the cc-pVXZ(X=D and T).

^e Basis set limit estimation with the cc-pVXZ(X=T and Q).

^f Basis set limit estimation with the cc-pVXZ(X=D, T, and Q).

^g Basis set limit estimation with the aug-cc-pVXZ(X=D and T).

^h Basis set limit estimation with the aug-cc-pVXZ(X=T and Q).

ⁱ Basis set limit estimation with the aug-cc-pVXZ(X=D, T, and Q).

[‡] Not available.

Table 2.1-2

		<i>Correlation functional</i>											
		VWN5	PL	TPSS	PBE	PW91	VWN	VP86	P86	LYP	HCTH93	HCTH	HCTH147
<i>Exchange functional</i>	B88	U	U	U	U	U	U	U	U	U	4.41	4.19	4.10
	HCTH	6.75	6.75	6.79	6.84	6.84	6.73	7.58	7.58	6.79	6.73	4.51	6.04
	OPTX	5.57	5.57	5.64	5.63	5.63	5.52	5.65	5.65	5.52	4.90	4.37	4.56
	MPW	5.48	5.48	5.57	5.56	5.55	5.44	5.43	5.42	5.03	4.22	4.12	4.01
	TPSS	5.04	5.15	5.03	5.00	4.96	4.95	4.55	4.55	4.63	4.14	4.22	3.96
	PBE	4.87	4.87	4.57	4.55	4.51	4.81	4.14	4.14	4.39	4.08	4.06	3.96
	PW91	4.81	4.81	4.59	4.57	4.54	4.75	4.14	4.14	4.41	4.07	4.05	3.95
	Slater	3.64	3.64	3.30	3.28	3.29	3.61	3.29	3.29	3.44	NA [‡]	NA [‡]	NA [‡]
	XAlpha	3.56	3.56	3.24	3.23	3.23	3.53	3.23	3.23	3.38	3.50	3.58	3.44

[‡]Not available

Table 2.1-3

		<i>Correlation functional</i>											
		VWN5	PL	TPSS	PBE	PW91	VWN	VP86	P86	LYP	HCTH93	HCTH	HCTH147
<i>Exchange functional</i>	B88	1.342	1.341	1.132	1.111	1.092	1.250	0.821	0.817	0.900	-0.018	-1.994	-0.602
	HCTH	-0.004	-0.004	-0.003	-0.003	-0.003	-0.005	-0.001	-0.001	-0.002	-0.002	-0.837	-0.010
	OPTX	-0.015	-0.016	-0.015	-0.015	-0.015	-0.027	-0.006	-0.006	-0.025	-0.169	-1.803	-0.443
	MPW	-0.063	-0.063	-0.059	-0.060	-0.060	-0.075	-0.045	-0.045	-0.080	-0.756	-2.818	-1.500
	TPSS	-0.057	-0.133	-0.066	-0.066	-0.067	-0.078	-0.121	-0.124	-0.175	-0.889	-3.248	-1.625
	PBE	-0.129	-0.130	-0.188	-0.191	-0.200	-0.156	-0.492	-0.499	-0.387	-1.391	-3.465	-2.226
	PW91	-0.347	-0.349	-0.411	-0.415	-0.424	-0.382	-0.693	-0.700	-0.591	-1.584	-3.659	-2.428
	Slater	-1.871	-1.886	-4.865	-5.120	-5.062	-2.070	-5.989	-6.014	-4.035	NA [‡]	NA [‡]	NA [‡]
	XAlpha	-2.126	-2.143	-5.403	-5.671	-5.601	-2.344	-6.580	-6.580	-4.484	-5.501	-7.012	-7.100

[‡]Not available

Table 2.1-4

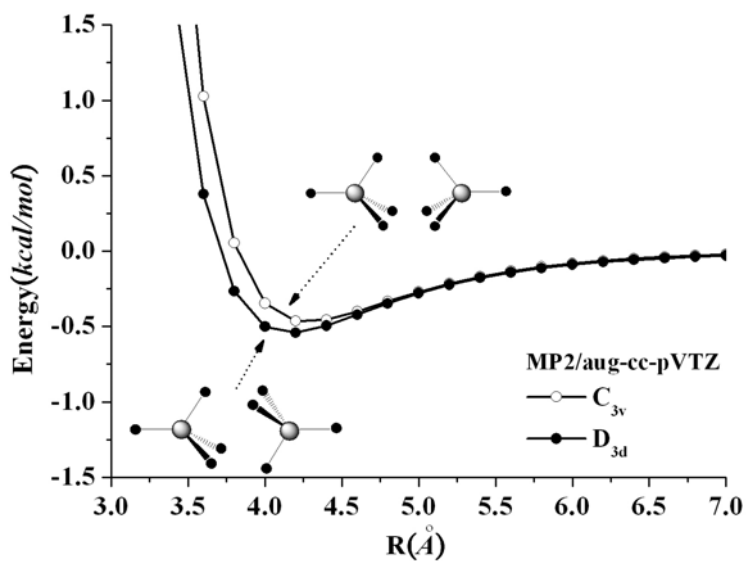


Fig. 2.1-1

FIG. 2.1-1. The BSSE corrected MP2 potentials using the aug-cc-pVTZ basis set for the D_{3d} and C_{3v} conformers of the silane dimer.

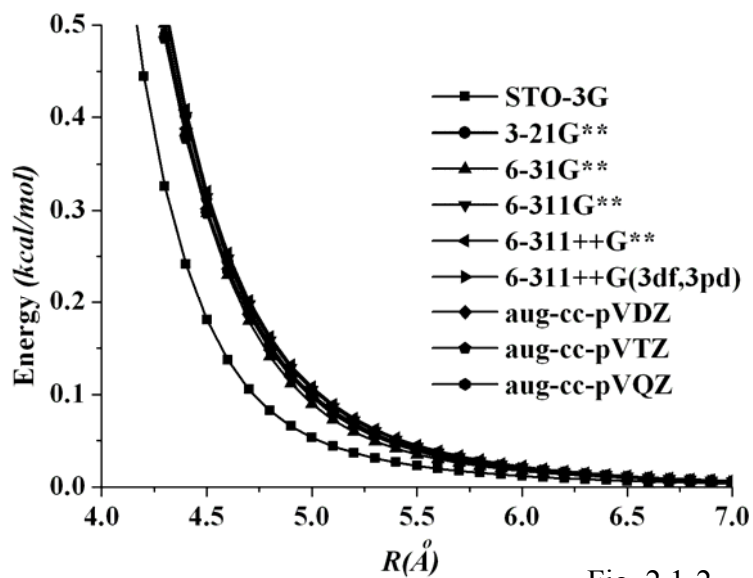


Fig. 2.1-2

FIG. 2.1-2. The BSSE corrected HF interaction potentials of the silane dimer using several basis sets.

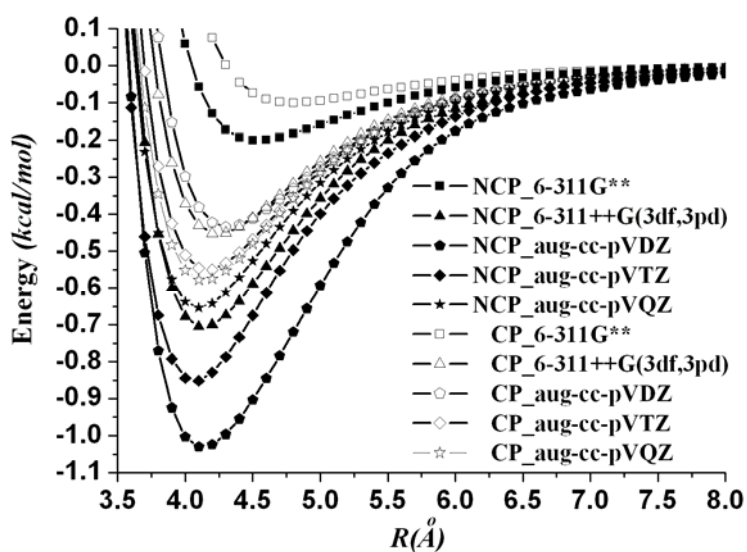


Fig. 2.1-3

FIG. 2.1-3. The BSSE corrected (CP) and uncorrected (NCP) MP2 potentials of the silane dimer using a series of basis sets.

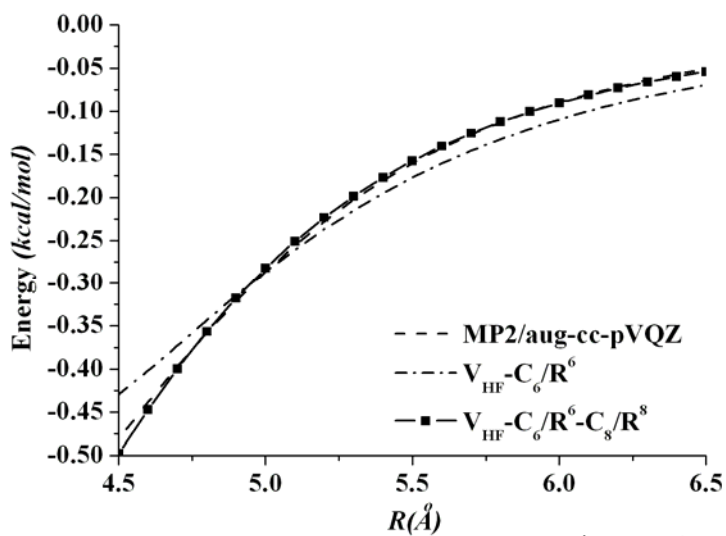


Fig. 2.1-4

FIG. 2.1-4. Comparison of the BSSE corrected MP2 potential curve calculated at the aug-cc-pVQZ basis set and the sum of the HF potential and the long-range dispersion potentials.

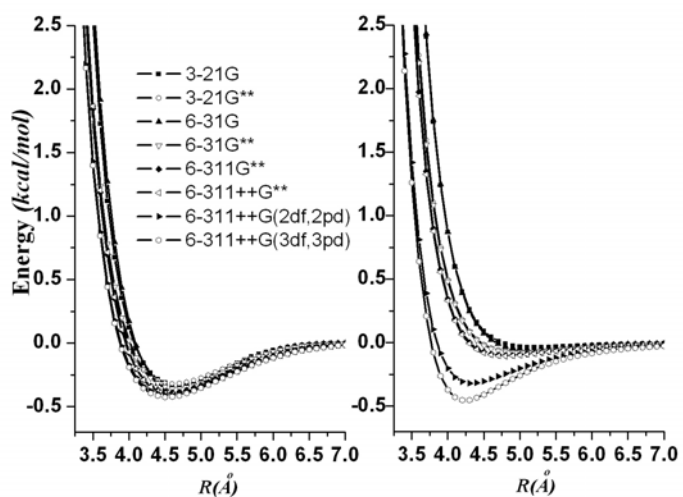


Fig. 2.1-5

FIG. 2.1-5. The basis set dependence of the DFT potentials calculated with the PW91PW91 functional (left panel). As a reference, the basis set dependence of the MP2 potentials is shown in the right panel.

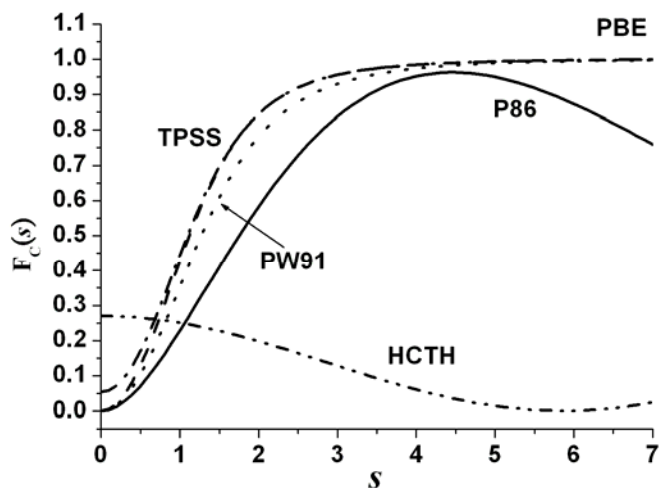


Fig. 2.1-6

FIG. 2.1-6. The GGA correlation enhancement factor as a function of s for the TPSS, PBE, PW91, P86, and HCTH correlation functionals. Here $r_s = 10$.

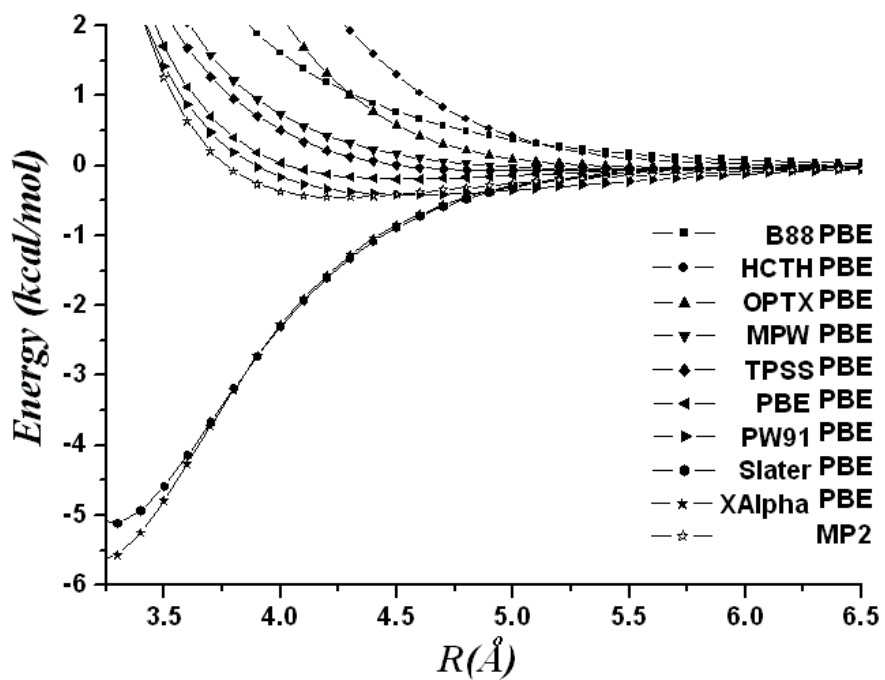


Fig. 2.1-7(a)

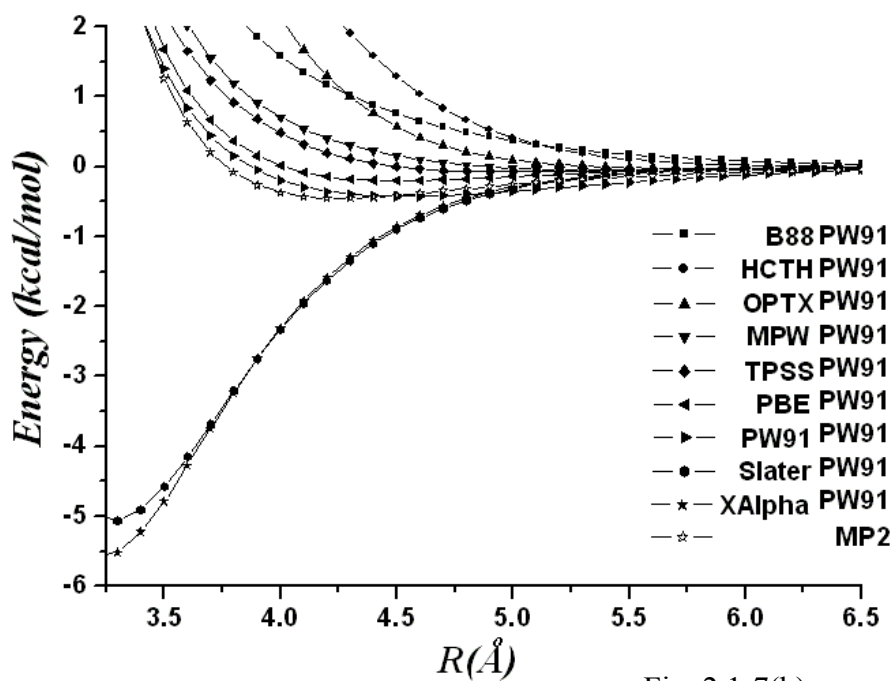


Fig. 2.1-7(b)

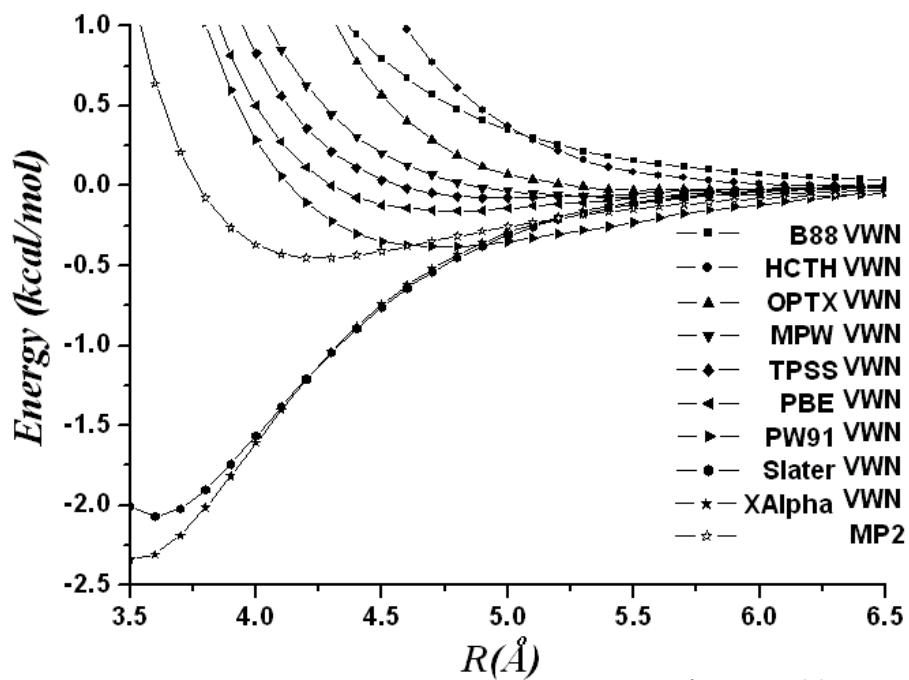


Fig. 2.1-7(c)

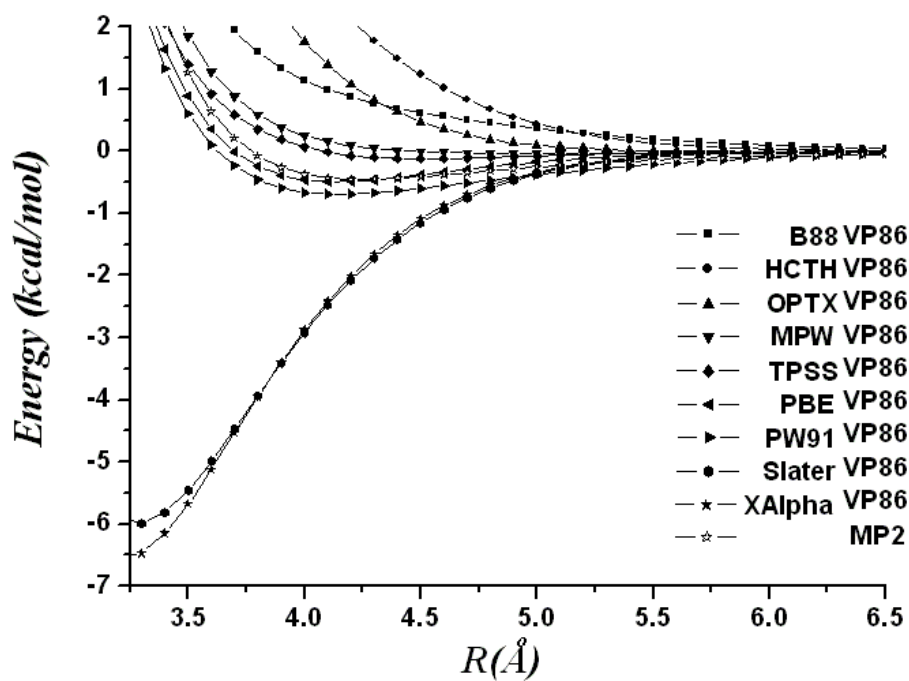


Fig. 2.1-7(d)

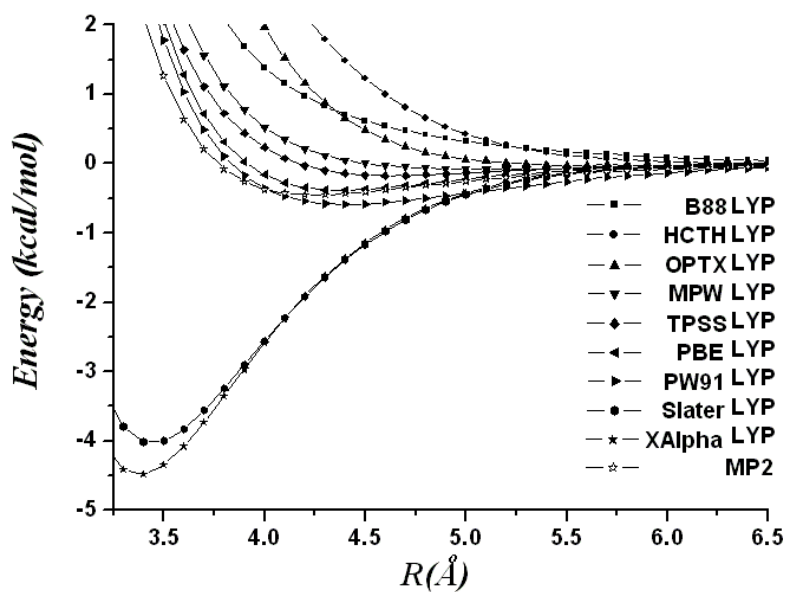


Fig. 2.1-7(e)

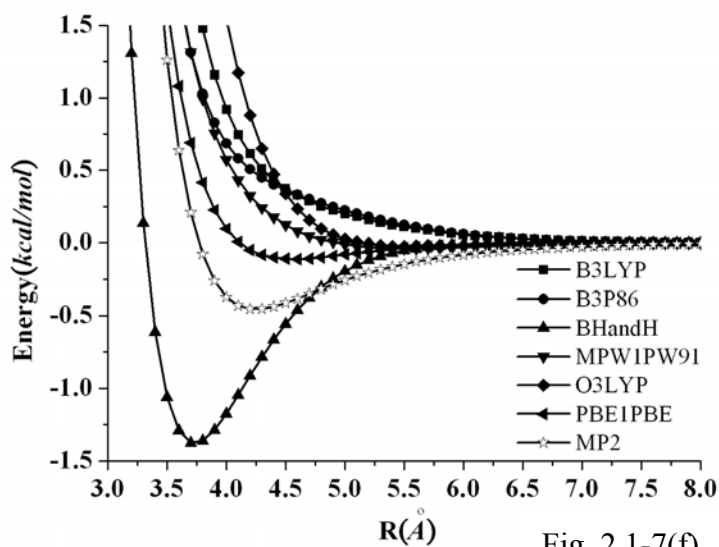


Fig. 2.1-7(f)

FIG. 2.1-7. The BSSE corrected DFT potential curves with varying exchange functionals by fixing (a) PBE, (b) PW91, (c) VWN, (d) VP86, and (e) LYP correlation functionals, respectively. (f) The DFT potentials using several hybrid functionals (B3LYP, B3P86, BHandH, MPW1PW91, O3LYP, and PBE1PBE) [59]. The MP2 potential curve is also shown as a reference.

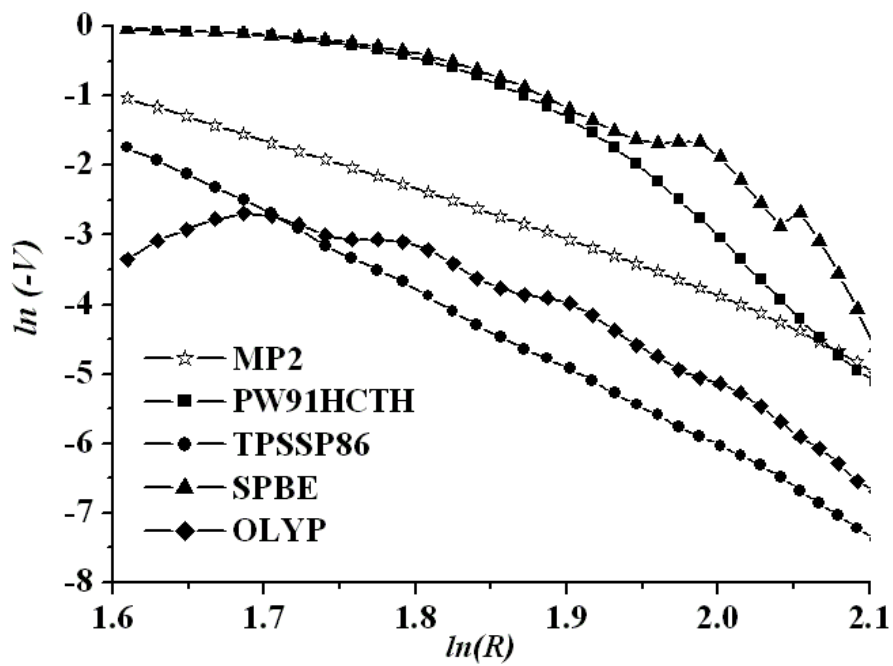
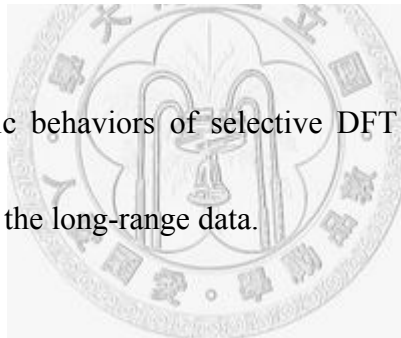


Fig. 2.1-8

FIG. 2.1-8. The asymptotic behaviors of selective DFT potentials versus the MP2 potential via an analysis of the long-range data.



2.2 Determination of a silane intermolecular force field potential model from an *ab initio* calculation

1. Introduction

Accurate determination of intermolecular interaction potentials or the van der Waals interactions has become much more important in the studies of materials chemistry and in optoelectronic or semiconductor industry. These interactions are crucial for understanding and predicting the thermodynamic properties of molecular liquids and solids [1], the energy and charge transfers among molecular complexes [2], and the conformational tertiary structures of nanostructure such as semiconductor manufacturing processes, aerospace engineering and MEMS [3-6]. For example, in semiconductor and optoelectronic industry, silane is widely used for the chemical vapor deposition of silicon and silicon dioxide thin layers. There were great interest in the downscaling of optoelectronic devices and the structural properties. However most of the studies have focused on the intramolecular potential energies, but only a few studies have been calculated the intermolecular potential energies of silane dimer in the recent past [7-10]. M. G. Govender *et al.* [7] has calculated single point geometry optimization at MP2/6-311++G (*d*, *p*) level. Y. Sakiyama *et al.* [8] have calculated the interaction energies of the silane dimer for nine relative orientations at the MP2/aug-cc-pVTZ level. Y. Sakiyama *et al.* [9] were done using the

MP2/aug-cc-pVTZ level with 162 different spatial configurations. Silane (SiH_4) structure is similar to the methane and it is another candidate to perform a prototype study. In previous studies, we have thoroughly calculated the interaction potentials of the methane and carbon tetrachloride dimers [11-16] and studied the dispersion energy. From our previous can be seen that the low level basis sets did not systematically converge to the expected potential curve. It is a good starting point to investigate the various factors affecting the contributions to the interaction energy, such as electrostatic, dispersion and exchange terms. Although the interaction potentials of the methane dimer have been studied extensively, there have been relatively few *ab initio* studies on the interaction potentials of the structurally similar silane dimer. In this paper, we perform high level calculation result on *ab initio* potential energies of the silane dimer in terms of the HF and MP2 methods, up to aug-cc-pV5Z and we also construct full intermolecular potential curves and potential energy surfaces. For understanding this system, the aim of the present study is to determine on Si-Si, Si-H and H-H force field parameters from *ab initio* potential energies to obtain an accurate representation of minimum structures. The Lennard-Jones potential is the most famous one with pair interaction [17]. Therefore, we show that Lennard-Jones 5-site potential can be parameterized to give excellent fits to both the repulsive and attractive regions of the potential energy curves. In this

paper, we are organized as follows. In Section II, we have shown details of the calculations. In Section III the results are presented and discussed. In Section IV, the summary and a brief perspective are given.

2. Methods and Calculations

All the quantum chemistry calculations have been performed by using the Gaussian 03 program package [18]. Similar to the methane dimer, a large part of the exchange repulsion interactions of the silane dimer can be calculated by the HF method. The calculation of electron correlation energies depends on the level of the correlation-corrected method, the size of the basis set, and the correction of the BSSE. (You did not introduce it before) The state-of-the-art choice of the correlation-corrected method is the Møller-Plesset (MP x , $x = 2-4$) perturbation method [19]. The isolated silane molecule was first optimized at the MP2/6-311++G (3df, 3pd) theory and was found to be at the tetrahedral configuration (T_d symmetry) with the Si-H bond length of 1.47 \AA which is consistent with the experimental data by Kattenberg and Oskam (Si-H bond length = $1.4806 \pm 0.0008 \text{ \AA}$) [20] and by Willetts *et al.* (Si-H bond length = 1.482 \AA) [21] and average value by Duncan (Si-H bond length = $1.4813 \pm 0.0006 \text{ \AA}$) [22] and linear fitting prediction data by Duncan *et al.* (Si-H bond length = $1.479 \pm 0.003 \text{ \AA}$) [23]. The 12 symmetric conformers chosen to

sample the orientational dependence are depicted in Fig. 2.1-1. Because of the high symmetry of the dimer configuration, the angular sampling should be wide enough to model the rotational dynamics in normal thermodynamic conditions. The MP2 method [19] has been used to treat the correlation effect. Pople's medium size basis sets [up to 6-311++G (3df, 3pd)] [24] and Dunning's correlation consistent basis sets (aug-cc-pVXZ, X=D, T, Q, 5) [25] were employed in the calculations. The basis set superposition errors (BSSEs) were corrected by the counterpoise method of Boys and Bernardi [26]. Subsequently the Si-Si distance, denoted as R , was sampled for a large range of 3.0 ~ 9.0 Å, with 31 configuration points for each conformer. A total of 372 configuration points were actually sampled and the energies calculated. During the scan we used rigid and symmetric conformer assumptions. The MP2 interaction energies at the basis set limit have been estimated using the methods of Martin [27] and Helgaker *et al.* [28] and a numerical extrapolation scheme based on the Lagrange formula [29]. The G and H conformer potential data with some basis sets are shown in Table I.

3. Results and Discussions

A. Hartree-Fock self-consistent field calculations

The BSSE corrected HF interaction potentials of the silane dimer in 12 symmetric

conformers are shown in Fig. 2.2-2. The HF calculations for all conformers yield purely repulsive potentials without minima for all the basis sets used. This can be attributed to the rather weak electrostatic interactions for the silane dimer. In the short range, the strong exchange-repulsion interaction dominates with little alternation from the electrostatic and induction attractions.

B. MP2 calculations

In Fig. 2.2-3 we show the MP2 potentials for the twelve conformers using high level aug-cc-pV5Z basis set. We see that the potentials become deeper when there are more inner hydrogen atoms and more close on distance contacts between the monomers. It has been found that the minimum-energy conformation corresponds to the C_s symmetry configuration (the G and H conformers). It is interesting to analyze the orientational dependence from the repulsive and the attractive components of the potentials separately. SiH_4 is a non-polar molecule and the dominant long-range attraction is thus due to the London dispersion force. On the other hand, the strong repulsive force almost comes from the exchange-repulsion interaction. Contrasting the HF and the MP2 potentials thus helps to delineate the relative importance of the dispersion energy in the overall intermolecular interactions. In Fig. 2.2-4 we show the MP2 potentials subtracting the corresponding HF potentials, dubbed as MP2-HF, for

the twelve conformers. The MP2-HF potentials largely represent the dispersion curves which are purely attractive. The dispersion interaction between molecules is a weak attraction due to an instantaneous dipole moment in one molecule inducing a dipole moment in another molecule. The dispersion energy (V_{disp}) of the form [30]

$$V_{disp} = -\frac{C_6}{R^6} \quad (1)$$

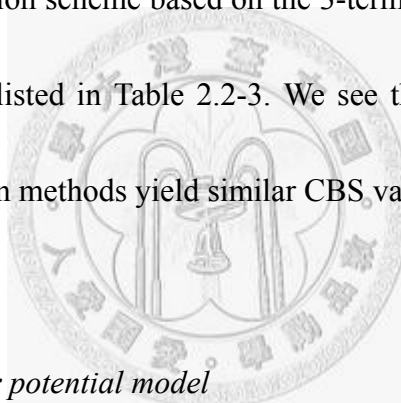
where the dispersion coefficient C_6 is a constant depending on the molecules in Fig.

2.2-5. The fitting C_6 values of Eq. (1) is compared to accurate literature values [31].

Up to the largest basis set used, the value of our calculation ($C_6 \doteq 342.35 \text{ eV}\text{\AA}$) has converged to the expected value from the literature ($C_6 \doteq 343.0 \text{ eV}\text{\AA}$) [31] and the calculation ($C_6 \doteq 343.9 \text{ eV}\text{\AA}$) [32] and ($C_6 \doteq 356.1 \text{ eV}\text{\AA}$) [33]. In our calculation, the aug-cc-pV5Z basis set underestimates only 0.19% for G conformer of the literature value (see Table II).

In Table 2.2-1 we present the G and H conformers of several basis sets with the MP2 method. R_0 is the distance at which the potential is zero and can be obtained from a two point interpolation of the calculated data. The bond length R_m and the binding energy E_b can be obtained through a harmonic modeling of the three lowest potential data near equilibrium regions. With increasing basis size, the equilibrium bond length converges at the aug-cc-pVTZ basis set to a 0.02\AA accuracy, while a pretty large basis

set, aug-cc-pV5Z, is required to converge the binding energy at a chemical accuracy (~ 0.03 kcal/mol). It is clear from Table 2.2-1 that the aug-cc-pVTZ basis set still underestimates the binding energy by about 33% and consistent with previous papers [8-9]. The strong basis set dependence and the slow convergence on the binding energy call for an estimation of the potential features at the complete basis set (CBS) limit. The CBS binding energies can be obtained by an extrapolation scheme with Dunning's basis sets. We consider the methods of Martin [27] and Helgaker *et al.* [28] and a numerical extrapolation scheme based on the 3-term Lagrange formula [29] and the MP2/CBS results are listed in Table 2.2-3. We see that using the aug-cc-pVXZ data, the three extrapolation methods yield similar CBS values.



C. Analytical site-site pair potential model

Unlike the methane dimer [11-15], in Fig. 2.2-3, we see that the twelve orientation potential energy curves of silane dimer are not systematically arranged in order. The configurations of I and J conformer energies are relative lower than G and H conformers. This indicates that not only the inner silicon-silicon interactions play a major role but also the interchange of influence of silicon-hydrogen interactions was very important. Besides, the central silicon atom size is larger and electronegativity is smaller than carbon atom. For those reasons, the calculation results shown the G

and H potential curves maybe more favorable stabilization than others. Therefore, we conclude that the inner silicon interactions and interplay silicon-hydrogen interactions are also the major components contributing to the potential anisotropy.

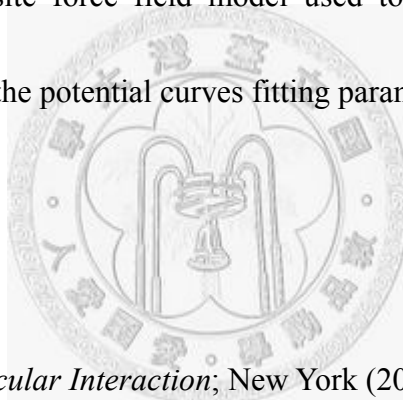
Based on these observations, an analytical 5-site model was proposed to represent the MP2/aug-cc-pV5Z potential data. The site-site interaction is represented by a Lennard-Jones (L-J) function [33].

$$U(r_{ij}) = 4\varepsilon_{ij} \left[\left(\frac{\sigma_{ij}}{r_{ij}} \right)^{12} - \left(\frac{\sigma_{ij}}{r_{ij}} \right)^6 \right] \quad (2)$$

where the indices i and j denote the atoms in separated monomers, respectively, and r_{ij} represent the silicon - silicon distance for a pair of monomer. In this model σ_{ij} and ε_{ij} are the potential parameters to be determined in the non-linear regression. No bias weights were put on specific configurations except that we excluded from the non-linear fitting some largest repulsive energy points in the regression to prevent their dominance in the least-squares cost function [43]. However, this latter constraint could effectively put more weight on deeper wells. For the 5-site model, the best fitting parameters we obtained are $\sigma_{HH}=2.754 \text{ \AA}$, $\varepsilon_{HH}=0.100 \text{ kcal/mol}$, $\sigma_{SiH}=3.070 \text{ \AA}$, $\varepsilon_{SiH}=0.006 \text{ kcal/mol}$, $\sigma_{SiSi}=4.150 \text{ \AA}$, $\varepsilon_{SiSi}=0.072 \text{ kcal/mol}$. In Fig. 2.2-7(a) and Fig. 2.2-7(b) we present the fitting curves and the *ab initio* data..

4. Conclusion

The present work extends our previous work [11-16] for calculating intermolecular potential energies to state-of-the-art methodology. We have systemically analyzed the intermolecular potential of silane dimer in twelve conformers. We also employed high level quantum chemistry calculation to obtain the potential data and consistent with previous literatures. The potentials exhibit significant anisotropy, which is analyzed and considered in the 5-site force field model used to fit the potential data and determine the accuracy of the potential curves fitting parameters.



5. Bibliography

- [1] I. G. Kaplan. *Intermolecular Interaction*; New York (2006).
- [2] P. Hobza and R. Zahradnik. *Intermolecular Complex: The Role of van der Waals Systems in Physical Chemistry and in the Biodisciplines* (Elsevier, New York, 1988)
- [3] J. Feng, W. Grochala, T. Jaron, R. Hoffmann, A. Bergara and N. W. Ashcroft, *Phys. Rev. Lett.* **96**, 017006 (2006).
- [4] O. Degtyareva, M. M. Canales, A. Bergara, X.-J. Chen, Y. Song and V. V. Struzhkin, *Phys. Rev. B.* **76**, 064123 (2007).

- [5] D. Y. Kim, R. H. Scheicher, S. Lebegue, J. Prasongkit, B. Arnaud, M. Alouani and R. Ahuja, *Proc. Natl. Acad. Sci. USA*. **105**, 16454 (2008).
- [6] M.-C. Miguel, A. R. Oganov, Y. Ma, Y. Yan, A. O. Lyakhov and A. Bergara, *Phys. Rev. Lett.* **102**, 087005 (2009).
- [7] M. G. Govender, S. M. Rootman and T. A. Ford, *Crystal Engineering*. **6**, 263 (2003).
- [8] Y. Sakiyama, S. Takagi and Y. Matsumoto, *Phys. of fluids*. **16**, 1620 (2004).
- [9] Y. Sakiyama, S. Takaga and Y. Matsumoto, *J. Chem. Phys.* **122**, 234501 (2005).
- [10] C.-C. Pai, A. H.-T. Li and S. D. Chao, *J. Phys. Chem.* **111**, 11922 (2007).
- [11] A. H.-T. Li and S. D. Chao, *J. Chem. Phys.* **125**, 094312 (2006).
- [12] A. H.-T. Li and S. D. Chao, *Phys. Rev. A*. **73**, 016701 (2006)
- [13] S. D. Chao and A. H.-T. Li, *J. Phys. Chem. A*. **111**, 9586 (2007).
- [14] S. W. Chao, A. H.-T. Li and S. D. Chao, *J. Comput. Chem.* **30**, 1839 (2009).
- [15] A. H.-T. Li and S. D. Chao, *J. Mol. Struct. Theo.* **897**, 90 (2009).
- [16] A. H.-T. Li, S.-C. Huang and S. D. Chao, *J. Chem. Phys.* **132**, 024506 (2010).
- [17] J. E. Lennard-Jones, *Proc. R. Soc. London, Ser. A*. **109**, 584 (1925).
- [18] M. J. Frisch, G. W. Trucks, H. B. Schlegel *et al.*, Gaussian 03, Revision D.02, Gaussian, Inc., Wallingford CT (2004).
- [19] C. Møller and M. S. Plesset, *Phys. Rev.* **46**, 618 (1934).

- [20] H. W. Kattenberg and A. Oskam, *J. Mol. Spectroscopy*. **49**, 52 (1974).
- [21] D. V. Willetts and W. J. Jones, *J. Mol. Spectroscopy*. **55**, 200 (1975).
- [22] J. L. Duncan, *J. Mol. Spectroscopy*. **60**, 225 (1974).
- [23] J. L. Duncan, J. L. Harvie and D. C. Mckean, *J. Mol. Struc.* **145**, 225 (1986).
- [24] R. Krishnan, J. S. Binkley, R. Seeger, and J. A. Pople, *J. Chem. Phys.* **72**, 650 (1980).
- [25] T. H. Dunning, Jr., *J. Chem. Phys.* **90**, 1007 (1989)
- [26] S. F. Boys and F. Bernardi, *Mol. Phys.* **19**, 553 (1970).
- [27] J. M. L. Martin, *Chem. Phys. Lett.* **259**, 669 (1996).
- [28] T. Helgaker, W. Klopper, H. Koch, and J. Noga, *J. Chem. Phys.* **106**, 9639 (1997).
- [29] W. H. Press, S. A. Teukolsky, W. T. Vetterling, and B. P. Flannery, *Numerical Recipe in C* (Cambridge University Press, Cambridge, 1996).
- [30] P. W. Atkins and R. S. Friedman. *Molecluar Quantum Mechanics*, 3rd ed. (Oxford University Press, New York, 1997).
- [31] M. K. Spackman, *J. Chem. Phys.* **94**, 1295 (1990)
- [32] A. Kumar, M. Kumar and W. J. Meath, *Chem. Phys.* **286**, 227 (2003).
- [33] E. R. Johnson and A. D. Becke, *J. Chem. Phys.* **123**, 024101 (2005).
- [34] J. E. Jones, *Proc. R. Soc. Lond. A.* **106**, 463 (1924).

Basis set	MP2					
	G conformer			H conformer		
	R_0 (Å)	R_m (Å)	E_b (kcal/mol)	R_0 (Å)	R_m (Å)	E_b (kcal/mol)
aug-cc-pVDZ	3.98	4.45	-0.484	3.98	4.46	-0.482
aug-cc-pVTZ	3.86	4.33	-0.594	3.87	4.34	-0.590
aug-cc-pVQZ	3.84	4.31	-0.622	3.85	4.31	-0.622
aug-cc-pV5Z	3.82	4.30	-0.651	3.83	4.30	-0.646
basis set limit	3.78	4.28	-0.712	3.79	4.29	-0.692

Table 2.2-1

Table 2.2-1. The basis set dependence of MP2 potentials for the G and H conformers

Conformer	Prediction (eVA^6)	Error (%)	^a Literature (eVA^6)
A	1507.75	339.57	343.0
B	1507.97	339.64	
C	641.75	87.10	
D	641.66	87.07	
E	497.82	45.14	
F	495.39	44.43	
G	342.35	0.19	
H	341.21	0.52	
I	301.10	12.22	
J	283.73	17.28	
K	480.63	40.12	
L	355.94	3.77	

^a Ref. [31-33]

Table 2.2-2

Table 2.2-2. Predicted C_6 coefficient value with literature in twelve conformers.

	aDZ^a	aTZ^a	aQZ^a	a5Z^a	
Number of basis function	126	284	536	902	
Extrapolation					
methods	aDT^b	aTQ^c	aQ5^d	aDTQ^e	aTQ5^f
<i>Martin</i>	-0.633	-0.638	-0.675	NA ^g	NA ^g
<i>Helgaker</i>	-0.640	-0.642	-0.681	NA ^g	NA ^g
<i>Numerical</i>	-0.682	-0.654	-0.693	-0.645	-0.712

Table 2.2-3

^aNumber of basis function with the MP2/aug-cc-pVXZ (X=D, T, Q and 5).

^bBasis set limit estimation with the aug-cc-pVXZ (X=D and T).

^cBasis set limit estimation with the aug-cc-pVXZ (X=T and Q).

^dBasis set limit estimation with the aug-cc-pVXZ (X=Q and 5).

^eBasis set limit estimation with the aug-cc-pVXZ (X=D, T and Q).

^fBasis set limit estimation with the aug-cc-pVXZ (X=T, Q and 5).

^gNot available.

Table 2.2-3. The estimated MP2/CBS binding energies for the G conformer

using the three extrapolation methods described in the text.

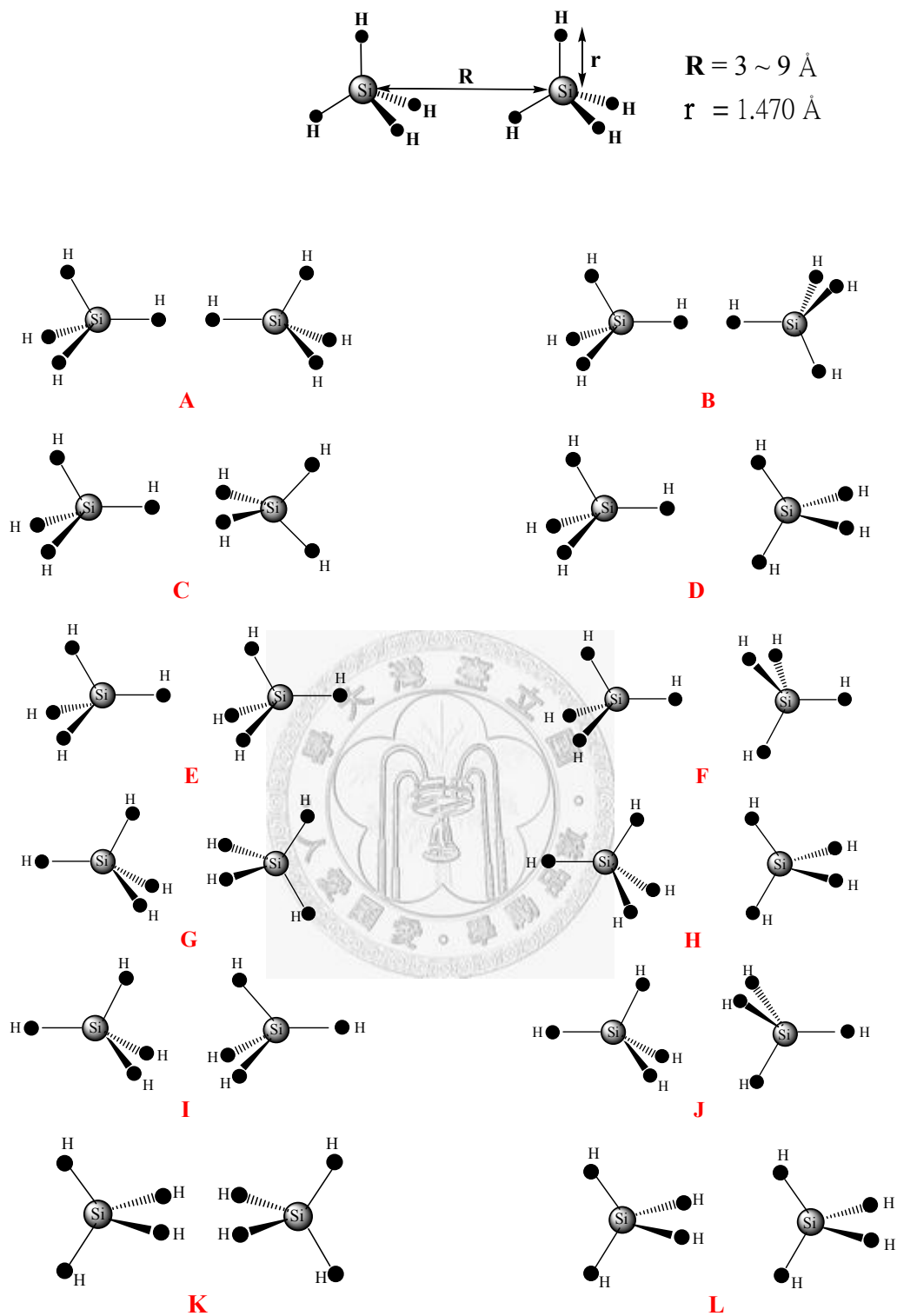


Fig. 2.2-1

FIG. 2.2-1. The twelve symmetric conformers of the silane dimer. We designate each conformer by a representative capital letter from A to L.

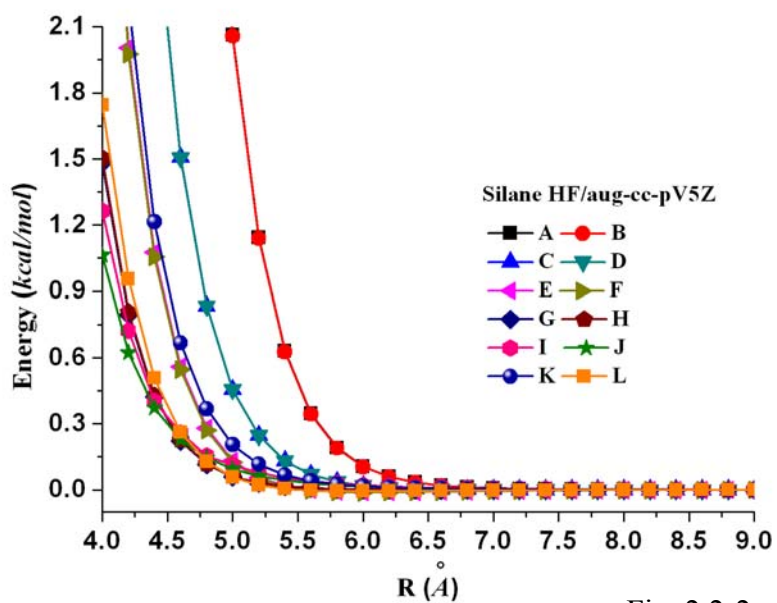


Fig. 2.2-2

FIG. 2.2-2. The HF potentials for the 12 orientations using the aug-cc-pV5Z basis set.

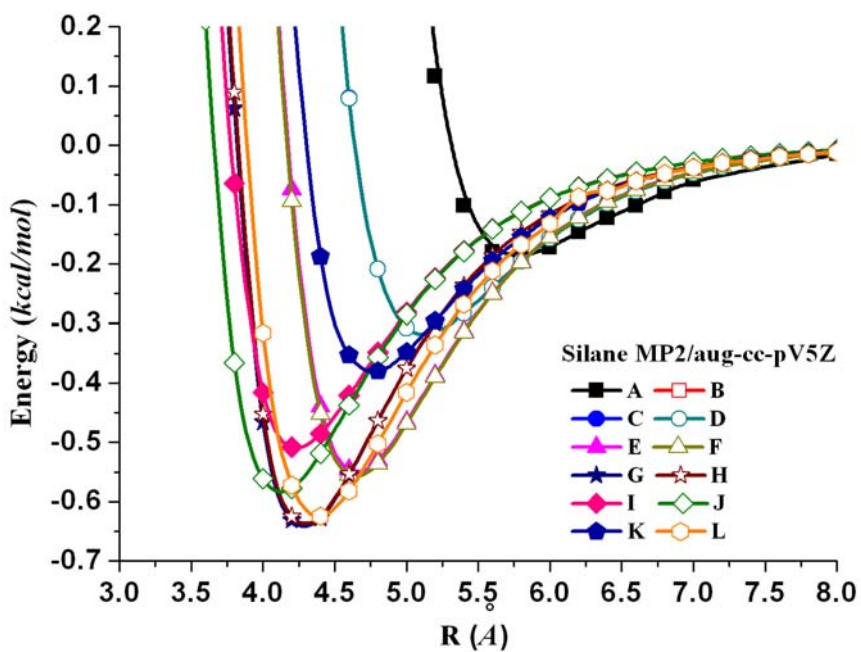


Fig. 2.2-3

FIG. 2.2-3. The MP2 potentials for the 12 orientations using the aug-cc-pV5Z basis

set.

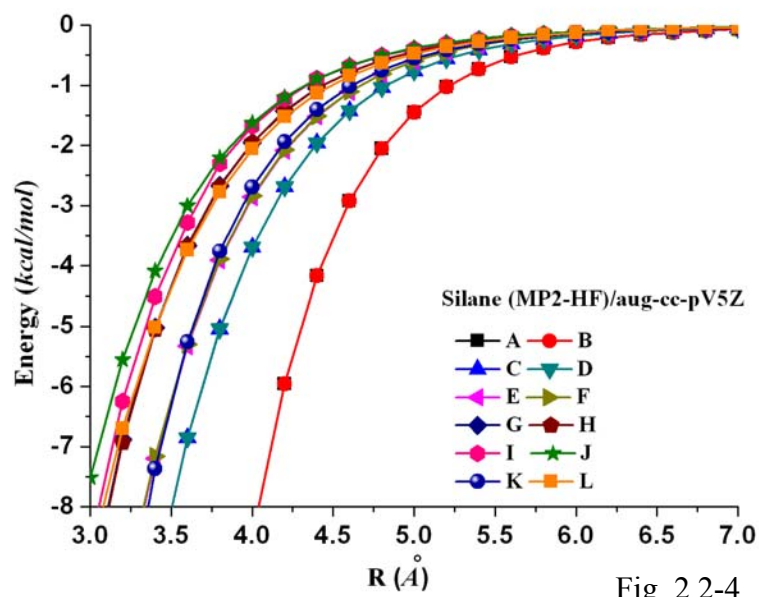


Fig. 2.2-4

FIG. 2.2-4. The MP2-HF potentials for the 12 orientations using the aug-cc-pV5Z

basis set.

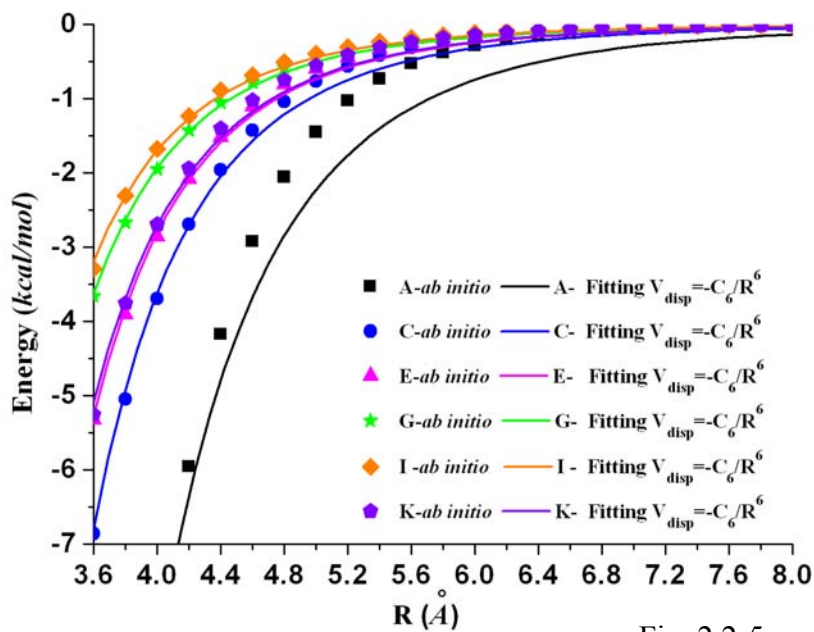


Fig. 2.2-5

FIG. 2.2-5. The C_6 coefficient value has been obtained by fitting to intermolecular

potential energy from *ab initio* calculation.

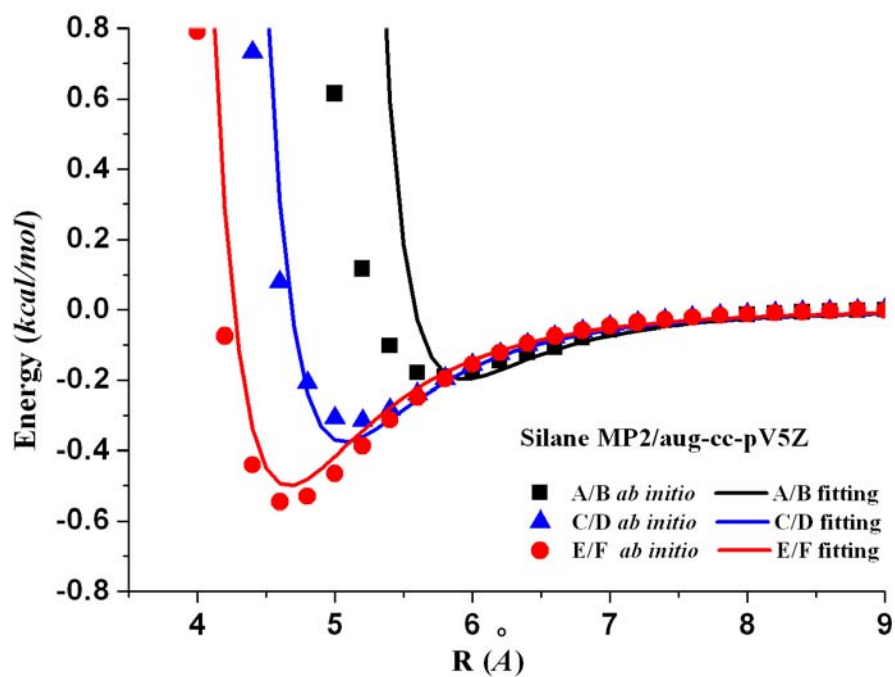


Fig. 2.2-6(a)

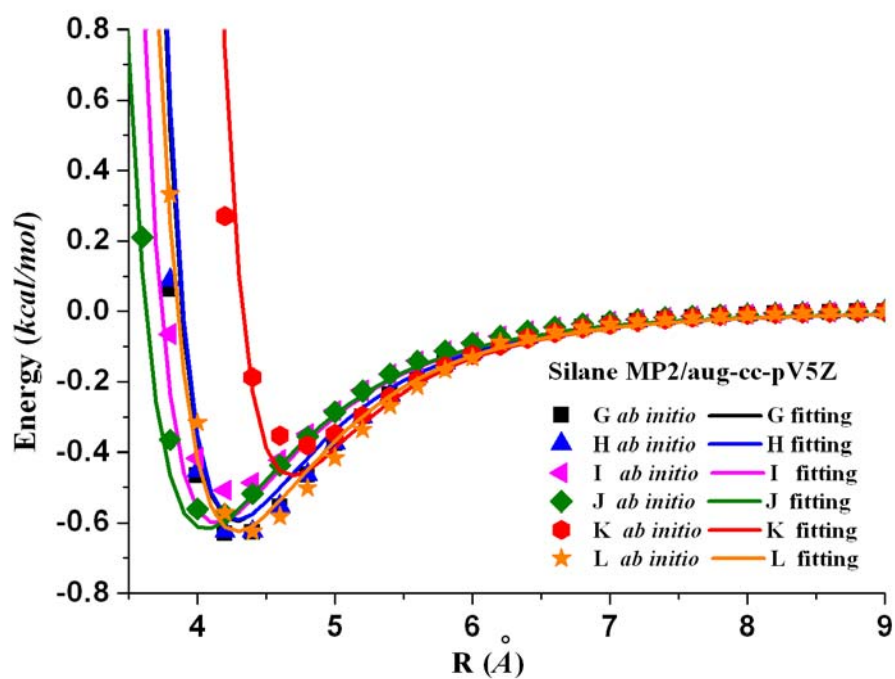


Fig. 2.2-6(b)

FIG 2.2-6(a)-6(b). Comparison of the fitting curves (line) and the potential data (symbol).

Chapter 3 Theoretical Studies on the Carbon Tetrachloride Dimers

3.1 *Ab initio* force field modeling and molecular dynamics simulation of liquid carbon tetrachloride

1. Introduction

Carbon tetrachloride (CCl_4) has been widely used as solvents in many industrial processing procedures such as petroleum separation processes or spectroscopic analyses [1-2]. CCl_4 is also one of the earliest systems exhibiting the plastic crystal phase behavior [3-8]. Therefore, the structural and thermodynamic properties of CCl_4 have long been intensely studied by experimental means, such as X-ray and neutron diffraction [9-13]. Despite of these valuable experimental data accumulated for decades, the issue of thermodynamic state dependence of the CCl_4 dimer structure in liquid or solid phase is still debating in recent literature [14-18]. Part of the reasons involved is due to the incompleteness of experimental sampling. For example, experiments using the X-ray crystallography or the laser luminescence spectroscopy mainly explore the equilibrium regions of the potential surface, while thermodynamic measurements in the fluid or solid phase often yield isotropic potential data without the desired stereochemical responses.

Computer simulations, such as molecular dynamics (MD) or Monte Carlo (MC) simulation can complement experiments in providing predictions await laboratory verification. However, most previous simulations used empirical force fields which were themselves not validated over extensive enough thermodynamic conditions, thus rendering great ambiguity in interpreting the simulation results. Because the efficacy of a simulation ultimately depends on the quality of the force field used, recent attention has been drawn to constructing the force field based on only quantum chemistry calculation, or the *ab initio* force field, without experimental data input.

Chang *et al.* [19] has constructed a polarizable potential model and calibrated it with the CCl₄ dimer interaction potential calculated at the MP2/aug-cc-pVDZ level of theory. Soetens *et al.* [20] have calculated the interaction energies of the CCl₄ dimer for 6 relative orientations at the MP2/aug-cc-pVDZ level and used the data to construct a 5-site model. Their MD simulations by and large reproduced the experimental data while some significant discrepancy was observed. They attributed the discrepancy to the inefficacy of their force field modeling, being too shallow.

Mahlanen *et al.* [21] calculated the dimer interaction for 11 orientations at the MP2/aug(df)-6-311G* level, resulting in 355 data points, and a 5-site potential functions were used to fit the *ab initio* data. However, there was no simulation result presented for comparison to experiments. Krongasuk *et al.* [14] have calculated the

interaction energies of the CCl_4 dimer for 800 configuration points at the MP2/6-31G** level and used the data to construct a 5-site model. Their MC simulations could well reproduce the experimental radial distribution functions.

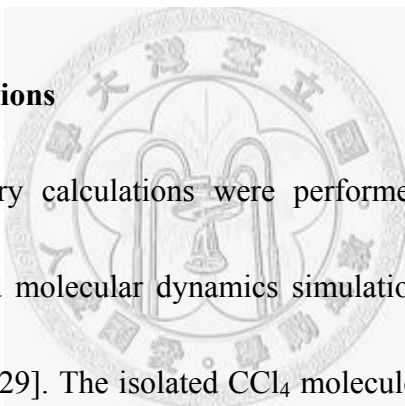
These previous works are either inaccurate enough in the *ab initio* potential data or are not validated against a wider enough range of experimental data. Currently, no *ab initio* force fields so far have been calculated at a spectroscopic accuracy level while at the same time can be used to reproduce the structural and transport properties of liquid CCl_4 . In previous studies [22-27], we have calculated the interaction potentials of the methane and silane dimers. Because of the similarity in structures, carbon tetrachloride is expected to have similar radial responses for the dimer potentials as methane and silane. However, because the disparity in the relative electronegativity and the apparent larger bond polarizability, the orientational response of the intermolecular interaction would be subtly different from that for the methane case.

In this paper we construct an *ab initio* force field using a high level theory, up to MP2/aug-cc-pVTZ, for 12 conformers of CCl_4 . We determine the accuracy of the constructed *ab initio* force field using MD simulations and the results are compared with experiments. Quantitative agreements with the measured radial distribution

functions, the self-diffusion coefficients, and the neutron and X-ray diffraction scattering functions for a wide range of thermodynamic conditions provide a proper justification on the validity of this force field.

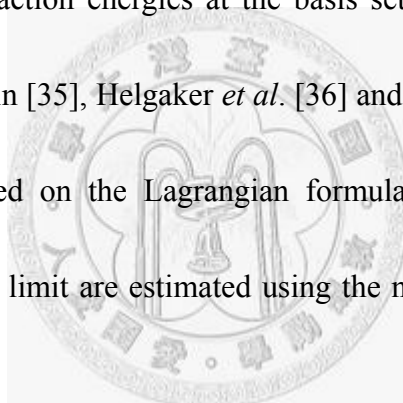
The paper is organized as follows. In Section II, we describe the details of these calculations. In Section III the results are presented and discussed. A summary and a brief perspective are given in Section IV.

2. Methods and Calculations



All the quantum chemistry calculations were performed using the Gaussian 03 program package [28] and molecular dynamics simulations were performed by the Materials Studio package [29]. The isolated CCl_4 molecule was first optimized at the MP2/6-311++G (3d, 3p) theory and was found to be at the tetrahedral configuration (T_d symmetry) with the C-Cl bond length of 1.768 \AA which is consistent with the experimental data 1.769 \AA [30]. The 12 symmetric conformers chosen to sample the orientational response are depicted in Fig. 3.1-1. Because of the high symmetry of the dimer configuration, the angular sampling should be wide enough to model the rotational dynamics in normal thermodynamic conditions. The MP2 method [31] has been used to treat the correlation effect. Pople's medium size basis sets [up to

6-311++G (3df, 3pd)] [32] and Dunning's correlation consistent basis sets (cc-pVXZ and aug-cc-pVXZ, X=D, T, Q) [33] were employed in the calculations. The basis set superposition errors were corrected by the counterpoise method of Boys and Bernardi [34]. Subsequently the carbon-carbon (C-C) distance, denoted as R , was sampled for a large range of 4~10 Å, with 31 configuration points for each conformer. A total of 372 configuration points were actually sampled and the energies calculated. During the scan we fixed the monomer geometry (rigid monomer assumption) and the conformer symmetry. The MP2 interaction energies at the basis set limit have been estimated using the methods of Martin [35], Helgaker *et al.* [36] and Feller [37] and a numerical extrapolation scheme based on the Lagrangian formula [38]. The other potential parameters at the basis set limit are estimated using the numerical extrapolation (see Table 3.1-1).



The MD simulations were performed in a rectangular cell with the periodic boundary conditions imposed on the three coordinate directions. A total of 500 carbon tetrachloride molecules were initially arranged in random configuration. An isobaric-isothermal (constant-NPT) ensemble was used with the temperature control by rescaling the center-of-mass velocities every 500 time steps. Equations of motion were solved using the velocity-Verlet algorithm with the time step of 1 fs. The system

was checked equilibrium after running 20 ps and allowed 200 ps for data collection. The cut-off radius was set to be half of the box size to avoid long range correlations. The simulated thermodynamic conditions cover a density range of 0.557~1.660 g/cm³ and a temperature range of 250.0 ~ 556.5 K, where the experimental data are available.

3. Results and Discussions

A. Hartree-Fock self-consistent field calculations

The BSSE corrected HF interaction potentials of the carbon tetrachloride dimer in 12 symmetric conformers are shown in Fig. 3.1-2. The HF calculations for most conformers yield purely repulsive potentials without minima for all the basis sets used except the C, D, E and F conformers. The C and D potentials have attractive wells. This might be due to the large bond polarizability. The E and F potentials exhibit weak wells. This can be attributed to the electrostatic attraction because the E and F orientations are favored by the multipole interactions. In the short range, the strong exchange-repulsion interaction dominates with little alternation from the electrostatic and induction attractions. We can model the HF potential for the J conformer using the repulsive Buckingham function [39]

$$V_{HF}(R) = Ae^{-\alpha R} \quad (1)$$

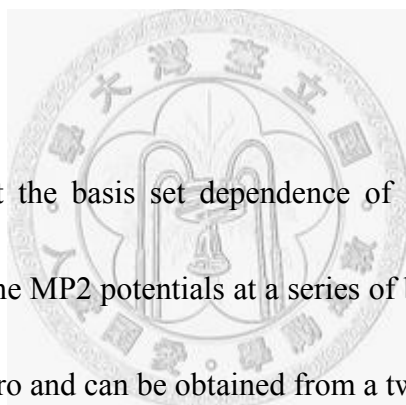
where R is the C-C distance, A and α (the repulsion exponent) are the fitting parameters. The fitting parameters are listed in Table 3.1-1. It is seen that the repulsion exponent converges quickly after the 6-31G** basis set being used.

B. MP2 calculations

In Fig. 3.1-3 we show the MP2 potentials for the twelve conformers using the aug-cc-pVTZ basis set. We see that the potentials become deeper when there are more inner chlorine atom contacts between the monomers. It is found that the minimum-energy conformation corresponds to the D_{3d} symmetry configuration (the J conformer), which is consistent with a previous energy dissection method [40]. It is interesting to analyze the orientational responses from the repulsive and the attractive components of the potentials separately. CCl_4 is a non-polar molecule and the dominant long-range attraction is thus due to the London dispersion force. On the other hand, the strong repulsive force almost comes from the exchange-repulsion interaction. Contrasting the HF and the MP2 potentials thus helps to delineate the relative importance of the dispersion energy in the overall intermolecular interactions.

In Fig. 3.1-4 we show the MP2 potentials subtracting the corresponding HF potentials, dubbed as MP2-HF, for the twelve conformers. The MP2-HF potentials largely represent the dispersion curves which are purely attractive. We see larger variations

for the repulsive components as compared to the attractive components. For example, at $R=6.00\text{\AA}$, the HF potentials (MP2-HF potentials) vary from 0.066 kcal/mol (-1.101kcal/mol) for the J conformer to 20.215 kcal/mol (-9.553 kcal/mol) for the A conformer. That is to say, compared to the others, the J conformer has actually the weakest attractive but also the weakest repulsive parts. Therefore, it is actually due to the stronger variation in the repulsive interactions, but not due to the stronger attraction as would be intuitively expected, that the J conformer is the most stable carbon tetrachloride dimer.



In Table 3.1-1 we present the basis set dependence of several important potential quantities extracted from the MP2 potentials at a series of basis sets. R_0 is the distance at which the potential is zero and can be obtained from a two point interpolation of the calculated data. The bond length R_m and the binding energy E_b can be obtained through a harmonic modeling of the three lowest potential data near equilibrium regions. With increasing basis size, the equilibrium bond length converges at the aug-cc-pVDZ basis set to a 0.1 \AA accuracy, while a pretty large basis set, aug-cc-pVTZ, is required to converge the binding energy at a spectroscopic accuracy ($\sim 0.1\text{ kcal/mol}$). This explains the inefficacy of the potential calculated by Soetons *et al.* [20] using the aug-cc-pVDZ basis set. The strong basis set dependence and the

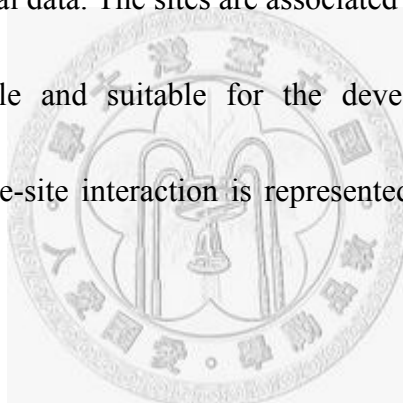
slow convergence on the binding energy call for an estimation of the potential features at the complete basis set (CBS) limit. The CBS binding energies can be obtained by an extrapolation scheme with Dunning's basis sets. We consider the methods of Martin [35], Helgaker *et al.* [36], Feller [37] and a numerical extrapolation scheme based on the 3-term Lagrange formula [38] and the MP2/CBS results are listed in Table II. We see that using the aug-cc-pVXZ data, instead of the cc-pVXZ data, the four extrapolation methods yield similar CBS values. This shows clearly that the quality of the extrapolation critically depends on the basis set functions used.

C. Analytical site-site pair potential model

Figure 3.1-3 shows interesting interplay among the contact atoms of CCl_4 dimer. First we notice that for the A~F conformers, the A and B, the C and D, and the E and F potential curves are numerically identical, respectively (hence we show only one respective curve of them in Fig. 3.1-3). This indicates that the inner chlorine-chlorine interactions play a major role, as compared with the outer chlorine-chlorine interactions, in determining the overall interaction energies. Next we observe that the G and H potential curves are almost identical, which indicates that some compensation among the inner chlorine atoms occurs to allow two possible degenerate 3-2 configurations. The same reasoning can be used to rationalize the

relative stability of the I and J conformers. For the J conformer, the inner 3-3 chlorine atoms manage to “avoid” each other to reach a more favorable stabilization over the I conformer where the chlorine atoms “head on”. Similar arguments apply to the K and L conformers also. Therefore, we conclude that the inner chlorine interactions are the major components contributing to the potential anisotropy.

Based on these observations, an analytical 4-site model was proposed to represent the MP2/aug-cc-pVTZ potential data. The sites are associated with the chlorine atoms and this model is very simple and suitable for the development of coarse-grained potentials [41-42]. The site-site interaction is represented by a Lennard-Jones (L-J) function.



$$U(r_{ij}) = 4\varepsilon \left[\left(\frac{\sigma}{r_{ij}} \right)^{12} - \left(\frac{\sigma}{r_{ij}} \right)^6 \right] \quad (2)$$

where the indices i and j denote the chlorine atoms in separated monomers, respectively, and r_{ij} represent the chlorine - chlorine distance for a pair of i and j chlorine atoms. In this model σ and ε are the potential parameters to be determined in the non-linear regression. No bias weights were put on specific configurations except that we excluded from the non-linear fitting some largest repulsive energy points in the regression to prevent their dominance in the least-squares cost function [43].

However, this latter constraint could effectively put more weight on deeper wells. The fitting parameters we obtained are $\sigma=3.45 \text{ \AA}$ and $\varepsilon=0.387 \text{ kcal/mol}$. In Fig. 3.1-5 we present the fitting curves and the *ab initio* data. Notice that the order of the potential data has been correctly represented by the fitting curves, which echoes the above physical arguments.

D. Molecular dynamics

We evaluate the force field model by running molecular dynamics simulations [29] on it. We calculate the atom(α)-atom(β) radial distribution functions (RDFs) by the definition [44-45]

$$g_{\alpha\beta}(r) = \frac{n(r)}{\rho 4\pi r^2 \Delta r} \quad (3)$$

where $g_{\alpha\beta}(r)$ is the radial distribution function for the α - β atom pair, $n(r)$ is the mean number of atoms in a shell of radius r and thickness Δr surrounding the atom, and ρ is the mean density for total system. The calculation of $g_{\alpha\beta}(r)$ consists of about 10000 trials, with each by selecting an α atom as the origin and counting the β atoms within the spherical shells of thickness $\Delta r=0.02\sigma$ using the histogram method. Fig. 3.1-6(a) ~ 6(c) present the simulated atom-atom radial

distribution functions for temperature from $T=260.0\text{ K}$ to $T=556.5\text{ K}$ and density $\rho=1.660\text{ g/cm}^3$ to $\rho=0.557\text{ g/cm}^3$. The path is roughly from the triple point to the critical point along the condensation line on the phase diagram. As we can see from the comparison of the calculated peak positions with the experimental data [3-5] as shown in Table 3.1-3, the overall agreement is satisfactory. The peak and valley positions are well reproduced for the RDF. We have also simulated the scattering functions from neutron and X-ray diffraction and compared with experiments at temperature 293 K in Fig. 3.1-7 and Fig. 3.1-8 respectively. The (not normalized) scattering functions

$$I(K) = \sum_j \sum_k f_j^* f_k \exp(i\mathbf{r}_{jk} \cdot \mathbf{K}) \quad (4)$$

where $f_{j,k}$ are the scattering lengths, can thus be obtained from the RDFs through a Fourier transform [20]. The simulated results from this model are in good quantitative agreement with the curves derived from our data.

Next, we have calculated the self-diffusion coefficients using the Green-Kubo formula [46-48],

$$D = \frac{1}{3N} \int_0^\infty \left\langle \sum_i^N \bar{v}_i(t) \cdot \bar{v}_i(0) \right\rangle dt \quad (5)$$

where \bar{v}_i is the velocity vector of particle i and the statistical average is the velocity

autocorrelation functions (VAFs). In Table 3.1-4, we present the comparison of the calculated self-diffusion coefficients with experiments from different research groups [49-50]. We see the results are generally in good agreement with the experiments. At lower temperature, the calculated D is higher than the experimental value. This is a characteristic feature that as the liquid freezes, it would approach first to the plastic crystal phase Ia, but not directly to the ordered phase II [6].

4. Conclusion

To simulate liquid carbon tetrachloride properties, we have employed quantum chemistry calculation to obtain the potential data. The potentials exhibit significant anisotropy, which is analyzed and considered in the 4-site force field model used to fit the potential data. We determine the accuracy of the constructed *ab initio* force field using MD simulations and the results are compared with experiments. Quantitative agreements with the observed radial distribution functions (RDFs), the self-diffusion coefficients and the scattering functions have been obtained for a wide range of thermodynamic conditions.

5. Bibliography

[1] M. P. Allen and D. J. Tildesley, *Computer Simulation of Liquids* (Oxford

university Press, Oxford, 1987).

- [2] A. A. Al-Kahtani, *Spectrochim, Acta, Part. A.* **58**, 2877 (2002).
- [3] A. N. Campell and R. M. Chatterjee, *Canadian J. Chem.*, **47**, 3893 (1969).
- [4] A. H. Narten, *J. Chem. Phys.*, **65**, 573 (1976).
- [5] S. Cohen, R. Powers and R. Rudman, *Acta. Cryst.* **B35**, 1670 (1979).
- [6] I. R. McDonald, D. G. Bounds, and M. L. Klein, *Mol. Phys.* **45**, 521 (1982).
- [7] A. Chahid, F. J. Bermejo, E. Enciso, M. G. Hernandez and J. L. Martinez, *J. Phys.:Condens. Matter* **4**, 1213 (1992).
- [8] L. Pusztai and R. L. McGreevy, *Mol. Phys.*, **90**, 533 (1997).
- [9] A. H. Narten, M. H. Danford and H. A. Levy, *J. Chem. Phys.*, **46**, 4875 (1967).
- [10] P. A. Egelstaff, D. I. Page and J. G. Powles, *Mol. Phys.*, **20**, 881 (1971).
- [11] J. B. van Tricht, *J. Chem. Phys.*, **85**, 1977 (1977).
- [12] F. J. Bermejo, E. Enciso, J. Alonso, N. Garcia and W. S. Howells, *Mol. Phys.*, **64**, 1169 (1988).
- [13] M. Misawa, *J. Chem. Phys.*, **91**, 5648 (1989).
- [14] S. Kongsuk, T. Kerdcharoen, M. Kiselev, S. Hannongbua, *Chem. Phys.*, **324**, 447 (2006).
- [15] R. Rossend, *J. Chem. Phys.*, **126**, 164506 (2007).
- [16] R. Rossend, *J. Phys. Chem. B*, **112**, 344 (2008).

- [17] R. Rossend, *J. Chem. Phys.*, **129**, 224509 (2008).
- [18] Sz. Pothoczki, L. Temleitner, P. Jovari, S. Kohara and L. Pusztai, *J. Chem. Phys.*, **130**, 064503 (2009).
- [19] T. M. Chang, K. A. Peterson and L. X. Dang, *J. Chem. Phys.*, **103**, 7502 (1995).
- [20] J. C. Soetens and G. Jansen, *Mol. Phys.*, **96**, 1003 (1999).
- [21] R. Mahlanen, J. P. Jalkanen and T. A. Pakkanen, *Chem. Phys.*, **313**, 271 (2005).
- [22] A. H.-T. Li and S. D. Chao, *J. Chem. Phys.*, **125**, 094312 (2006).
- [23] A. H.-T. Li and S. D. Chao, *Phys. Rev. A.*, **73**, 016701 (2006)
- [24] S. D. Chao and A. H.-T. Li, *J. Phys. Chem. A.*, **111**, 9586 (2007).
- [25] C. C. Pai, A. H.-T. Li and S. D. Chao, *J. Phys. Chem. A.*, **111**, 11922 (2007).
- [26] S. W. Chao, A. H.-T. Li and S. D. Chao, *J. Comput. Chem.*, **30**, 1839 (2009).
- [27] A. H.-T. Li and S. D. Chao, *J. Mol. Struct. Theo.*, **897**, 90 (2009).
- [28] M. J. Frisch, G. W. Trucks, H. B. Schlegel *et al.*, Gaussian 03, Revision D.02, Gaussian, Inc., Wallingford CT, 2004.
- [29] <http://accelrys.com/products/materials-studio/>
- [30] J. Haase and W. Zell, *Phys. Chem.*, **45**(3/4), 202 (1965).
- [31] C. Møller and M. S. Plesset, *Phys. Rev.* **46**, 618 (1934).
- [32] R. Krishnan, J. S. Binkley, R. Seeger, and J. A. Pople, *J. Chem. Phys.*, **72**, 650 (1980).

- [33] T. H. Dunning, Jr., *J. Chem. Phys.*, **90**, 1007 (1989).
- [34] S. F. Boys and F. Bernardi, *Mol. Phys.*, **19**, 553 (1970).
- [35] J. M. L. Martin, *Chem Phys Lett.*, **259**, 669 (1996).
- [36] T. Helgaker, W. Klopper, H. Koch, and J. Noga, *J. Chem. Phys.*, **106**, 9639 (1997).
- [37] D. Feller, *J. Chem. Phys.*, **96**, 6104 (1992).
- [38] W. H. Press, S. A. Teukolsky, W. T. Vetterling, and B. P. Flannery, *Numerical Recipe in C* (Cambridge University Press, Cambridge, 1996).
- [39] F. Jensen, *Introduction to Computational Chemistry*. Wiley:New York (1999)
- [40] M. M Szczesniak, G. Chalasinski, S. M. Cybulski and S. Scheiner, *J. Chem. Phys.*, **93**, 4243 (1990).
- [41] S. D. Chao, J. D. Kress, and A. Redondo, *J. Chem. Phys.* **120**, 5558 (2004).
- [42] S. D. Chao, J. D. Kress, and A. Redondo, *J. Chem. Phys.* **122**, 234912 (2005).
- [43] J. M. Hayes, J. C. Greer, and D. A. Morton-Blake, *J. Comp. Chem.* **25**, 1953 (2004).
- [44] D. C. Rapaport, *The Art of Molecular Dynamics Simulation* (Cambridge University Press, New York, 1995).
- [45] F. Jensen, *Introduction to Computational Chemistry* (Wiley, New York, 1999).
- [46] M. S. Green, *J. Chem. Phys.*, **20**, 1281 (1952).

[47] M. S. Green, *J. Chem. Phys.*, **22**, 398 (1954).

[48] Kubo, R. "Statistical Mechanical Theory of Irreversible Processes. I. General Theory and Simple Applications to Magnetic and Conduction Problems", *J. Phys. Soc. Jpn.*, **12**, 570 (1957).

[49] R. Dawson, F. Khoury, and R. Kobayashi, *AIChE J.* **16**, 725 (1970).

[50] K. R. Harris and N. J. Trappeniers, *Physica A.* **104**, 262 (1980).



Basis set	MP2	HF		MP2		
	Number of basis function	A (kcal/mol)	α (\AA^{-1})	R_0 (\AA)	R_m (\AA)	E_b (kcal/mol)
STO-3G	82	48397683	3.75	5.66	6.29	-0.010
3-21G	122	1299506	2.79	5.49	6.03	-0.123
6-31G	122	1617627	2.84	5.43	6.00	-0.135
3-21G**	170	1046010	2.75	4.98	5.57	-0.397
cc-pVDZ	172	1243814	2.79	4.78	5.36	-0.581
6-31G**	182	1422093	2.81	4.87	5.43	-0.473
aug-cc-pVDZ	262	1347998	2.81	4.28	4.81	-2.310
cc-pVTZ	332	1440544	2.82	4.36	4.87	-1.722
6-311++G(3df,3pd)	454	2401632	2.93	4.24	4.77	-2.609
aug-cc-pVTZ	492	1314163	2.79	4.17	4.70	-2.968
cc-pVQZ	582	1269782	2.78	4.20	4.72	-2.581
aug-cc-pVQZ	832	1266359	2.78	4.13	4.65	-3.220
Basis set limit		1161130	2.76	4.08	4.58	-3.523

Table 3.1-1.

Table 3.1-1. The basis set dependence of some potential parameters of the HF and MP2 potentials for the J conformer.

	DT^a	TQ^b	DTQ^c	aDT^d	aTQ^e	aDTQ^f
<i>Martin</i>	-2.123	-3.076	NA ^g	-3.200	-3.365	NA ^g
<i>Helgaker</i>	-2.020	-3.207	NA ^g	-3.245	-3.326	NA ^g
<i>Feller</i>	NA ^g	NA ^g	-2.684	NA ^g	NA ^g	-3.376
<i>Numerical</i>	-2.949	-3.721	-4.045	-3.718	-3.585	-3.523

Table 3.1-2

^aBasis set limit estimation with the cc-pVXZ(X=D and T).

^bBasis set limit estimation with the cc-pVXZ(X=T and Q).

^cBasis set limit estimation with the cc-pVXZ(X=D, T, and Q).

^dBasis set limit estimation with the aug-cc-pVXZ(X=D and T).

^eBasis set limit estimation with the aug-cc-pVXZ(X=T and Q).

^fBasis set limit estimation with the aug-cc-pVXZ(X=D, T, and Q).

^gNot available.

Table 3.1-2. The estimated MP2/CBS binding energies for the J conformer. using the four extrapolation methods

described in the text.

	g _{cc1}			g _{cc1}		
	EXP	4 sites	Error (%)	EXP	4 sites	Error (%)
1 st peak	4.91	5.09	3.54	3.80	3.76	1.06
1 st valley	5.95	6.17	3.57	4.79	4.90	2.24
2 nd peak	7.06	6.99	1.00	6.07	6.23	2.57
2 nd valley	8.71	8.70	0.11	7.49	7.62	1.71

Table 3.1-3

Table 3.1-3. Comparison of the calculated peak and valley positions of the RDF with the experiment [5].

T (K)	ρ (g/cm ³)	D-Theory (10 ⁻⁹ m ² /s)	D-Exp. (10 ⁻⁹ m ² /s)
260	1.66	0.706	0.300
293	1.58	1.306	1.284
328	1.53	1.801	NA ^a
453.2	1.25	6.638	NA ^a
556.5	0.56	40.040	NA ^a

^aNot available

Table 3.1-4

Table 3.1-4. The self-diffusion coefficients using the Green-Kubo formula [46-48] as compared to the available experimental data [7].

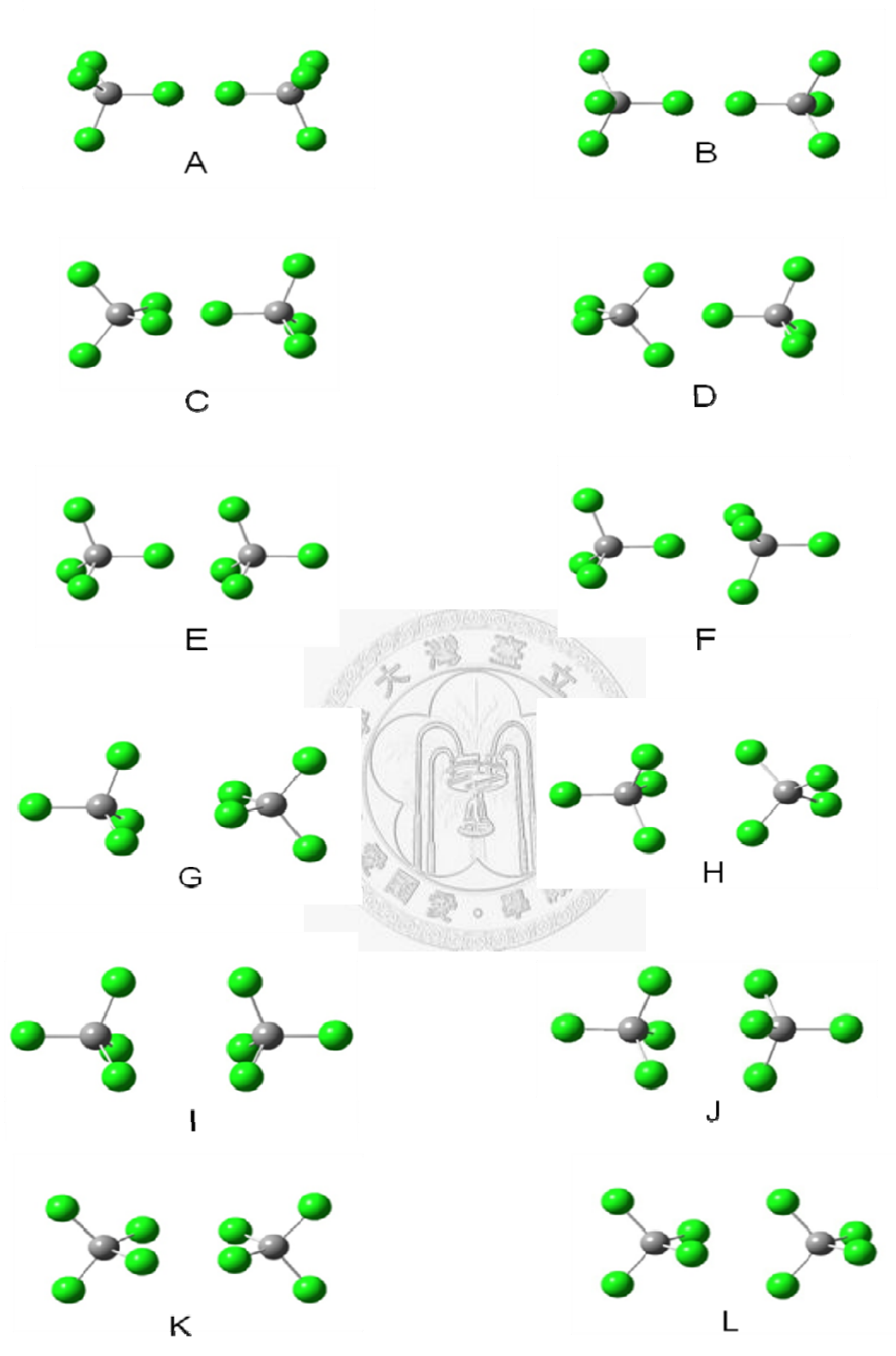


Fig. 3.1-1

FIG. 3.1-1. The twelve symmetric conformers of the carbon tetrachloride dimer. We designate each conformer by a representative capital letter from A to L.

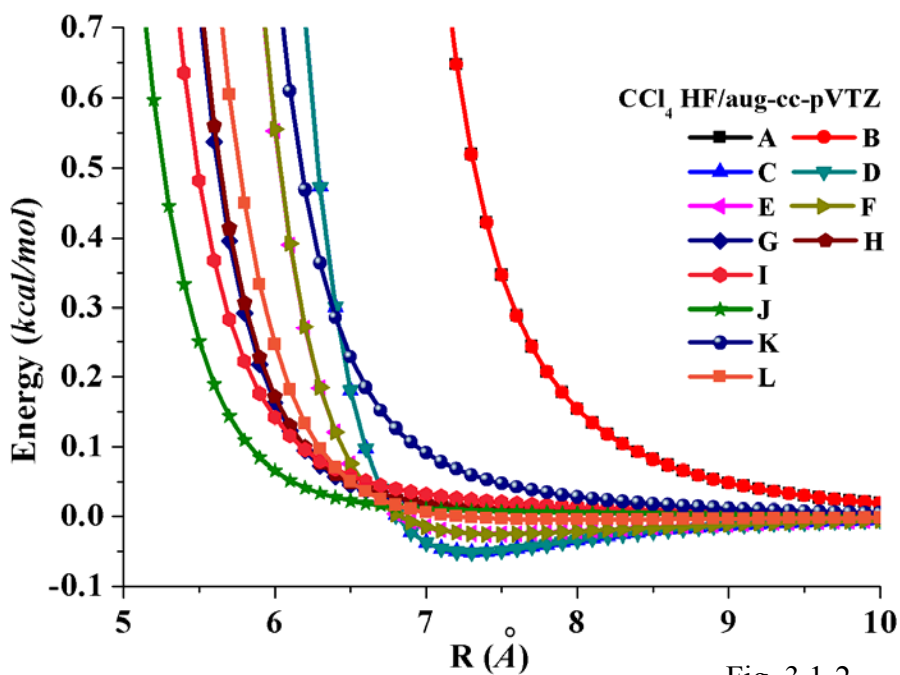


Fig. 3.1-2

FIG. 3.1-2. The HF potentials for the 12 orientations using the aug-cc-pVTZ basis set.

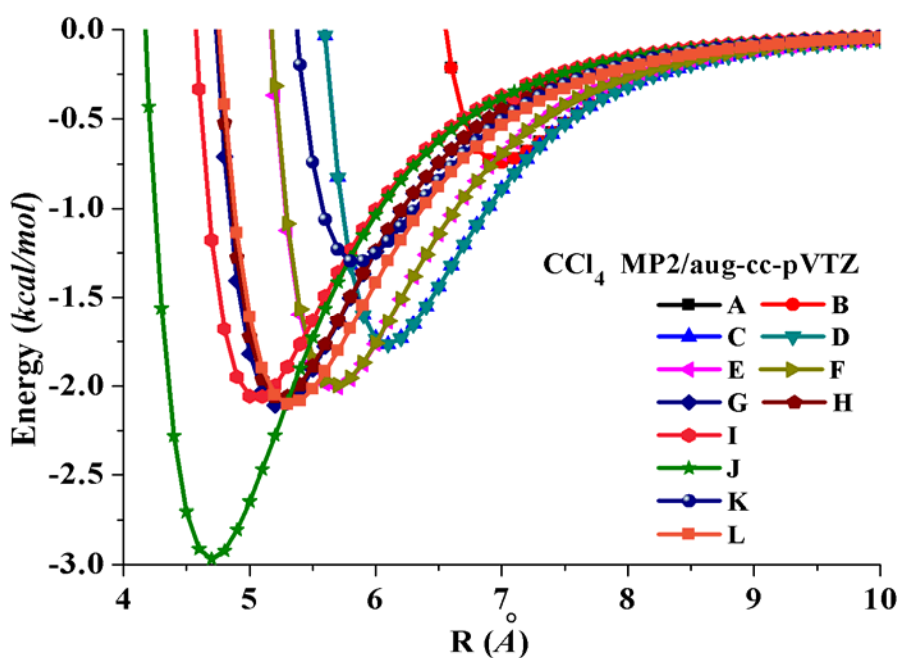


Fig. 3.1-3

FIG. 3.1-3. The MP2 potentials for the 12 orientations using the aug-cc-pVTZ basis

set.

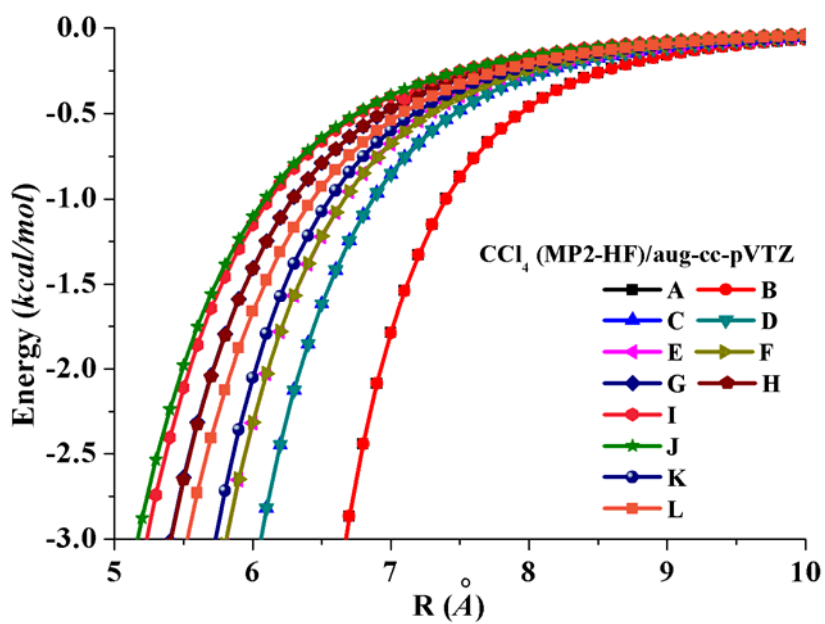


Fig. 3.1-4

FIG. 3.1-4. The MP2-HF potentials for the 12 orientations using the aug-cc-pVTZ basis set.

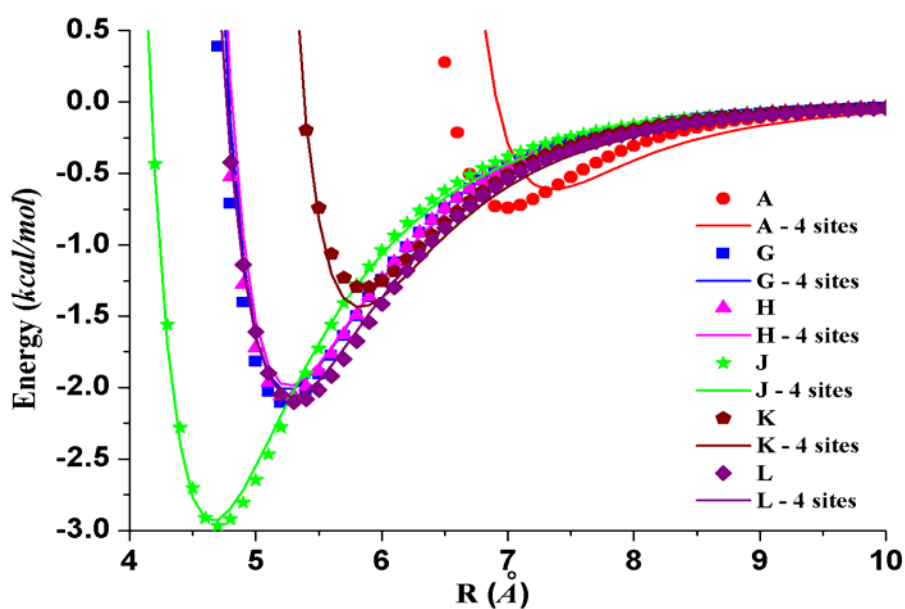


Fig. 3.1-5

FIG. 3.1-5. Comparison of the fitting curves (line) and the potential data (symbol).

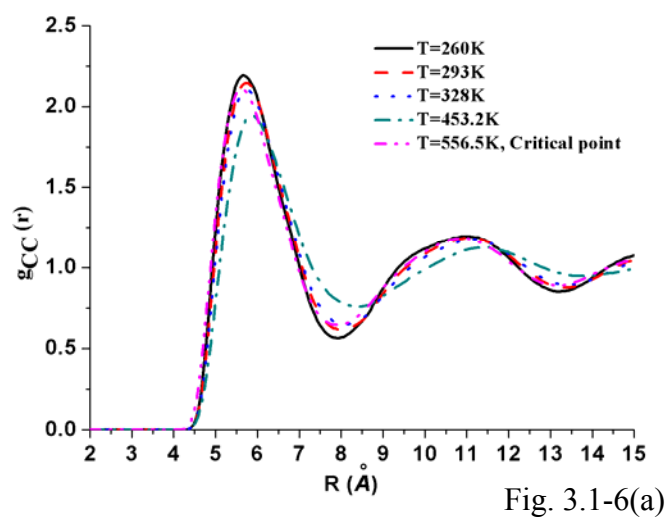


Fig. 3.1-6(a)

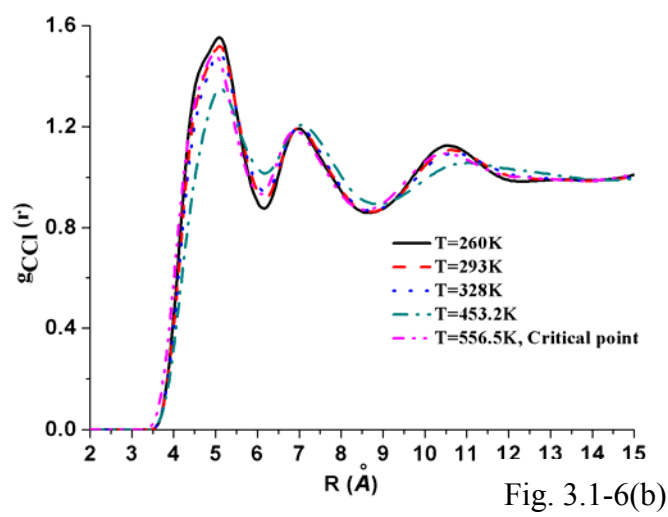


Fig. 3.1-6(b)

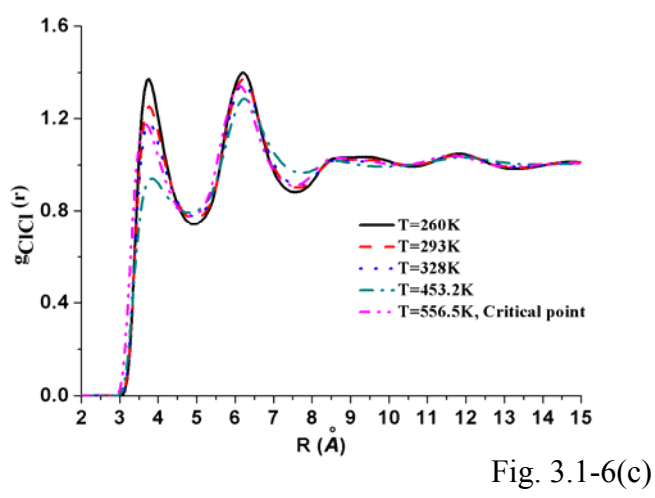


Fig. 3.1-6(c)

FIG. 3.1-6(a) ~ 6(c). The calculated C-C, C-Cl and Cl-Cl radial distribution function g_{CC} , g_{CCl} , g_{ClCl} for a range of thermodynamic conditions.

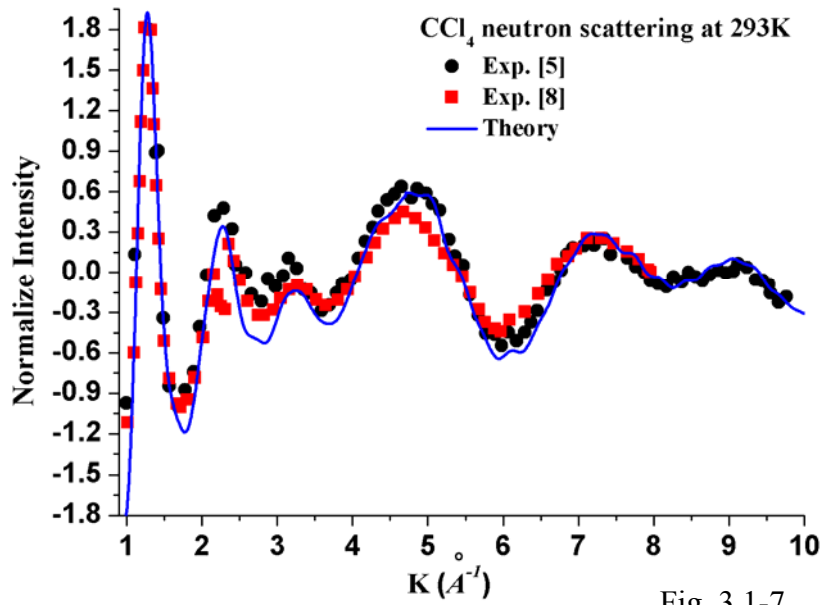


Fig. 3.1-7

FIG. 3.1-7. Comparison of theory curve (line) and neutron scattering functions (symbol).

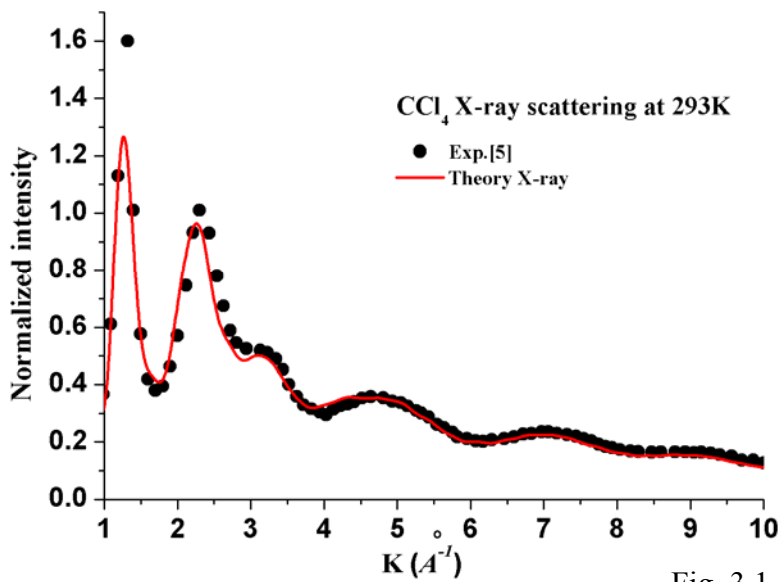


Fig. 3.1-8

FIG. 3.1-8. Comparison of theory curve (line) and X-ray scattering functions (symbol).

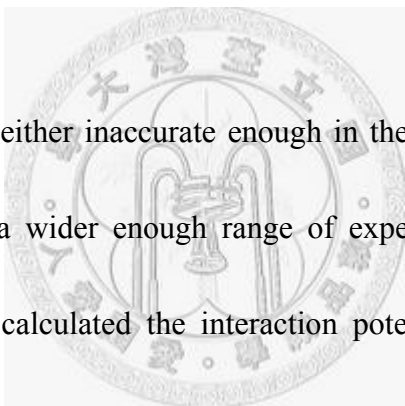
3.2 Intermolecular potentials of the carbon tetrachloride dimer calculated with Møller-Plesset perturbation theory and density functional theory

1. Introduction

Carbon tetrachloride (CCl₄) has been widely used as solvents in many industrial processing procedures such as petroleum separation processes or spectroscopic analyses [1-2]. CCl₄ is also one of the earliest system exhibiting the plastic crystal phase behavior [3-8]. Therefore, the structural and thermodynamic properties of CCl₄ have long been intensely studied by experimental means, such as X-ray and neutron diffraction [9-13]. Despite of these valuable experimental data accumulated for decades, the issue of thermodynamic state dependence of the CCl₄ dimer structure in liquid or solid phase is still debating in recent literature [14-18].

It is now well recognized that intermolecular potentials can be calculated in terms of correlation-corrected quantum chemistry methods [19-21] or density functional theory (DFT) [22-23] with improved generalized gradient approximation (GGA) functionals. These calculations are normally done with the supermolecular scheme in which the intermolecular potential is defined as the total energy difference between the supermolecule and the isolated subsystems. Chang *et al.* [24] has constructed a polarizable potential model and calibrated it with the CCl₄ dimer interaction potential

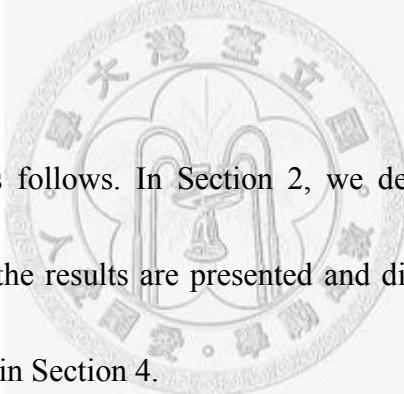
calculated at the MP2/aug-cc-pVDZ level of theory. Soetens *et al.* [25] have calculated the interaction energies of the CCl₄ dimer for 6 relative orientations at the MP2/aug-cc-pVDZ level. Mahlanen *et al.* [26] calculated the dimer interaction for 11 orientations at the MP2/aug(df)-6-311G* level, resulting in 355 data points. However, there was no simulation result presented for comparison to experiments. Krongasuk *et al.* [14] have calculated the interaction energies of the CCl₄ dimer for 800 configuration points at the MP2/6-31G** level.



These previous works are either inaccurate enough in the *ab initio* potential data or are not validated against a wider enough range of experimental data. In previous studies [27-32], we have calculated the interaction potentials of the methane and silane dimers. Because of the similarity in structures, carbon tetrachloride is expected to have similar radial responses for the dimer potentials as methane and silane. However, because the disparity in the relative electronegativity and the apparent larger bond polarity, the orientational dependence of the intermolecular interaction would be subtly different from that for the methane case.

In this paper, we perform a comprehensive study on interaction potentials of the CCl₄ dimer in terms of the HF, MP2, and DFT methods to gain better understanding of this

system for D_{3d} conformers of CCl_4 . Moreover, in this paper we will assess the utilities of using the available implementation of the density functional theory in determining the intermolecular interactions. From the studies of atomic dimers, it has been found that conventional exchange-correlation functionals based on the local density approximation (LDA) and generalized gradient approximation (GGA) cannot calculate the intermolecular interactions to a satisfying level of accuracy [33]. It is thus desirable to investigate to what extent the DFT calculations using available functionals can serve as an alternative for *ab initio* molecular orbital calculations.



The paper is organized as follows. In Section 2, we describe the details of these calculations. In Section 3 the results are presented and discussed. A summary and a brief perspective are given in Section 4.

2. Methods and Calculations

All the HF, MP2 and DFT calculations are performed using the Gaussian 03 program package [34] on a single-node two processor AMD 250 PC cluster with distributed memory. The isolated CCl_4 molecule was first optimized at the MP2/6-311++G (3d, 3p) theory and was found to be at the tetrahedral configuration (T_d symmetry) with the C-Cl bond length of 1.768 \AA which is consistent with the experimental data 1.769 \AA

[35]. Because of the high symmetry of the dimer configuration, the angular sampling should be wide enough to model the rotational dynamics in normal thermodynamic conditions. The MP2 method [36] has been used to treat the correlation effect. Pople's medium size basis sets [up to 6-311++G (3df, 3pd)] [37] and Dunning's correlation consistent basis sets (cc-pVXZ and aug-cc-pVXZ, X=D, T, Q) [38] were employed in the calculations. The basis set superposition errors were corrected by the counterpoise method of Boys and Bernardi [39]. Subsequently the carbon-carbon (C-C) distance, denoted as R , was sampled for a large range of 4~10 Å, with 61 configuration points for each conformer. A total of 732 configuration points were actually sampled and the energies calculated. During the scan we fixed the monomer geometry (rigid monomer assumption) and the conformer symmetry. From a previous energy dissection method, [40] it is found that for a general tetrahedral molecule either the D_{3d} or the C_{3v} conformer would be possibly the most stable conformer. We have thus first calculated the potential interaction energies for these two conformers at the MP2/aug-cc-pVTZ level of theory. In Figure 3.2-1, we show the comparison of the potential curves for the D_{3d} and the C_{3v} conformers. As can be seen, the D_{3d} conformer is more stable than the D_{3v} one. Therefore, we will focus on the D_{3d} conformer in this paper.

3. Results and Discussions

A. Hartree-Fock self-consistent field calculations

The BSSE corrected HF interaction potentials of the carbon tetrachloride dimer in D_{3d} conformer using several basis sets are shown in Fig. 3.2-2. The HF calculations for D_{3d} conformer yield purely repulsive potentials without minima for all the basis sets used. In the short range, the strong exchange-repulsion interaction dominates with little alternation from the electrostatic and induction attractions. We can model the HF potential for the J conformer using the repulsive Buckingham function [41]

$$V_{HF}(R) = Ae^{-\alpha R}$$

where R is the C-C distance, A and α (the repulsion exponent) are the fitting parameters. The fitting parameters are listed in Table 3.2-1. It is seen that the repulsion exponent converges quickly after the 6-31G** basis set being used.

B. MP2 calculations

In Figure 3.2-3, we compare the MP2 potentials with and without the BSSE corrections (denoted as CP and NCP, respectively). We see very strong dependence of the interaction potentials on the BSSE corrections. The potentials without the BSSE corrections fluctuate with increasing basis size and do not systematically converge to the expected curve at the basis set limit. On the contrary, the BSSE corrected potentials systematically approach the expected curve with increasing basis size.

Therefore, the BSSE correction must be considered in calculating the intermolecular interactions, in particular for small basis sets.

In Table 3.2-1 we present the basis set dependence of several important potential quantities extracted from the MP2 potentials at a series of basis sets. R_0 is the distance at which the potential is zero and can be obtained from a two point interpolation of the calculated data. The bond length R_m and the binding energy E_b can be obtained through a harmonic modeling of the three lowest potential data near equilibrium regions. With increasing basis size, the equilibrium bond length converges at the aug-cc-pVDZ basis set to a 0.1 Å accuracy, while a pretty large basis set, aug-cc-pVTZ, is required to converge the binding energy at a spectroscopic accuracy (~ 0.1 kcal/mol). This explains the inefficacy of the potential calculated by Soetons *et al.* [25] using the aug-cc-pVDZ basis set.

C. Density functional theory

We have examined the basis set effect on the DFT potentials in a similar manner as in the HF and MP2 calculations. We found that in general the DFT potentials converge at a larger basis set than the HF potentials but at a smaller basis set than the MP2 potentials. Therefore, only the aug-cc-pVTZ basis set is used to obtain the DFT

potentials which are compared to the MP2 potentials calculated at the same basis set.

The density functionals used in the present work include the 80 combinations chosen among 8 exchange (B88 [42], MPW [43], PBE [44], PW91 [45], TPSS [46], Slater [47], HCTH [48], and XAlpha [49]) and 10 correlation (TPSS [46], PBE [44], PW91 [45], P86 [50], HCTH [48], VWN5 [51], PL [52], VWN [51], and LYP [53]) functionals. We intend to examine the relative performance of the chosen exchange and correlation functionals in determining the interaction potentials for the CCl_4 dimer.

The chosen functionals are selective representations among the most commonly used density functionals employed in current literature.

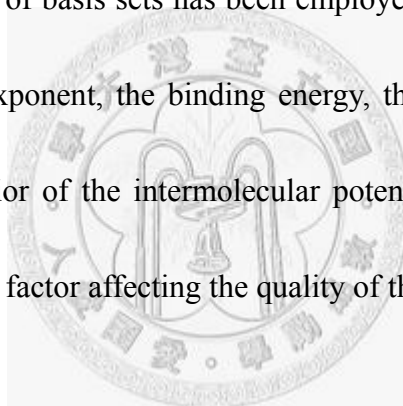
In Table 3.2-2 we show the bond lengths of the calculated DFT potentials using the 80 exchange-correlation functionals, displayed as the row and the column items, respectively. Roughly the bond lengths descend across the row and down the column.

We find that the SVWN5 and SPL functionals yield a value (4.49 \AA) close to the MP2 result (4.70 \AA). Table 3.2-3 presents the calculated binding energies using the 80 exchange-correlation functionals in a particular order in which the (negative) DFT potentials descend across the row and down the column. The results clearly demonstrate the relative performance of the exchange and the correlation functionals

in the DFT calculations. In Fig. 3.2-5 and Fig. 3.2-6, we also find that the SVWN5 and SPL functions yield a value (-3.063 and - 3.088 *kcal/mol*, respectively) close to the MP2 result (-2.968 *kcal/mol*).

4. Conclusion

In this paper, we have systematically studied the calculated intermolecular potentials of the carbon tetrachloride dimer at D_{3d} conformation using the HF, MP2, and DFT methods. A wide selection of basis sets has been employed to determine the basis set effects on the repulsion exponent, the binding energy, the equilibrium bond length, and the asymptotic behavior of the intermolecular potentials. BSSE corrections are considered as an important factor affecting the quality of the calculated potentials.



5. Bibliography

- [1] M. P. Allen and D. J. Tildesley, *Computer Simulation of Liquids* (Oxford university Press, Oxford, 1987).
- [2] A. A. Al-Kahtani, *Spectrochim. Acta, Part. A.* **58**, 2877 (2002).
- [3] I. R. McDonald, D. G. Bounds, and M. L. Klein, *Mol. Phys.* **45**, 521 (1982).
- [4] A. N. Campell and R. M. Chatterjee, *Canadian J. Chem.*, **47**, 3893 (1969).
- [5] A. H. Narten, *J. Chem. Phys.*, **65**, 573 (1976).

- [6] S. Cohen, R. Powers and R. Rudman, *Acta. Cryst.* **B35**, 1670 (1979).
- [7] A. Chahid, F. J. Bermejo, E. Enciso, M. G. Hernandez and J. L. Martinez, *J. Phys.:Condens. Matter* **4**, 1213 (1992).
- [8] L. Pusztai and R. L. McGreevy, *Mol. Phys.*, **90**, 533 (1997).
- [9] P. A. Egelstaff, D. I. Page and J. G. Powles, *Mol. Phys.*, **20**, 881 (1971).
- [10] A. H. Narten, M. H. Danford and H. A. Levy, *J. Chem. Phys.*, **46**, 4875 (1967).
- [11] J. B. van Tricht, *J. Chem. Phys.*, **85**, 1977 (1977).
- [12] F. J. Bermejo, E. Enciso, J. Alonso, N. Garcia and W. S. Howells, *Mol. Phys.*, **64**, 1169 (1988).
- [13] M. Misawa, *J. Chem. Phys.*, **91**, 5648 (1989).
- [14] S. Kongsuk, T. Kerdcharoen, M. Kiselev, S. Hannongbua, *Chem. Phys.*, **324**, 447 (2006).
- [15] R. Rossend, *J. Chem. Phys.*, **126**, 164506 (2007).
- [16] R. Rossend, *J. Phys. Chem. B*, **112**, 344 (2008).
- [17] R. Rossend, *J. Chem. Phys.*, **129**, 224509 (2008).
- [18] Sz. Pothoczki, L. Temleitner, P. Jovari, S. Kohara and L. Pusztai, *J. Chem. Phys.*, **130**, 064503 (2009).
- [19] A. K. Rappe, E. R. Bernstein, *J. Phys. Chem. A.*, **104**, 6117 (2000).
- [20] E. R. Chalasinski, M. M. Szczesniak, *Chem. Rev.*, **100**, 4227 (2000).

- [21] R. J. Wheatley, A. S. Tulegenov, E. Bichoutskaia, *Int. Rev. Phys. Chem.* **23**, 151 (2004).
- [22] Y. Zhao, D. G. Truhlar, *J. Chem. Theory Comput.*, **1**, 415 (2005).
- [23] S. Grimme, *J. Comp. Chem.*, **25**, 1463 (2004).
- [24] T. M. Chang, K. A. Peterson and L. X. Dang, *J. Chem. Phys.*, **103**, 7502 (1995).
- [25] J. C. Soetens and G. Jansen, *Mol. Phys.*, **96**, 1003 (1999).
- [26] R. Mahlanen, J. P. Jalkanen and T. A. Pakkanen, *Chem. Phys.*, **313**, 271 (2005).
- [27] S. W. Chao, A. H.-T. Li and S. D. Chao, *J. Comput. Chem.*, **30**, 1839 (2009).
- [28] C. C. Pai, A. H.-T. Li and S. D. Chao, *J. Phys. Chem. A.*, **111**, 11922 (2007).
- [29] A. H.-T. Li and S. D. Chao, *J. Mol. Struct. Theo.*, **897**, 90 (2009).
- [30] S. D. Chao and A. H.-T. Li, *J. Phys. Chem. A.*, **111**, 9586 (2007).
- [31] A. H.-T. Li and S. D. Chao, *J. Chem. Phys.*, **125**, 094312 (2006).
- [32] A. H.-T. Li and S. D. Chao, *Phys. Rev. A.*, **73**, 016701 (2006)
- [33] K. Burke, J. P. Perdew, Y. Wang, *In Electronic Density Functional Theory: Recent Progress and New Directions*; J. F. Dobson, G. Vignale, M. P. Das. Eds.; Plenum: New York, 1998.
- [34] M. J. Frisch, G. W. Trucks, H. B. Schlegel *et al.*, Gaussian 03, Revision D.02, Gaussian, Inc., Wallingford CT, 2004.
- [35] J. Haase and W. Zell, *Phys. Chem.*, **45**(3/4), 202 (1965).

- [36] C. Møller and M. S. Plesset, *Phys. Rev.* **46**, 618 (1934).
- [37] R. Krishnan, J. S. Binkley, R. Seeger, and J. A. Pople, *J. Chem. Phys.*, **72**, 650 (1980).
- [38] T. H. Dunning, Jr., *J. Chem. Phys.*, **90**, 1007 (1989).
- [39] S. F. Boys and F. Bernardi, *Mol. Phys.*, **19**, 553 (1970).
- [40] M. M. Szczesniak, G. Chalasinski, S. M. Cybulski and S. Scheiner, *J. Chem. Phys.* **93**, 4243 (1990).
- [41] F. Jensen, *Introduction to Computational Chemistry*. Wiley:New York, 1999
- [42] A. D Becke, *Phys. Rev. A.*, **38**, 3098 (1988).
- [43] C. Adamo and V. Barone, *J. Chem. Phys.*, **108**, 664 (1998).
- [44] J. P. Perdew, K. Burke and M. Ernzerhof. *Phys. Rev. Lett.*, **77**, 3865 (1996).
- [45] K. Burke, J. P. Perdew, Y. Wang, In *Electronic Density Functional Theory: Recent Progress and New Directions*; Dobson, J. F., Vignale G, Das, M. P., Eds.; (Plenum, New York, 1998).
- [46] J. Tao, J. P. Perdew, V. N. Staroverov, and G. E. Scuseria, *Phys. Rev. Lett.*, **91**, 146401 (2003).
- [47] W. Kohn, L. Sham, *J. Phys. Rev.*, **140**, A1133 (1965).
- [48] A. D. Boese and N. C. Handy, *J. Chem. Phys.*, **114**, 5497 (2001); see also the supplemental material EPAPS Document No. E-JCPA6-114-301111.

- [49] J. C. Slater, *Quantum Theory of Molecular and Solids*. Vol. 4: The Self-Consistent Field for Molecular and Solids; McGraw-Hill: New York, 1974.
- [50] J. P. Perdew, *Phys. Rev. B.*, **33**, 8822 (1986).
- [51] S. H. Vosko, L. Wilk, and M. Nusair, *Can. J. Phys.*, **58**, 1200 (1980).
- [52] J. P. Perdew and A. Zunger, *Phys. Rev. B.*, **23**, 5048 (1981).
- [53] C. Lee, W. Yang, and R. G. Parr, *Phys. Rev. B.*, **37**, 785 (1988).

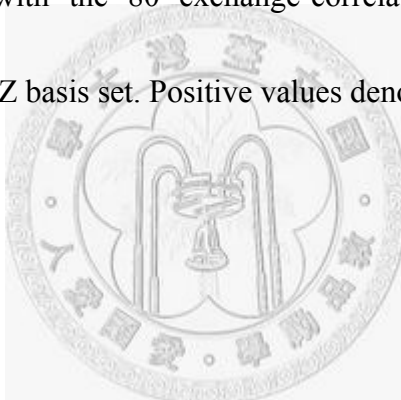


Table captions

Table 3.2-1. The basis set dependence of some potential parameters for the HF and MP2 potentials.

Table 3.2-2. Comparison of the bond lengths (in \AA) of the interaction potential calculated with the 80 exchange-correlation functionals using the aug-cc-pVTZ basis set.

Table 3.2-3. Comparison of the binding energies (in kcal/mol) of the potential calculated with the 80 exchange-correlation functionals using the aug-cc-pVTZ basis set. Positive values denote unbound structure.



Basis set	HF		MP2	
	A (kcal/mol)	α (\AA^{-1})	R _m (\AA)	E _b (kcal/mol)
STO-3G	48397683	3.75	6.29	-0.010
3-21G	1299506	2.79	6.03	-0.123
6-31G	1617627	2.84	6.00	-0.135
3-21G**	1046010	2.75	5.57	-0.397
cc-pVDZ	1243814	2.79	5.36	-0.581
6-31G**	1422093	2.81	5.43	-0.473
aug-cc-pVDZ	1347998	2.81	4.81	-2.310
cc-pVTZ	1440544	2.82	4.87	-1.722
6-311++G(3df,3pd)	2401632	2.93	4.77	-2.609
aug-cc-pVTZ	1314163	2.79	4.70	-2.968
cc-pVQZ	1269782	2.78	4.72	-2.581
aug-cc-pVQZ	1266359	2.78	4.65	-3.220
Basis set limit	1161130	2.76	4.58	-3.523

Table 3.2-1

		<i>Correlation functional</i>									
		VWN5	PL	VWN	TPSS	PBE	PW91	LYP	P86	VP86	HCTH
<i>Exchange functional</i>	HCTH	7.19	7.24	7.09	U ^a	7.20	7.20	U ^a	7.76	U ^a	5.45
	B	U	U	7.59	U ^a	5.05					
	MPW	6.43	6.42	6.37	6.49	6.48	6.47	6.25	6.34	6.34	4.99
	TPSS	6.19	6.19	6.14	6.02	6.02	6.01	5.59	5.41	5.41	4.94
	PBE	5.68	5.68	5.66	5.48	5.46	5.44	5.20	5.01	5.01	4.91
	PW91	5.68	5.68	5.65	5.52	5.50	5.48	5.24	5.03	5.04	4.91
	S	4.49	4.49	4.47	4.15	4.11	4.12	4.24	4.00	4.00	NA ^b
	XA	4.42	4.42	4.39	4.00	4.00	4.00	4.17	4.00	4.00	4.37

^a Unbound

^b Not available

Table 3.2-2

		<i>Correlation functional</i>									
		VWN5	PL	VWN	TPSS	PBE	PW91	LYP	P86	VP86	HCTH
<i>Exchange functional</i>	HCTH	-0.003	-0.009	-0.012	0.007	-0.017	-0.016	0.003	-0.012	0.002	-1.225
	B	0.001	0.000	-0.004	0.020	0.029	0.018	0.010	0.017	0.017	-3.383
	MPW	-0.085	-0.085	-0.102	-0.081	-0.080	-0.079	-0.126	-0.051	-0.051	-4.613
	TPSS	-0.132	-0.133	-0.154	-0.111	-0.112	-0.115	-0.291	-0.237	-0.232	-5.039
	PBE	-0.239	-0.242	-0.298	-0.283	-0.291	-0.307	-0.671	-0.854	-0.842	-5.753
	PW91	-0.548	-0.552	-0.610	-0.586	-0.591	-0.611	-0.934	-1.100	-1.089	-5.992
	S	-3.063	-3.088	-3.367	-6.828	-7.235	-7.303	-7.305	-9.740	-9.698	NA ^a
	XA	-3.441	-3.468	-3.758	-7.518	-8.036	-8.086	-8.079	-10.753	-10.709	-12.513

^aNot available

Table 3.2-3

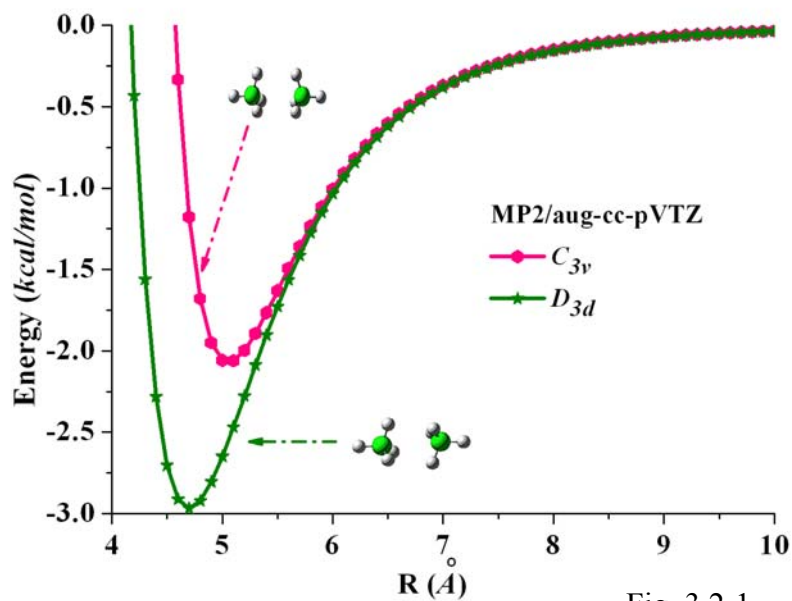


Fig. 3.2-1

FIG. 3.2-1. The BSSE corrected MP2 potentials using the aug-cc-pVTZ basis set for the D_{3d} and C_{3v} conformers of the carbon tetrachloride dimer.

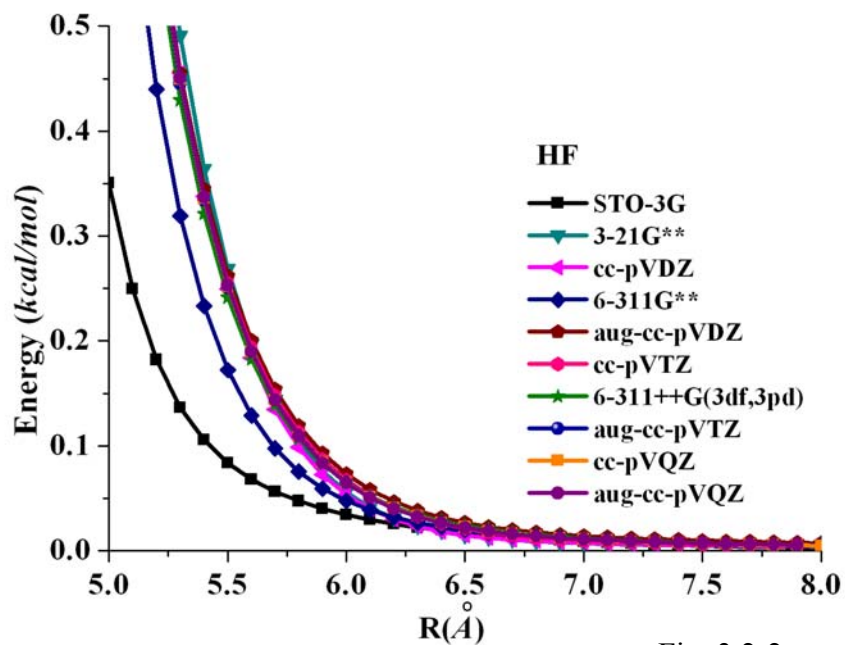


Fig. 3.2-2

FIG. 3.2-2. The BSSE corrected HF interaction potentials of the carbon tetrachloride dimer using several basis sets.

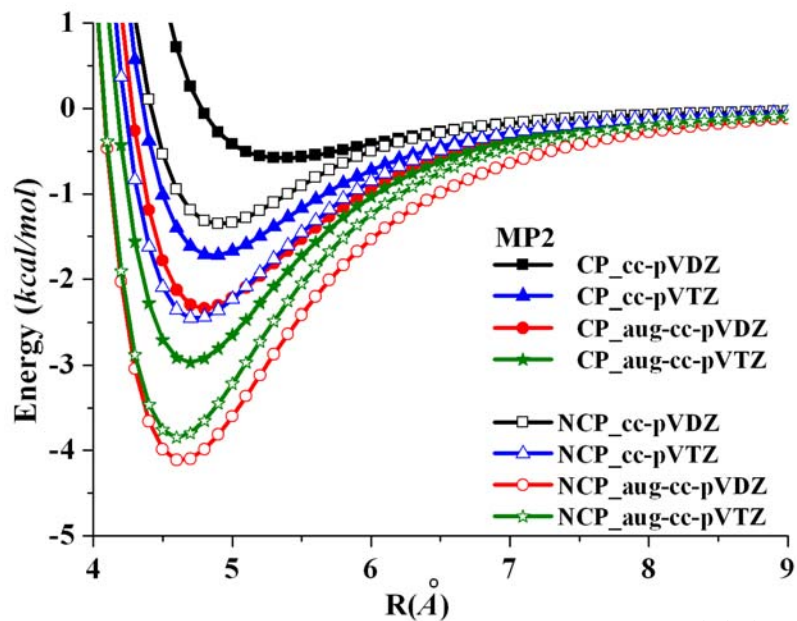


Fig. 3.2-3

FIG. 3.2-3. The BSSE corrected (CP) and uncorrected (NCP) MP2 interaction potentials of the carbon tetrachloride dimer using a series of basis sets.

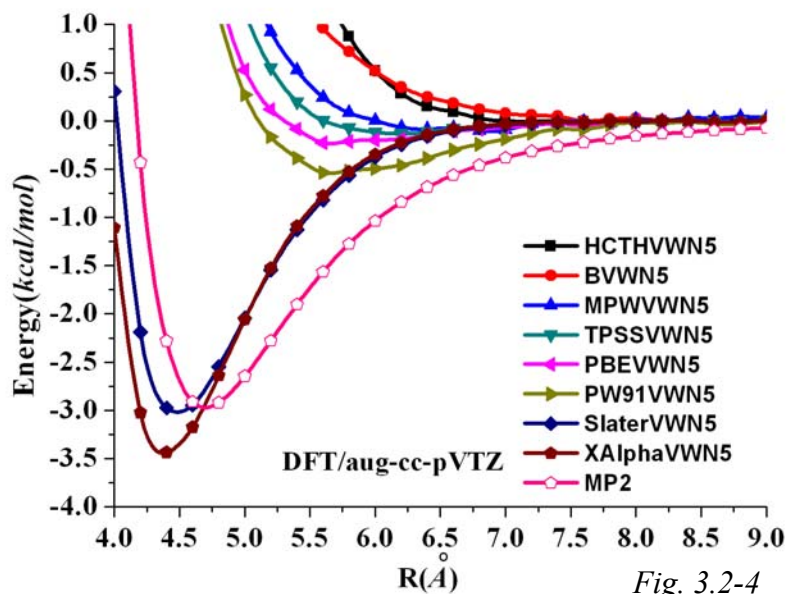


Fig. 3.2-4

FIG. 3.2-4. The BSSE corrected DFT potential curves with varying exchange functional by fixing VWN5 correlation functionals. The MP2 potential curve is also shown as a reference.

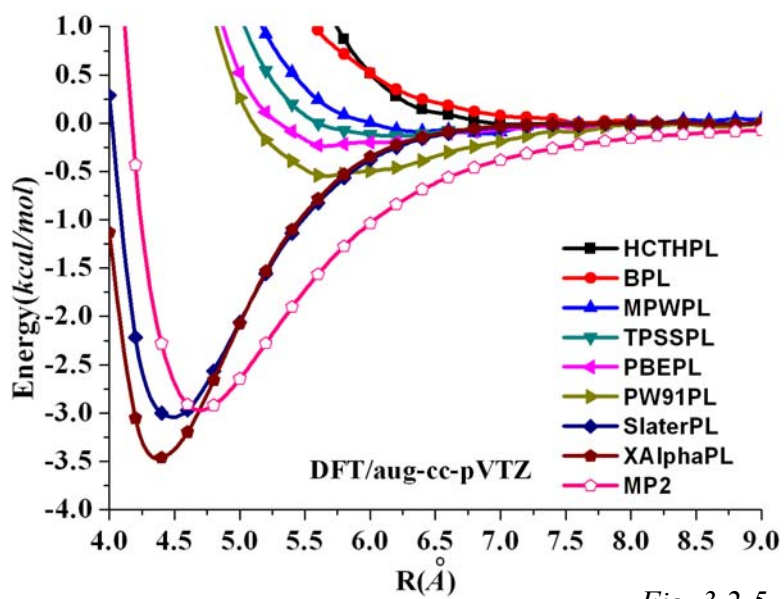
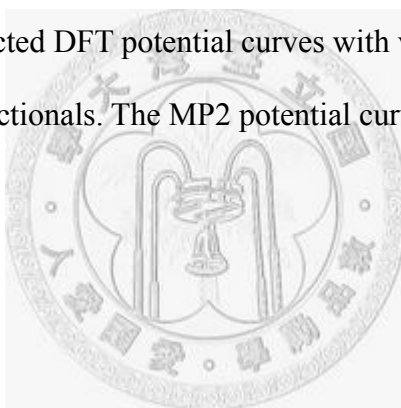


Fig. 3.2-5

FIG. 3.2-5. The BSSE corrected DFT potential curves with varying exchange functional by fixing PL correlation functionals. The MP2 potential curve is also shown as a reference.



Chapter 4 Conclusion

We have calculated the intermolecular potentials of dimers of methane, silane and carbon tetrachloride using quantum chemistry HF, DFT, MP2 and CCSD(T) methods. The fitted parameters are then used to examine the thermodynamics properties, molecular dynamics simulations and perform theoretical analysis on the simulation results. All the simulations are compared to their corresponding finer simulations to check convergence and accuracy. One of the distinguishing points from most other united-atom simulation schemes is that our theory considers properly the actual molecular shape effect on the interaction and would capture the main microscopic features of macromolecular interactions.

(1) *Ab initio* Calculations

We performed *ab initio* calculations on dimers of methane, silane and carbon tetrachloride at several relative configurations, using the Gaussian 03 and Gaussian 09 package. The calculations of those dimers were performed at the HF, DFT, MP2 and CCSD(T) theory using the STO-3G ~ aug-cc-pV5Z basis set level for twelve different orientations. The basis set is pretty large and has been used to calibrate empirical force fields for liquid alkane in the literature. The energy scans were performed for a quite dense grid of spatial points for each definite configuration. Counterpoise corrections (CPC) to the basis set superposition error were performed using the new counterpoise feature in Gaussian 03 and Gaussian 09.

(2) Molecular Dynamics Simulations

We performed a molecular dynamics simulation for a system of model CH₄, SiH₄ and CCl₄ dimers using both the constructed 4-site and 5-site models. We show the simulated

radial distribution functions and velocity autocorrelation functions using our 4-site and 5-site models at phase points along the gasification line and melting line from the triple point to the critical point. We compare the simulated diffusion constants in different conditions with the experimental results. We see the theoretical results are in agreement with those from X-ray scattering and Neutron scattering factor experiments.

